



HAL
open science

Interaction sol-structure non-linéaire en analyse sismique

Alex Nieto Ferro

► **To cite this version:**

Alex Nieto Ferro. Interaction sol-structure non-linéaire en analyse sismique. Autre. Ecole Centrale Paris, 2013. Français. NNT : 2013ECAP0006 . tel-00944139

HAL Id: tel-00944139

<https://theses.hal.science/tel-00944139>

Submitted on 10 Feb 2014

HAL is a multi-disciplinary open access archive for the deposit and dissemination of scientific research documents, whether they are published or not. The documents may come from teaching and research institutions in France or abroad, or from public or private research centers.

L'archive ouverte pluridisciplinaire **HAL**, est destinée au dépôt et à la diffusion de documents scientifiques de niveau recherche, publiés ou non, émanant des établissements d'enseignement et de recherche français ou étrangers, des laboratoires publics ou privés.



Nonlinear Dynamic Soil-Structure Interaction in Earthquake Engineering

THÈSE

présentée et soutenue publiquement le 17/01/2013
pour l'obtention du grade de

Docteur de l'École Centrale Paris
(spécialité mécanique)

par

Alex Nieto Ferro

sous la direction du Prof. Didier Clouteau

Composition du jury

Président : M. Frédéric Ragueneau (ENS Cachan, France)
Rapporteurs : M. Marc Bonnet (CNRS, France)
M. Geert Degrande (KU Leuven, Belgique)
Examineurs : M. Didier Clouteau (École Centrale Paris, France)
M. Nicolas Greffet (EDF R&D, France)
M. Jean-François Semblat (IFSTTAR, France)

Acknowledgements

First of all, I would like to express my most sincere gratitude to Prof. Didier Clouteau, for his invaluable guidance and his precious capacity to convey knowledge. Prof. Clouteau woke up my interest in the fascinating field of computational structural dynamics and it has been a great pleasure for me to work with him during these years at the École Centrale Paris.

I am also deeply indebted to my supervisors of the EDF R&D team, Nicolas Greffet and Georges Devésa, for their timely support and suggestions. Because meeting them and working with them has been an enriching experience in both scientific and human terms.

I also want to extend my appreciation to the many friends, students, professors and research engineers with whom, somehow, I shared time and lots of enjoyable moments. For their generosity, help and friendship, I am highly grateful to: Dzifa, Quang Anh, Christelle, Fernando, Dina, Phuong, Irmela, Vinicius, François, Tatiana, El Hadi, Cédric, Nazir, Amélie, Ali, Ana, Régis, Luis, Denis, and to many others that will certainly remain in my memories for ever. Thanks also to my EDF R&D team managers, Thomas and Vincent, who left me the freedom to pursue my own research unfettered by the actual industrial interests, and allowing me to do a profitable but also scientifically rigorous work.

I am beholden to Prof. Lehel Banjai and to Dr. Stijn François for receiving me warmly at the Max Planck Institute of Leipzig and at the KU Leuven, respectively, and for giving me the opportunity to work with them. Also to Prof. Christian Lubich, from Universität Tübingen, and Prof. Antonio Laliena, from Universidad de Zaragoza. Many thanks for their fruitful advice and help at some stages of this work.

Finally, I would like to express special thanks to my family: to my parents, because they have always encouraged me to do my best, and foremost, to my beloved wife, Ana, who has been beside me from the beginning, providing me with all the necessary support during these years in Paris.

A. NIETO FERRO
Paris, January 17th, 2013

Contents

| | |
|--|-------------|
| Acknowledgements | i |
| List of Symbols | vii |
| List of Figures | xiii |
| List of Tables | xvii |
| Introduction and Outline | 1 |
| Industrial context | 2 |
| Methodology and original contributions | 3 |
| Organisation of the text | 4 |
| 1 An overview on dynamic soil-structure interaction | 7 |
| 1.1 Literature review | 7 |
| 1.1.1 The direct method | 8 |
| 1.1.2 The substructure method | 10 |
| 1.2 Dynamic SSI problem in earthquake engineering | 13 |
| 1.2.1 Seismic incident field | 15 |
| 1.2.2 Linear governing equations | 15 |
| 1.2.3 Variational formulation | 16 |
| 1.2.4 The soil impedance operator | 18 |
| 1.3 Spatial semi-discretization: the BE-FE coupled equations | 21 |
| 1.3.1 BE discretization | 22 |
| 1.3.2 FE discretization | 23 |
| 1.3.3 Extension to the nonlinear case | 24 |
| 1.4 Conclusions | 26 |

| | | |
|----------|--|-----------|
| 2 | The Hybrid Laplace-Time Domain Approach | 27 |
| 2.1 | State of the art | 28 |
| 2.2 | Time domain discretization | 29 |
| 2.2.1 | Family of Newmark time integration schemes | 30 |
| 2.2.2 | Convolution Quadrature Method | 31 |
| 2.3 | The Hybrid Laplace-Time Domain Approach | 34 |
| 2.3.1 | General formulation | 35 |
| 2.3.2 | Application to SSI problems: <i>MKC formulation</i> | 36 |
| 2.3.3 | MKC identification | 40 |
| 2.4 | Coupling to the time integration scheme used for the FE system | 41 |
| 2.4.1 | Stability properties | 41 |
| 2.4.2 | Implicit algorithm | 42 |
| 2.4.3 | Explicit algorithm | 43 |
| 2.5 | Comparison with the Hybrid Frequency-Time domain Approach | 44 |
| 2.5.1 | Evaluation of the SSI interaction forces in the time domain | 45 |
| 2.5.2 | Illustrative numerical example | 47 |
| 2.6 | Conclusions | 52 |
| 3 | Numerical experiments and validation | 53 |
| 3.1 | Preliminaries | 53 |
| 3.1.1 | Numerical implementation of the CQ Method | 53 |
| 3.1.2 | The soil impedance in the time domain | 54 |
| 3.1.3 | Hysteretic damping model | 56 |
| 3.1.4 | Soil matrices identification approach | 57 |
| 3.1.5 | Interpolation of the interaction forces in the time domain | 58 |
| 3.2 | Linear analysis | 60 |
| 3.2.1 | Reference solution | 60 |
| 3.2.2 | Lumped-parameter model | 61 |
| 3.2.3 | Large-scale FE model | 62 |
| 3.2.4 | Structure-soil-structure interaction model | 67 |
| 3.3 | Nonlinear framework | 70 |
| 3.4 | Conclusions | 74 |

| | |
|---|------------|
| 4 Industrial numerical application | 77 |
| 4.1 Introduction and methodology | 77 |
| 4.1.1 The structural FE model | 78 |
| 4.1.2 The viscoelastic soil domain | 80 |
| 4.2 Soil-structure interaction modelling | 82 |
| 4.2.1 Full FEM resolution | 83 |
| 4.2.2 Frequency domain BE-FE coupling | 85 |
| 4.2.3 Hybrid Laplace-Time Domain Approach | 86 |
| 4.3 Comparative study | 87 |
| 4.3.1 Loads | 87 |
| 4.3.2 Linear analysis | 89 |
| 4.3.3 Nonlinear analysis | 92 |
| 4.3.4 Efficiency of the considered approaches | 94 |
| 4.4 Conclusions | 97 |
| Conclusions and perspectives | 99 |
| Bibliography | 103 |
| A Functional spaces | 115 |
| B Earthquake Response Spectra | 117 |

List of Symbols

Acronyms

| | |
|------------|--|
| 3SI | Structure-Soil-Structure Interaction |
| ABC | Artificial Boundary Condition |
| BC | Boundary Conditions |
| BDF | Backward Differentiation Formula |
| BDF1, BDF2 | Backward Differentiation Formula of first and second order |
| BE, BEM | Boundary Element, Boundary Element Method |
| BVP | Boundary Value Problem |
| CEA | Commissariat à l'Énergie Atomique et aux énergies alternatives |
| CIFECM | Consistent Infinitesimal Finite-Element Cell Method |
| CPU | Central Processing Unit |
| CQM | Convolution Quadrature Method |
| DoF | Degree-of-Freedom |
| DSM | Direct Solution Method |
| DSSI | Dynamic Soil-Structure Interaction |
| DtN | Dirichlet to Neumann |
| EDF | Électricité de France |
| FD | Finite Difference |
| FE, FEM | Finite Element, Finite Element Method |
| FFT | Fast Fourier Transform |
| FreqBFA | Frequency domain BE-FE Approach |
| FSI | Fluid-Structure Interaction |
| GLRC | Global Law of Reinforced Concrete |
| GMRES | Generalized Minimum RESidual method |
| HFTA | Hybrid Frequency-Time domain Approach |
| HHT | Hilber-Hughes-Taylor time integration method |
| HLTA | Hybrid Laplace-Time domain Approach |
| IE | Infinite Element |
| IFFT | Inverse Fast Fourier Transform |
| LDLT | Cholesky decomposition |

| | |
|-------|---|
| NOAA | National Oceanic and Atmospheric Administration |
| NRBC | NonReflecting Boundary Conditions |
| NUPEC | Nuclear Power Electric Corporation |
| PML | Perfectly Matched Layer |
| PGA | Peak Ground Acceleration |
| PGD | Peak Ground Displacement |
| PSA | Pseudo-Spectral Acceleration |
| RMS | Root Mean Square |
| R&D | Research and Development |
| RS | Response Spectra |
| SA | Spectral Acceleration |
| SBFEM | Scaled Boundary Finite-Element Method |
| SD | Spectral Displacement |
| SDOF | Single Degree-of-Freedom |
| SMART | Seismic design and best-estimate Methods Assessment for Reinforced concrete buildings subjected to Torsion and non-linear effects |
| SSI | Soil-Structure Interaction |
| TLM | Thin Layer Method |

General symbols and conventions

| | |
|------------------------------|---|
| \mathbf{x}, x_i | Cartesian coordinates |
| r | radial direction |
| \mathbf{e}_i | unit vector along the axis i |
| \mathbf{I}_d | identity tensor |
| t | time |
| f | frequency |
| δ_{ij} | Kronecker Delta |
| $\delta(\diamond)$ | Dirac Delta distribution |
| ω | Fourier transform variable, angular frequency |
| s | complex Laplace transform variable |
| z | complex z-transform variable |
| $\Re(\diamond)$ | real part of a variable \diamond |
| $\Im(\diamond)$ | imaginary part of a variable \diamond |
| $i = \sqrt{-1}$ | imaginary unit |
| $\overline{\diamond}$ | complex conjugate of \diamond |
| $\mathcal{F}(\diamond)$ | Fourier Transform of \diamond |
| $\mathcal{F}^{-1}(\diamond)$ | Inverse Fourier Transform of \diamond |
| $\mathcal{L}(\diamond)$ | Laplace Transform of \diamond |

| | |
|------------------------------|---|
| $\mathcal{L}^{-1}(\diamond)$ | Inverse Laplace Transform of \diamond |
| $\partial_t \diamond$ | first order time derivative of the variable \diamond |
| $\partial_{tt} \diamond$ | second order time derivative of the variable \diamond |
| $(\diamond * \circ)(t)$ | time convolution between functions $\diamond(t)$ and $\circ(t)$ |
| $\diamond : \circ$ | double contraction product between tensors \diamond and \circ |
| $\diamond \cdot \circ$ | scalar product between vectors \diamond and \circ |
| \diamond^T | transpose of a matrix \diamond |
| $\nabla \diamond$ | gradient of a vector field \diamond |
| $\nabla \cdot \diamond$ | divergence of a vector field \diamond |
| $\hat{\diamond}$ | Laplace transform of \diamond |
| $O(\diamond)$ | Big O notation (Landau notation) |
| $\diamond _{\Gamma}$ | trace of \diamond on Γ |

Dynamic Soil-Structure Interaction

| | |
|--------------------------------------|--|
| Ω_b | structural domain |
| Ω_s | soil domain |
| Γ | soil-structure interaction interface |
| Γ_{bo} | free boundary of the structural domain |
| Γ_{ABC} | boundary with ABC |
| Γ_D | boundary with Dirichlet BC |
| Γ_N | boundary with Neumann BC |
| S_0 | free boundary of the soil domain |
| λ_α | first Lamé constant of the domain α |
| μ_α | second Lamé constant, shear modulus of the domain α |
| $\mathbf{C}_\alpha, C_{\alpha,ijkl}$ | constitutive tensor of the domain α |
| ν_α | Poisson's ratio of the domain α |
| ρ_α | density of the domain α |
| E_α | Young's modulus of the domain α |
| η_s | viscous damping coefficient of the soil domain |
| β_s | hysteretic damping coefficient of the soil domain |
| λ_s^* | complex first Lamé constant of the soil domain |
| μ_s^* | complex second Lamé constant of the soil domain |
| C_P | dilatational wave velocity in the soil model |
| C_S | shear wave velocity in the soil model |
| $t_{prop,P}$ | dilatational wave propagation delay in the soil |
| $t_{prop,S}$ | shear wave propagation delay in the soil |
| \mathbf{n}_α | outer unit normal vector of the domain α |
| \mathbf{u}_α | displacement field in the domain α |

| | |
|--------------------------|--|
| ϵ_α | strain field in the domain α |
| σ_α | stress field in the domain α |
| t_{n_α} | traction vector field defined by n_α |
| \mathbf{u}^{inc} | incident displacement field |
| \mathbf{u}_{sc} | scattered displacement field |
| \mathbf{u}_{rad} | radiated displacement field into the soil |
| \mathbf{u}_{loc} | locally diffracted displacement field |
| \mathbf{t}^{inc} | traction vector field corresponding to the incident wave field |
| t_{bo} | traction vector field defined on Γ_{bo} |
| $\hat{\mathbf{U}}_s^G$ | first Green's tensor of a layered half-space |
| $\hat{\mathbf{T}}_s^G$ | second Green's tensor of a layered half-space |
| \mathbf{T}^0 | tensor used for the regularization of the BIE |
| \mathcal{M} | sesquilinear form of mass |
| \mathcal{K} | sesquilinear form of stiffness |
| ℓ_b | linear form associated to the forces applied on Ω_b |
| ℓ_s | linear form associated to the forces applied on Γ |
| \mathcal{Z}_V | sesquilinear form defined in Ω_b |
| \mathcal{Z} | sesquilinear form of the dynamic soil impedance defined on Γ |
| \mathcal{U} | first bilinear form associated to the BIE |
| \mathcal{T} | second bilinear form associated to the BIE |
| $\hat{\mathcal{Z}}(s)$ | Laplace domain bounded linear operator associated to \mathcal{Z} |
| $\hat{\mathcal{U}}(s)$ | Laplace domain bounded linear operator associated to \mathcal{U} |
| $\hat{\mathcal{T}}(s)$ | Laplace domain bounded linear operator associated to \mathcal{T} |
| \mathbf{N}_b | matrix collecting the finite element shape functions |
| \mathbf{M}_s | matrix collecting the boundary element shape functions |
| \mathbf{D}_b | constitutive matrix of the structure |
| \mathbf{M}_b | mass matrix of the structure |
| \mathbf{K}_b | stiffness matrix of the structure |
| \mathbf{L} | matrix with space derivative operators |
| \mathbf{L}_t | matrix with time derivative operators |
| $\hat{\mathcal{S}}$ | Laplace transform of \mathbf{L}_t operator |
| $\diamond_{\alpha\beta}$ | matrix blocks of matrix \diamond corresponding to DoF's $\alpha\beta$ |
| $\hat{\phi}(s)$ | prescribed displacement field on Γ |
| $\hat{\mathbf{U}}(s)$ | Laplace domain BE matrix, the spatial discretization of $\hat{\mathcal{U}}(s)$ |
| $\hat{\mathbf{T}}(s)$ | Laplace domain BE matrix, the spatial discretization of $\hat{\mathcal{T}}(s)$ |
| $\hat{\mathcal{Z}}(s)$ | Laplace domain dynamic soil impedance matrix (from $\hat{\mathcal{Z}}(s)$) |
| $\hat{\mathcal{Z}}_V(s)$ | Laplace domain matrix associated to $\hat{\mathcal{Z}}(s)$ |
| \diamond | \diamond is a FE-basis vector |
| \diamond | \diamond is a BE-basis vector |

| | |
|--------------------------------|---|
| Λ_s | diagonal matrix with BE surface |
| T_q | BE to FE transfer matrix |
| \underline{R}_T | SSI forces at FE nodes |
| \underline{F}^{int} | vector of the internal nonlinear forces at FE nodes |
| \underline{F}^{ext} | vector of the external forces at FE nodes |
| $\underline{r}(\underline{u})$ | vector of the residual term of the force balance equation |
| S_T | tangent matrix operator on $\underline{r}(\underline{u})$ |
| $\gamma_f(t)$ | free-field acceleration |
| Ψ_{CB} | Craig-Bampton transformation matrix |
| Λ_{QQ} | diagonal matrix containing the square of eigenfrequencies |
| ξ | modal damping |
| α_{R1}, α_{R2} | Rayleigh damping parameters |
| l_{EF} | boundary element size |
| λ_S | shear wave wavelength |
| f_{max} | upper bound of the frequency interval of interest |

Hybrid Laplace-Time domain Approach

| | |
|---------------------|--|
| Δt | time step |
| A | left hand-side Newmark operator |
| B | right hand-side Newmark equivalent forces vector |
| β | first Newmark parameter |
| γ | second Newmark parameter |
| α_d | Newmark numerical damping parameter |
| G | growth matrix (stability analysis) |
| L_n | vector depending on the excitation at time step n (stability analysis) |
| $r(z)$ | rational function associated to the CQM |
| ρ | CQM parameter |
| ϵ_{CQM} | CQM precision |
| w_n | CQM weights |
| \diamond_n | discretized field \diamond at time step n |
| $\hat{Z}_s(\omega)$ | Fourier domain dynamic soil impedance matrix |
| $\hat{Z}(s)$ | Laplace domain dynamic soil impedance matrix |
| $Z(t)$ | time domain dynamic soil impedance matrix |
| $\underline{u}(t)$ | nodal displacement vector |
| $\hat{Z}_{nsin}(s)$ | Laplace domain non-singular dynamic soil impedance matrix |
| $Z_{nsin}(t)$ | time domain non-singular dynamic soil impedance matrix |
| $\hat{Z}_{sin}(s)$ | Laplace domain singular dynamic soil impedance matrix |
| $Z_{sin}(t)$ | time domain singular dynamic soil impedance matrix |

| | |
|------------------------------|--|
| \mathbf{M}_Γ | mass matrix of the structure at SSI DoF's |
| \mathbf{C}_Γ | damping matrix of the structure at SSI DoF's |
| \mathbf{K}_Γ | stiffness matrix of the structure at SSI DoF's |
| $\tilde{\diamond}$ | estimate of matrix \diamond |
| $\mathbf{Z}_M(t)$ | time domain impedance of inertia |
| $\mathbf{Z}_C(t)$ | time domain impedance of damping |
| $\mathbf{Z}_K(t)$ | time domain impedance of stiffness |
| $\mathbf{\Psi}_k^n$ | dynamic soil impedance matrix k at time step n |
| $\check{\mathbf{\Psi}}_k^n$ | generalized dynamic soil impedance matrix k at time step n |
| $\mathbf{\Theta}^n$ | dynamic soil flexibility matrix at time step n |
| $\tilde{\mathbf{\Theta}}^n$ | dynamic soil flexibility matrix at time step n (MKC formulation) |
| $\mathbf{R}_{\Gamma,n}$ | nodal SSI forces at time step n |
| $\mathbf{R}_{\Sigma(n-1)}$ | time history of dynamic SSI forces |
| $\mathbf{\Phi}_\Gamma$ | matrix containing Ritz vectors |
| $\boldsymbol{\alpha}_\Gamma$ | modal coordinates vector |

Hybrid Frequency-Time domain Approach

| | |
|-----------------------|--|
| $\hat{\mathbf{F}}(s)$ | Laplace domain dynamic soil flexibility matrix |
| $\mathbf{F}(t)$ | time domain dynamic soil flexibility matrix |
| \mathbf{F}^n | dynamic soil flexibility matrix at time step n |
| \mathbf{Q}_n | nodal SSI forces at time step n (within a flexibility formulation) |
| $\phi(t)$ | time domain interpolation function |
| $\varphi(t)$ | $\phi(t)$ modified by the Heaviside function |

List of Figures

| | | |
|-----|--|----|
| 1 | (a) Model at 1/3 scale of a reactor at Hualien, Taiwan. (b) Dynamic response of the corresponding numerical model. | 2 |
| 2 | Simplified model of a SSI system where the superstructure is modelled using a FE method and the layered soil, using a BE method. (a) The <i>superstructure</i> refers at least to the structure and its foundations since (b) may also include a surrounding part of soil. | 4 |
| 3 | Simplified scheme to represent (a) the effects of the linear unbounded soil and (b) the final global resolution of the SSI problem. | 5 |
| 1.1 | (a) Simplified model of a SSI-system. (b) The whole SSI system, bounded with an artificial NRBC boundary is discretized using FE. . . | 9 |
| 1.2 | (a) Modelling using the Thin Layer Method. (b) Modelling using the Scaled Boundary Finite Element Method. | 11 |
| 1.3 | Subdomain Ω_b (modelled in FE) may include the nonlinear structure and also the nonlinear soil. It is separated from the linear unbounded soil Ω_s by the interface Γ (modelled in BE). | 13 |
| 1.4 | Simplified model of the exterior Boundary Value Problem considered. The image boundary represented with dashed lines concerns the regularization approach. | 19 |
| 2.1 | Backward differentiation formulas of order P on the complex plane. . . | 34 |
| 2.2 | Real and imaginary parts of the interpolation function in the frequency domain (time steps 0.02 s and 0.01 s). | 47 |
| 2.3 | Real and imaginary parts of the interpolation function in the frequency domain (time steps 0.01 s and 0.005 s). | 47 |
| 2.4 | Lumped-parameter model of the soil-foundation-structure system. . . | 48 |
| 2.5 | Acceleration at m_1 computed with the Hybrid Frequency-Time domain Approach (HFTA) compared to the reference solution for $M_\Gamma = m_{2,2}$. . . | 50 |
| 2.6 | For $M_\Gamma = 10 m_{2,2}$, acceleration at m_1 computed with the HFTA and compared to the reference solution. | 51 |
| 2.7 | Ratio between time flexibility functions calculated by both approaches: the BDF2-based Hybrid Laplace-Time domain Approach (HLTA) and the HFTA. | 51 |

| | | |
|------|---|----|
| 2.8 | Acceleration at m_1 computed with the multistep BDF1-based HLTA compared to the reference solution. | 52 |
| 3.1 | (a) Simplified model of one-layer soil overlying a bedrock. (b) Simplified model of a homogeneous soil. | 54 |
| 3.2 | (a) Horizontal and (b) vertical components of the time impedance evolution for a soil consisting of a 150 m-layer. | 55 |
| 3.3 | (a) Horizontal component of the time impedance function for a homogeneous soil. (b) Idem with different y -axis limits. | 56 |
| 3.4 | Time impedance function containing hysteretic damping. | 57 |
| 3.5 | Simplified model of a structure on a square surface foundation. | 62 |
| 3.6 | Free-field accelerogram applied to m_2 | 63 |
| 3.7 | Displacement at m_1 in the x -direction computed with the HLTA and compared to the reference solution. | 63 |
| 3.8 | Different views of the FE model of reactor building considered in this study. | 64 |
| 3.9 | Free-field acceleration applied on x -direction (a) in time domain and (b) in frequency domain. | 64 |
| 3.10 | Comparison between rigid and flexible foundation responses in (a) displacement and (b) in acceleration at the top of the building for the reference solution. | 65 |
| 3.11 | (a) Time-history of impedance $Z_K(t)$ and (b) of impedance $Z_M(t)$ | 65 |
| 3.12 | Comparison between rigid and flexible responses in (a) displacement and (b) in acceleration at the top of the building for HLTA without MKC formulation. | 65 |
| 3.13 | Comparison between rigid and flexible foundation responses in (a) displacement and (b) in acceleration at the top of the building for HLTA with MKC formulation. | 66 |
| 3.14 | Comparison between HLTA using an MKC formulation, without MKC decomposition and the reference solution for (a) displacement and (b) acceleration in the time domain at the top of the building. | 66 |
| 3.15 | (a) Real view of the single embedded building. (b) Two identical closely spaced embedded buildings used within the NUPEC benchmark. | 67 |
| 3.16 | Simplified model of the NUPEC 3SI application: (a) diagram of dimensions and a (b) view of the FE model. | 67 |
| 3.17 | (a) Transient free-field accelerogram applied on the x -direction and (b) the modulus of its Fourier transform (FFT). | 68 |
| 3.18 | (a) Transient free-field accelerogram applied on the y -direction and (b) the modulus of its Fourier transform (FFT). | 68 |
| 3.19 | Soil profile with the thickness of each soil layer and its relative position respect to the buildings. | 68 |
| 3.20 | (a) Time impedance $Z(t)$ and (b) the $Z_K(t)$ coming from an MKC formulation. | 69 |

| | | |
|------|---|----|
| 3.21 | Transient accelerations at the top of one of the buildings in the (a) x -direction and (b) y -direction respect to the reference solutions. . . . | 70 |
| 3.22 | Numerical model used for the computation of the nonlinear reference solution. | 70 |
| 3.23 | (a) Simplified model of a structure on a square surface foundation. (b) Linear kinematic work hardening law of the nonlinear spring K | 71 |
| 3.24 | Displacement at m_1 in the x -direction computed with the HLTA and compared to the reference solution and to the linear response for F_y . . | 72 |
| 3.25 | Displacement at m_1 in the x -direction computed with the HLTA and compared to the reference solution for a yield load of $6.5F_y$ | 72 |
| 3.26 | (a) Displacement and (b) acceleration at the top of the building for linear and nonlinear responses. | 73 |
| 3.27 | (a) Displacement and (b) acceleration in the x -direction using the HLTA with an MKC formulation. | 73 |
| 3.28 | Zoom at the acceleration response obtained with an MKC formulation for some (a) strong and (b) weak shaking instants. | 74 |
| 3.29 | (a) Displacement and (b) acceleration at the top of the building (in the x -direction) for a HLTA applied with an M formulation. | 74 |
| 4.1 | Experimental set-up. | 77 |
| 4.2 | Schematic view of the soil-structure system to be modelled. | 78 |
| 4.3 | (a) and (b) Bending modes shape around x and y axis, (c) Torsional mode shape and (d) Pumping mode shape. | 79 |
| 4.4 | Numerical FE model of the SMART building and its foundations. . . . | 80 |
| 4.5 | Vertical soil profile as a function of the shear velocity. | 81 |
| 4.6 | Modal damping ratio for an average value of 2.5% between 3 Hz and 30 Hz and the original formula enforcing 2.5% only at endpoints of the same frequency range. | 82 |
| 4.7 | (a) FE model of the SSI system using a rectangular meshing. (b) Zoom of the same FE model near the structure. | 83 |
| 4.8 | (a) FE model of the SSI system using a radial meshing. (b) Zoom of the same FE model near the structure. | 84 |
| 4.9 | FE model used for the BE-FE coupling approach. | 86 |
| 4.10 | View from the top of the building. Red points indicate where acceleration responses have been measured. | 87 |
| 4.11 | Time history and the corresponding Pseudo Spectral Acceleration (PSA) of the free-field accelerogram for (a) and (b) x -direction, (c) and (d) y -direction and, (e) and (f) z -direction. | 88 |
| 4.12 | Comparison between PSA's: one with a hysteretic damping model within the the bounded FE soil and the other, with a viscous damping for (a) x -direction, (b) y -direction and (c) z -direction. | 90 |
| 4.13 | Linear calculation comparing FreqBFA and full FE solutions in (a) x -direction, (b) y -direction and (c) z -direction. | 91 |

| | | |
|------|---|----|
| 4.14 | PSA of linear and nonlinear transient full FEM solution in (a) x -direction, (b) y -direction and (c) z -direction. | 92 |
| 4.15 | PSA of the nonlinear transient full FEM solution compared with the HLTA based on both surface and embedded SSI-interface, for (a) x -direction, (b) y -direction and (c) z -direction. | 93 |
| 4.16 | For a full FEM modelling under the action of the weight: damage iso-values to traction, (a) front view and (b) side view. (c) Damage iso-values to bending, front view. | 95 |
| 4.17 | For a full FEM modelling under the action of the earthquake: ultimate damage iso-values on traction, (a) front view and (b) side view. (c) Ultimate damage iso-values on bending, front view. | 95 |
| 4.18 | For the HLTA solution: damage iso-values on traction when (a) an embedded SSI-interface and (b) a surface SSI-interface are considered. The same for the case of damage on bending: (c) embedded SSI-interface and (d) surface SSI-interface. | 96 |

List of Tables

| | | |
|-----|---|----|
| 2.1 | Generating polynomials of some k -step time integration methods | 34 |
| 2.2 | Properties of the structure-foundation lumped system | 49 |
| 2.3 | Properties of the soil modelled by a lumped-parameter impedance | 49 |
| 2.4 | RMS errors of the acceleration response computed, for different type of formulations, using the Hybrid Laplace-Time domain Approach (HLTA) and the Hybrid Frequency-Time domain Approach (HFTA) | 51 |
| 3.1 | Properties of the structure (m_1, m_2, k, c) and the soil (ρ, E, ν, β_s) | 62 |
| 3.2 | Properties of the soil layers ranged by depth (NUPEC SSI application) | 69 |
| 3.3 | Relative errors of the HLTA computed acceleration response respect to the reference solution for different yield loads (nonlinear analysis) | 73 |
| 4.1 | First eigenfrequencies of the base-clamped SMART structure | 79 |
| 4.2 | First eigenfrequencies of the entire FE soil-structure system | 83 |

Introduction and Outline

“Soil-structure interaction is an interdisciplinary field of endeavor which lies at the intersection of soil and structural mechanics, soil and structural dynamics, earthquake engineering, geophysics and geomechanics, material science, computational and numerical methods, and diverse other technical disciplines.”

EDUARDO KAUSEL, 2009

EARTHQUAKES are one of the most devastating of all natural disasters. On March 11th, 2011, a 9.0-magnitude undersea earthquake occurred near the north-eastern coast of Tohoku, Japan. The unleashed tsunami, with wave heights of about ten meters, swept away buildings, vehicles and debris across the farmlands. The degree and extent of the damage was unprecedented, more than 15 000 people were killed and many other thousands, injured and missing. Almost two years later, Japanese still suffer from the Fukushima Daiichi nuclear disaster, classified by the press media as the second worst nuclear accident ever. The World Bank estimated economic losses around US\$235 billion, which is enormous compared with the economic costs of other recent natural disasters, i.e. for the Hurricane Katrina (U.S., 2005), the National Oceanic and Atmospheric Administration (NOAA) announced \$81 billion of damage cost.

But the case of the Tohoku earthquake is only one among many others. During the last decade, seismic events have taken the life of thousands of people. In December 2004 a 9.1-magnitude Tsunami struck the coasts of Sumatra, Indonesia, killing over 200 000 people. In October 2005, a 7.6-magnitude earthquake devastated Kashmir, Pakistan, toppling buildings and originating landslides that buried more than 85 000 people. Just over two years later, about the same number of people died in Wenchuan, China, resulting in economic costs of about \$29 billion (according to the World Bank). On January 12th, 2010, a 7.0-magnitude earthquake destroyed Port-au-Prince, Haiti, sweeping more than 230 000 people to death and collapsing buildings and infrastructure. Within the same year, also Chile was hit by a very strong earthquake. Indeed, approximately two-thirds of the total record of economic losses in 2011 correspond to earthquakes accidents.

Earthquake engineering focuses on the protection of society and man-made structures from seismic events by limiting the damage to acceptable socio-economic levels. Earthquake engineers try to understand why some of the existing structures collapse when an earthquake occurs and thus, to improve the more recent dimensioning techniques. In this framework, and due to the lately exponentially growing world of

computing, numerical simulation stands as a good choice for predicting the response of structures under seismic loading.

Industrial context: challenges and motivations

Large and heavy structures such as power plants or dams have always been designed and constructed to withstand full seismic loading. However, the definition of seismic loading is not absolute and it actually evolves with technology. Indeed, the improvement of data acquisition techniques has recently shown that last seismic levels recorded in France are greater than those used for the initial dimensioning of those structures. As a result, Électricité de France (EDF) –the main electricity operator in France and the principal funder of this research work– has to respond to this new scenario by providing new seismic risk assessments of the entire power production sites.

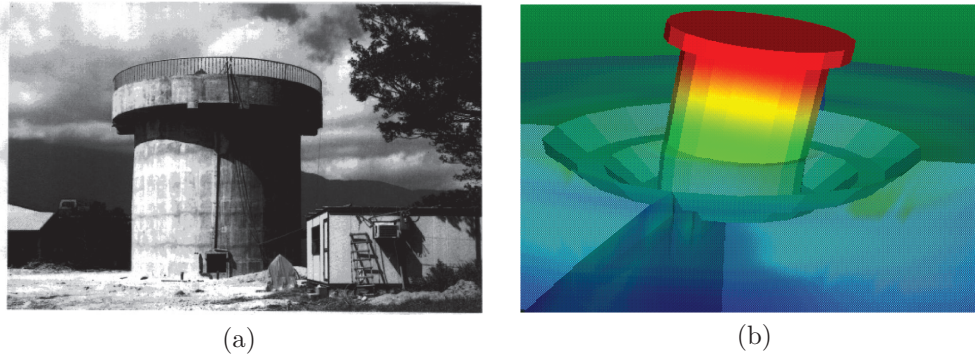


Figure 1: (a) Model at 1/3 scale of a reactor at Hualien, Taiwan. (b) Dynamic response of the corresponding numerical model.

This industrial need is quite interesting since the problem at hand slightly differs from the classical engineering way of thinking. Indeed, the role of engineers generally consists in doing calculations for the correct dimensioning of the buildings during their conception, usually using safety factors. However, in our case, the structures to assess were built some decades ago and therefore, the role of the engineer here is mainly focused on the evaluation of their resistance in order to satisfy the current seismic risk regulation. Thus the most important thing is not much to obtain fast and reliable calculations but to master the dimensioning margins and the possibly additional reinforcing costs. The best way to update seismic safety factors is to perform more accurate simulations that account for new physical phenomena at stake. These simulations refer mainly to dynamic SSI effects but not only, since numerical models can also be enriched by considering soil nonlinear behaviour, uplift of foundation, deformable slab, seismic spatial variability, inclined incidence waves, etc.

Within this context, the Research and Development (R&D) division of EDF is interested in developing new numerical tools that model more accurately SSI problems (Fig. 1). This interest is not new, and other Ph.D. thesis, such as Cottureau [35] or Obrembski *et al.* [107], have also been done under their support and collaboration. Relying on a BE-FE coupling strategy, most of their work contributed to improve

different functionalities of *Code_Aster*¹ (an open-source FE code developed within EDF R&D) and MISS3D² (a frequency-based BE code developed at the École Centrale Paris by Prof. D. Clouteau). This BE-FE coupling approach was historically adopted by EDF to enhance the advantages of the FE and BE methods and to reduce at the same time the main drawbacks of both. In fact, they are somehow two complementary spatial discretization methods: while the BE method is generally used to solve some kind of linear problems, the FE method seems to be well-adapted to problems showing complex nonlinear behaviour and geometry. Additionally, and in contrast to the FE method which is restricted to the discretization of bounded domains, the BE method is also able to deal with unbounded domains for mainly two reasons. First, it takes implicitly into account the radiation condition at infinity of the unbounded media; second, it is based on the discretization of only the boundaries, not the whole domain as in FE-based methods. It obviously reduces by one the dimension of the domain of discretization, but to the detriment of the resulting algebraic system which is characterized by fully-populated and possibly non-symmetric matrices. For further information on BE methods, the reader can refer to Bonnet [18] and Domínguez [44]. The work of Zienkiewicz *et al.* [159] is recommended for further reading on FE methods.

Keeping on this BE-FE coupling strategy and because of the industrial need standing behind, both codes (*Code_Aster* and MISS3D) have also been used in the framework of this Ph.D. thesis and our main original contributions have actually been implemented in *Code_Aster*.

Methodology and original contributions

The present work addresses a computational methodology –baptized here as the Hybrid Laplace-Time Domain Approach (HLTA)– which essentially solves a dynamic problem coupling time and Laplace domain discretizations. This approach is based on a domain decomposition technique where one subdomain (i.e. the *unbounded linear* soil) is solved in the Laplace domain –or *complex frequency domain*– using the BE method implemented in MISS3D. The other subdomain (i.e. the bounded nonlinear superstructure or *generalized structure*) is solved at each time step with a FE method in *Code_Aster*. This methodology, which applies for deterministic and probabilistic analysis, allows to account for three-dimensional nonlinear dynamic soil-structure interaction in seismic calculations by using an efficient BE-FE coupling approach.

The expression *generalized superstructure* refers not only to the structure and its foundations but also to the domain of soil surrounding the structure that possibly exhibits nonlinear behaviour (see Fig. 2). This domain is bounded and hence modelled using a FE method, which accounts for nonlinear material laws in a straightforward way. It is important to notice, however, that in the vicinity of the SSI-interface –which basically corresponds to the BE-FE interface– an elastic behaviour must be assumed to avoid spurious reflections back inside the FE domain. Otherwise, the SSI-interface must be moved away into a linear region of soil. Hereafter, it would be assumed that the word *structure* also includes the irregular soil region and thus the expression *generalized* is omitted.

¹<http://www.code-aster.org>

²http://www.mssmat.ecp.fr/cms/lang/en/mssmat/moyens/moyens_techniques_logiciels/miss

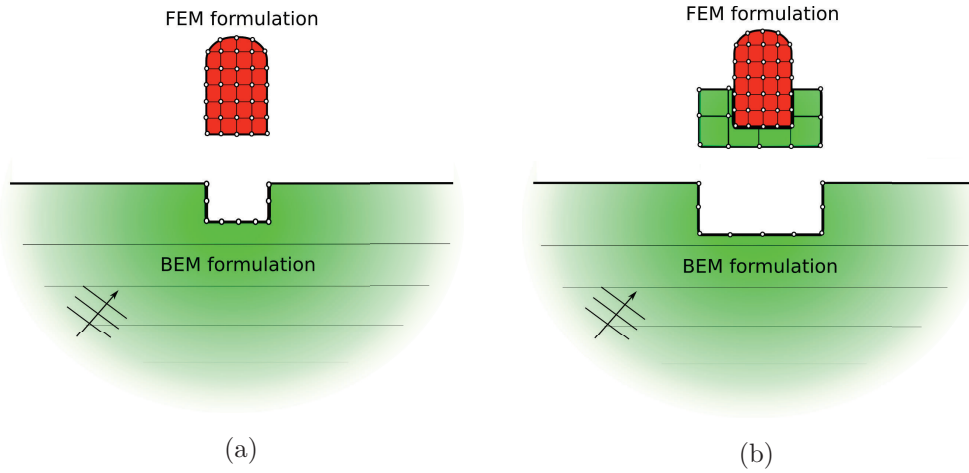


Figure 2: Simplified model of a SSI system where the superstructure is modelled using a FE method and the layered soil, using a BE method. (a) The *superstructure* refers at least to the structure and its foundations since (b) may also include a surrounding part of soil.

The remaining soil, which can have a horizontally stratified profile, is modelled using a soil impedance matrix as shown in Fig. 3a. This matrix, computed in the Laplace domain using MISS3D, can also be expressed on a modal basis constituted by dynamic interface modes. The equivalent soil impedance matrix in the time domain is obtained by means of the HLTA. This time impedance matrix allows the evaluation of the SSI-interaction forces that appear at the *SSI-interface*, evaluation that is not trivial, since it involves the computation of a time integral convolution. If an incident field is also considered, MISS3D allows for the calculation of the corresponding equivalent seismic force applied at the *SSI-interface*.

Once the equivalent seismic force and the time impedance matrix are computed, the effects of seismic waves and the unbounded soil can be taken into account. Therefore, the dynamic response of the structural domain accounting for SSI can be solved in *Code_Aster* as outlined in Fig. 3b.

The HLTA has been implemented in *Code_Aster* allowing EDF, for the first time using a substructuring approach, to account for full nonlinear behaviour in industrial three-dimensional soil-structure interaction calculations under deterministic or stochastic seismic loading.

Organisation of the text

This PhD dissertation has been mainly divided into four parts organized as follows:

Chapter 1 presents the main difficulties of the numerical modelling of DSSI problems as well as a general literature review on the numerical approaches to deal with the spatial domain discretization. The governing equations of both the soil and the structure are formulated. Once the variational form of the problem within a domain decomposition approach introduced, the soil impedance operator coming

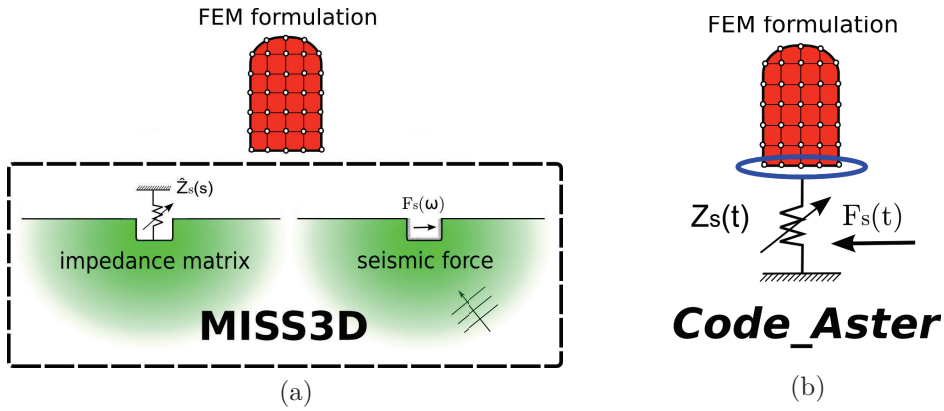


Figure 3: Simplified scheme to represent (a) the effects of the linear unbounded soil and (b) the final global resolution of the SSI problem.

from an integral boundary formulation is briefly defined. Some of its properties are also recalled. Finally, the problem is spatially discretized and the BE-FE coupling equations are presented in the linear (Laplace domain) and nonlinear (time domain) frameworks.

Chapter 2 constitutes the core of this dissertation since it addresses the Hybrid Laplace-Time domain Approach. It deals with the time domain discretization of the SSI problem. The HLTA is thus presented first from a general point of view and afterwards, from the perspective of SSI problems. The extension to modal basis is also provided. In order to give some other insights, the HLTA formulation, which is developed in terms of both stiffness and flexibility, is compared to a Hybrid Frequency-Time Domain approach. The last section analyzes the BE-FE time integration schemes couplings within the HLTA.

Chapter 3 is related to the validation of the HLTA and its implementation. To that end, the SSI problem is numerically discretized with respect to space and time using MISS3D and *Code_Aster*. In this context, time impedance evolutions are analyzed as well as particular numerical considerations that have to be taken into account. Afterwards, different numerical applications involving surface and embedded foundations, modal reduction techniques, linear and nonlinear calculations and different soil profiles are considered.

Chapter 4 is focused on a seismic assessment of a semi-industrial numerical model. Different modellings are tested involving full FE discretizations and hybrid substructuring approaches in order to carry out linear and a nonlinear analysis. Nonlinearities are confined in the structure and thus, the whole domain of soil remains linear elastic.

And finally, after some conclusions and perspectives for further research, the dissertation is complemented with **Appendix A** and **B** which recall respectively some useful mathematical definitions and some concepts commonly used in earthquake engineering.

Chapter 1

An overview on dynamic soil-structure interaction

“The sources must be sources, not sinks of energy. The energy which is radiated from the sources must scatter to infinity; no energy may be radiated from infinity into the prescribed singularities of the field.”

ARNOLD SOMMERFELD, 1949

1.1 Literature review

The growing complexity of SSI systems prevents the use of analytical approaches to carry out engineering analysis. Spatial discretization techniques, such as the FE method or the Finite Difference (FD) method, must be adopted. In particular, the FE method is a good choice for the discretization of geometrically complex domains and boundaries and it is thus the approach considered hereafter. However, it allows only the discretization of bounded domains whereas the modelling of infinite domains rises as one of its main challenges. Since an SSI analysis involves the effects of an unbounded domain –the soil– the standard FE method is not sufficient and engineers must proceed in a different way so that the Sommerfeld’s condition [133] is met. This condition, which is also known as radiation condition, ensures the absence of energy flow going back from the infinity to the free-surface of the soil and it is of great importance for a rigorous representation of the infinite or semi-infinite medium.

Therefore, if a FE method is to be used at least over a part of the whole SSI system (for instance, the part involving inhomogeneities and nonlinearities), a domain decomposition technique must be used and two subdomains should be defined. To this aim, an artificial boundary that bounds one of the subdomains has to be introduced, leading thus to one bounded subdomain (the structure) and one unbounded subdomain (the soil). The artificial boundary, which would be referred to the following as *SSI interface*, allows then the use of a FE technique over the structure. Recall that the term *structure* accounts for the superstructure domain, which certainly includes the building but which may also contain part of the soil surrounding it. The soil extending to infinity is generally modelled by means of a so-called Artificial Boundary

Condition (ABC) applied on the artificial boundary. The problem simply reads:

$$\left\{ \begin{array}{ll} \nabla \cdot \boldsymbol{\sigma}_b(\mathbf{x}, t) + \mathbf{f}_b(\mathbf{x}, t) - \rho \partial_{tt} \mathbf{u}_b(\mathbf{x}, t) = \mathbf{0} & \text{in the bounded structure} \\ \text{Dirichlet BC} & \text{on } \Gamma_D \\ \text{Neumann BC} & \text{on } \Gamma_N \\ \text{Artificial BC} & \text{on } \Gamma_{ABC} \end{array} \right.$$

where $\nabla \cdot \boldsymbol{\sigma}_b(\mathbf{x}, t)$ denotes the divergence of the stress tensor $\boldsymbol{\sigma}_b(\mathbf{x}, t)$ and $\mathbf{f}_b(\mathbf{x}, t)$, ρ and $\mathbf{u}_b(\mathbf{x}, t)$ stand respectively for the body prescribed forces, the density and the displacement field.

In order to model the ABC's and thus, the unbounded domain, literature proposes several methods. To help the reader, it may be useful to make a general classification of them. For instance, according to Zhenpeng [157], all these methods can be easily gathered into two major groups: those based on the *substructure method* and those based on the *direct method*. The classification depends simply on the location of the artificial boundary with respect of the SSI interface. If the latter coincides with the artificial boundary, a substructuring approach would be adopted; otherwise, if the artificial boundary encloses not only the superstructure subdomain but also a part of the unbounded soil, a direct method would be considered. ABC's are known, depending on the approach, under many other names such as absorbing, transmitting or nonreflecting boundary conditions, force-motion relationship, etc.

1.1.1 The direct method

In this section the structural domain, which is bounded, is assumed to be modelled with a FE method. The unbounded soil is modelled either with FE *plus* nonreflecting boundary conditions, or with Infinite Elements (IE).

Nonreflecting boundary conditions

The aim of Nonreflecting Boundary Conditions (NRBC) is to absorb outgoing waves or to minimize reflections in order to account for unbounded domains, i.e. the soil. In this framework, the simplest modelling comes from the works of Lysmer and Kuhlemeyer [90] and involves the use of viscous boundaries which behave as simple dashpots. Alternatively, an approach relying on paraxial approximations was presented by Clayton and Engquist [29] for elastic wave propagation problems. Since then, several versions of the latter approach, including high-order boundaries, have been proposed [64, 118] and used in many different applications. These techniques can be combined with a more intuitive approach [78] that is based on layers of damping materials that attenuate the displacement field near the artificial boundary.

Nevertheless, all these techniques do not absorb incident waves perfectly. In fact, spurious reflections are always generated at the edges of the domain yielding to inaccurate results. Perfect NRBC are called Perfectly Matched Layers (PML). Berenger [13] pioneered the use of an artificial material that rapidly attenuate –electromagnetic– waves avoiding thus reflections regardless of the frequency and the incidence angle. Similar formulations can be found in literature for the case of elastodynamic mediums [25, 34]. Particularly interesting are the PML's formulated in the time domain [10] since they could be coupled to a nonlinear analysis.

As mentioned before, NRBC are commonly combined with a FE modelling of the unbounded soil, but they can also be used with other type of modellings such as the Thin Layer Method (see Fig. 1.1b and 1.2a).

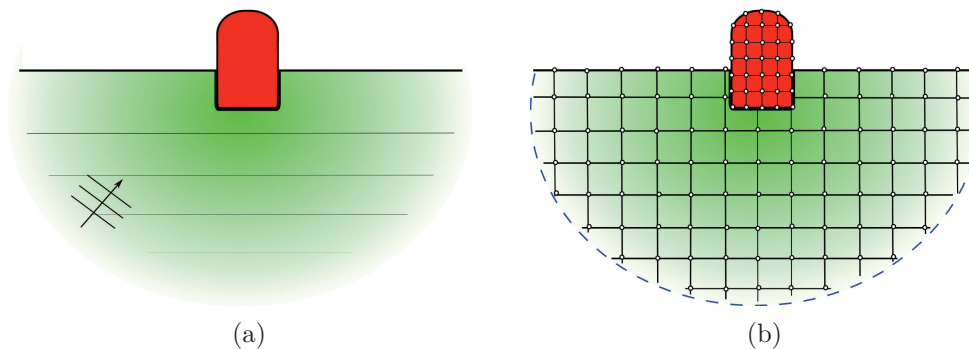


Figure 1.1: (a) Simplified model of a SSI-system. (b) The whole SSI system, bounded with an artificial NRBC boundary (dashed lines) is discretized using FE.

Infinite elements

As mentioned before, FE method allows the discretization of finite domains. On the contrary, since no radiation conditions can be directly satisfied on the boundaries of the domain, it is not well-adapted to exterior wave propagation problems. To overcome this drawback, the FE method can be combined to the so-called Infinite Element (IE) method. The latter is a new concept developed in the 70's by Ungless [142] that accounts for radiation conditions at infinity. The idea is to combine the standard shape functions of the classical FE framework with some oscillatory decay functions. These functions can exhibit different asymptotic behaviours such as reciprocal ($\propto \frac{1}{r^n}$) or exponential ($\propto e^{-nr}$) in the radial direction r . Several authors, such as Bettess [15] and Astley [2], have worked on different decay functions and on special integration schemes (Gauss-Laguerre, Gauss-Legendre...) in order to correctly account for the different propagating and, even evanescent, modes (P-waves, S-waves, Rayleigh waves...) arising in three dimensional wave propagation problems. Other research lines were based on a different type of IE, the *mapped IE* [16], which allowed to apply the IE method to exterior domains bounded by cylindrical, spherical or ellipsoidal artificial boundaries [22, 158]. In fact, the IE of Zienkiewicz was, at least from the point of view of Bettess [16], the best IE choice "because of its simplicity and theoretical advantages". However, some parameters, such as the phase velocity or the decay function behaviour, have to be priorly estimated by means of empirical results or analytical solutions [96, 132], and that is one of the main drawbacks of the approach.

Regarding to dynamic SSI problems, some references exist in literature that have used IE's to model a homogeneous half-space or even a layered infinite media. Although most of them worked under axisymmetric assumptions (refer for instance to Chuhan and Chongbin [28], Medina and Taylor [95], Rajapakse and Karasudhi [116], Yang and Yun [153]), Seo *et al.* [130] and [122], among others, developed an IE formulation based on a Cartesian coordinate system. It is particularly interesting to

notice that these referred SSI analyses have been done in the frequency domain, the reason is mainly because the IE method actually has some difficulties to cope with transient calculations [132]. In fact, Astley and Hamilton [3] studied the stability of IE schemes in transient acoustics and concluded that IE mesh geometries giving non-zero mass matrices do not yield stable solutions, and thus geometry has to be properly worked out. Nevertheless, nonlinear SSI calculations have also been carried out [26, 27] by means of a time-frequency coupling approach: the structure and the near field behaving both nonlinear are solved in the time domain with a FE method; the –linear– far-field is modelled by an axisymmetric IE method, formulated in the frequency domain. The latter –substructuring– approach makes easier the evaluation of the time integral convolutions arising in the FE-IE interface since the IE formulation is also based in stiffness, damping and mass matrices.

1.1.2 The substructure method

If the SSI problem is solved in the superstructure domain bounded by the artificial boundary, a discretization technique based on FE can be used. The ABC, which complements the set of BC applied on the superstructure domain, is usually expressed by a force-displacement relationship defined on the SSI-interface by means of the so-called impedance operator. This motion relationship can be written in both frequency and time domains.

Literature proposes several approaches to obtain this impedance operator and they are briefly discussed in the following paragraphs. It is important to have in mind that these approaches will be necessarily combined to a FE method, which is the technique adopted for the discretization of the superstructure domain.

Procedures based on a BE method

The Boundary Element (BE) method was originally proposed by [119] in 1967 within the field of electrostatics. This technique is based on the discretization of only the domain boundaries and thus, it can be considered as a mesh reduction approach. It is generally restricted to linear problems although some authors have applied it on some kind of nonlinearities [18]. This discretization technique involves singular integrations and thus a lot of research has been done on regularization techniques or convergence analysis [18, 44]. Despite these numerical problems, the BE method is very well-adapted to deal with unbounded domains, making this feature as one of the main advantages of the method. Therefore, the coupling of a BE-FE method to account for dynamic soil-structure interaction is an interesting choice that many authors have explored. Among them, it can be mentioned for instance the work of von Estorff and Kausel [143], which presents a time domain formulation of the BE method. Besides, there is the work of Belytschko and Lu [12] who proposed, some years later, a variational formulation based on the full-space transient fundamental solutions. Nevertheless, the use of half-space Green's functions had been also used by Triantafyllidis [141]. Despite the vast number of articles that have focused on transient BE-FE formulations [46, 48, 50], mainly because of the interest to solve nonlinear problems [49], the BE-FE coupling can obviously be formulated also in the frequency domain. Indeed, this is particularly useful when layered medium should be accounted for [109, 137].

The main drawback of the BE method is that it has to deal with fully populated (and possibly non-symmetric) matrices. The latter, for large models yields to very important computational costs. In order to improve this feature, current research exists to reduce the number of operations through Fast Multipole formulations [23].

Scaled Boundary Finite-Element Method

The Scaled Boundary Finite-Element Method (SBFEM), also known as the Consistent Infinitesimal Finite-Element Cell Method (CIFECM), is an effective alternative to the BE method for the modelling of infinite or semi-infinite domains having heterogeneous material properties that was proposed by Wolf and Song [134, 135, 136, 150, 151]. In fact, this approach combines the advantages of both the FE and the BE methods: while only the boundaries have to be discretized, no fundamental solution is required. The limitation of the SBFEM comes from the geometric requirements that have to be satisfied for the similarity relationships but this problem can be overcome by coupling the SBFEM to other approaches such as the FE method [21, 58, 152].

This approach is inspired of a technique based on similarity that was first proposed by Dasgupta [41]. In order to understand the idea, the example of a 2D homogeneous half-space proposed in [157] is also followed here (see Fig. 1.2b). Suppose that the similarity centre O , which is the point of reference, is placed on the free-surface of a bounded region of soil and coincides with the origin of x and y axis. If all coordinates of the original SSI-interface are multiplied by a positive constant, the corresponding part of the boundary can be scaled resulting in a new SSI-interface and thus a characteristic distance r can be defined for the former and latter interface. The dynamic soil impedance modelling the unbounded domain of soil can be thus determined formulating some similarity relationships between the dynamic impedances of each SSI-interface and between the corresponding FE nodes of the motion equation.

Literature proposes different versions of the SBFEM to deal with the representation of homogeneous half-spaces and full-spaces in 2D or 3D problems [79, 82]. Recently, the SBFEM has also been applied to 3D-layered systems allowing dynamic SSI analysis in complex models [17]. However, the latter approach appears to be computationally expensive and further research is currently ongoing.

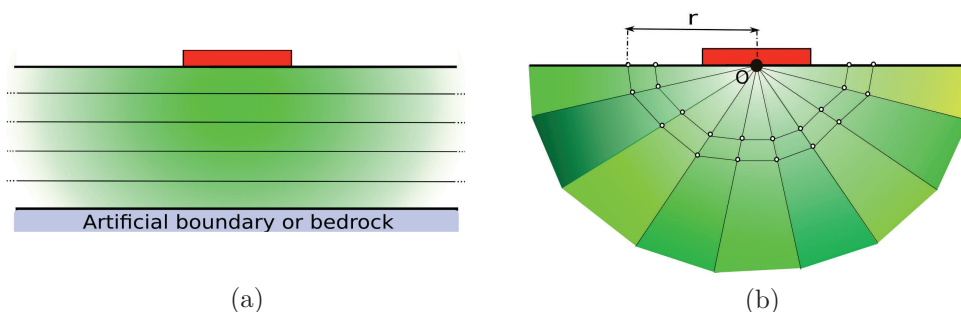


Figure 1.2: (a) Modelling using the Thin Layer Method. (b) Modelling using the Scaled Boundary Finite Element Method (only the boundary is discretized as in the BE method).

The Thin Layer Method

The Thin Layer Method (TLM), which was originally applied by Lysmer [89] in 1970 to study seismic Rayleigh waves propagation, is based on the partial discretization of the wave equation, mainly in the direction of soil layering (usually the vertical one). This allows the use of a FE solution for that coordinate while other different approaches that account for radiation conditions at infinity, such as closed-form solutions or ABC's, can be used for the remaining coordinate directions (see Fig. 1.2a). Hence the main advantage of the TLM: no additional computational effort is needed for a layered soil respect to the case of a homogeneous soil.

Since 1970, the TLM has been extended to 2D-problems (SV-P and SH waves) in the frequency or time domain and applied for the formulation of absorbing layers and perfectly matched layers [8, 69, 91]. It has also been used to study the dynamic response of circular foundations and earth dams [20, 139].

However, perhaps the most important application of the TLM came for the calculation of the Green's functions for point loads acting on or within layered domains. In particular, Kausel and Peek [70] proposed the framework to deal with loads showing arbitrary spatial and temporal distributions. Thus, the Green's functions of a layered medium that are now implemented in some well-known programs, such as SASSI, were presented by Kausel and Roesset [71] allowing thus the computation of the TLM soil stiffness (or impedance) matrix. These Green's functions were later adapted to the case of layered media over elastic half-spaces using paraxial boundaries [72]. Other approaches showing similar aspects to the TLM apply for the computation of the soil stiffness matrix, i.e. Haskell-Thomson transfer matrix approach [61, 140] or the stiffness matrices technique of Seale and Kausel [128]. Nevertheless, the advantage of the TLM respect to others is that transcendental functions can be linearized within layers due to the assumption of sufficiently thin layers and therefore, they are easier to be computed.

More recently, the works of Geller and Ohminato [57] and Geller and Hatori [56] presented the so-called Direct Solution Method (DSM) which is a modification of TLM to handle laterally and vertically heterogeneous domains and which has also been used for the computation of 3D synthetic seismograms [38].

Lumped-parameter models

In order to account for soil-structure interaction, other approaches are based on lumped-parameter models, such as the pioneering spring method [47] which relied on a set of springs, one for each degree-of-freedom, attached at the base of the structure (even for the case of embedded foundations [73]). The spring method has been afterwards enriched with dashpots and masses [9, 149] yielding to more accurate models. However, this approach presents some difficulties when an incident seismic field is considered [43].

Another similar approach, called the macroelement method, arises by the hand of Nova and Montrasio [106] in 1991. A macroelement is, from a FE point of view, an input-output system defined at the foundation centre. If displacements are given as input, forces are obtained as a result. Thus, this method allows to account for nonlinear constitutive laws in static and dynamic analysis [24, 59].

1.2 Dynamic SSI problem in earthquake engineering

First of all, the geometry of the SSI system must be defined (see Fig. 1.3). Let Ω_b be a bounded subset of \mathbb{R}^3 with smooth boundary $\Gamma \cup \Gamma_{bo}$ where Γ represents the interface between Ω_b and the unbounded subdomain Ω_s . And let S_0 be the free-surface of the layered half-spaced Ω_s .

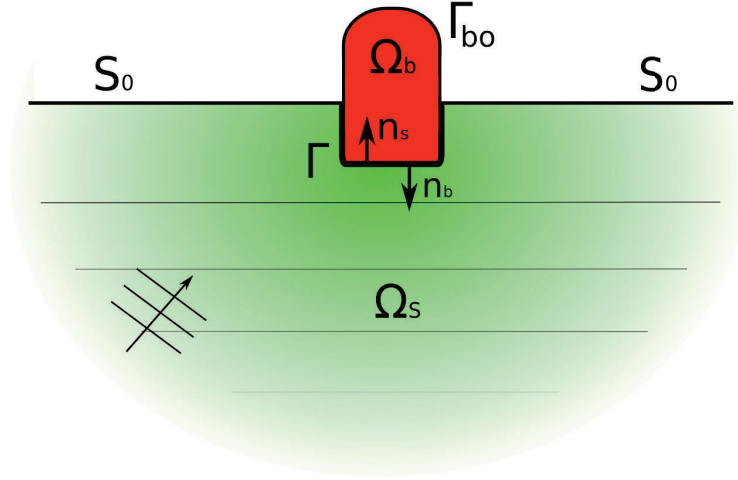


Figure 1.3: Subdomain Ω_b (modelled in FE) may include the nonlinear structure and also the nonlinear soil. It is separated from the linear unbounded soil Ω_s by the interface Γ (modelled in BE).

In order to set the unknown fields of this problem, let the permanent displacement fields on Ω_s and Ω_b due to static loads (e.g. the weight) be first defined. They are respectively denoted by \mathbf{u}_{so} and \mathbf{u}_{bo} and assumed to be known parameters. The dynamic perturbations of these fields due to dynamic loadings are denoted by $\mathbf{u}_b(\mathbf{x}, t)$ and $\mathbf{u}_s(\mathbf{x}, t)$. Latter displacement fields are assumed to be small enough to allow a linear approximation of the constitutive and equilibrium equations in the vicinity of the static state $(\mathbf{u}_{so}, \mathbf{u}_{bo})$. Therefore, the dynamic perturbations of the stress tensors denoted by $\boldsymbol{\sigma}_s(\mathbf{u}_s)$ and $\boldsymbol{\sigma}_b(\mathbf{u}_b)$ can also be expressed respectively as linear functions of the dynamic fluctuation of the strain tensors $\boldsymbol{\epsilon}_s(\mathbf{u}_s)$ and $\boldsymbol{\epsilon}_b(\mathbf{u}_b)$, for $\alpha \in \{s, b\}$ the classical linear elastic law reads:

$$\boldsymbol{\sigma}_\alpha(\mathbf{u}_\alpha) = \mathbf{C}_\alpha : \boldsymbol{\epsilon}_\alpha(\mathbf{u}_\alpha) \quad (1.1)$$

with \mathbf{C}_α being a four-rank tensor and $:$ denoting the double contraction product between two tensors of arbitrary tensor order. In particular, for an isotropic and homogeneous material, its components $C_{\alpha,ijkl}$ can be written using index notation as:

$$C_{\alpha,ijkl} = \lambda_\alpha \delta_{ij} \delta_{kl} + \mu_\alpha (\delta_{ik} \delta_{jl} + \delta_{il} \delta_{jk}) \quad (1.2)$$

where δ_{ij} denotes the Kronecker Delta and λ_α and μ_α the Lamé's coefficients. It is important to notice that these Lamé constants may have space dependent values.

They can be written in terms of the Young's modulus E_α and the Poisson's ratio ν_α as follows:

$$\lambda_\alpha = \frac{E_\alpha \nu_\alpha}{(1 + \nu_\alpha)(1 - 2\nu_\alpha)} \quad (1.3)$$

$$\mu_\alpha = \frac{E_\alpha}{2(1 + \nu_\alpha)} \quad (1.4)$$

Using Eq. (1.1) and (1.2), the constitutive law reads:

$$\boldsymbol{\sigma}_\alpha(\mathbf{u}_\alpha) = \lambda_\alpha (\nabla \cdot \mathbf{u}_\alpha) \mathbf{I}_d + 2\mu_\alpha \boldsymbol{\epsilon}_\alpha(\mathbf{u}_\alpha) \quad (1.5)$$

$$\boldsymbol{\epsilon}_\alpha = \frac{1}{2} (\nabla \mathbf{u}_\alpha + \nabla^T \mathbf{u}_\alpha) \quad (1.6)$$

where $(\cdot)^T$ denotes the transposed and \mathbf{I}_d the identity tensor.

The traction fields $\mathbf{t}_{\mathbf{n}_\alpha}(\mathbf{u}_\alpha)$ applied on a given interface and with unit outward normal vector \mathbf{n}_α can be obtained according to Cauchy's stress principle as:

$$\mathbf{t}_{\mathbf{n}_\alpha}(\mathbf{u}_\alpha) = \boldsymbol{\sigma}_\alpha(\mathbf{u}_\alpha) \cdot \mathbf{n}_\alpha \quad (1.7)$$

Damping models for the soil domain

There are mainly two different ways to account for dissipation in an isotropic and homogeneous soil: either by viscous damping or by hysteretic damping. The former can be introduced by means of the following visco-elastic constitutive equation:

$$\boldsymbol{\sigma}_s(\mathbf{u}_s) = (1 + \partial_t \eta_s) (\lambda_s \nabla \cdot \mathbf{u}_s + 2\mu_s \boldsymbol{\epsilon}_s(\mathbf{u}_s)) \quad (1.8)$$

where η_s corresponds to the viscous damping coefficient. When this damping model is considered no energy is dissipated at very low frequencies since the amount of energy dissipated is proportional to the frequency. Besides, seismic waves reaching the free-surface of the soil usually concentrate their energy in a low range of frequencies. Since experiments have shown the present of constant dissipation over this frequency range [129], a viscous damping model is not appropriate for earthquake engineering systems.

To overcome this problem, hysteretic damping can be considered. In this case, stress-strain hysteretic cycles appear even for zero frequency and thus, this damping mechanism always introduces dissipation. It is usually modelled by casting Lamé constants to complex-valued parameters:

$$\lambda_s^* = \lambda_s (1 + i\beta_s(\omega)) \quad (1.9)$$

$$\mu_s^* = \mu_s (1 + i\beta_s(\omega)) \quad (1.10)$$

where $\beta_s(\omega)$ denotes the hysteretic damping coefficient. However, due to the frequency-independent behaviour of the imaginary part of Lamé constants over the frequency range of interest, the equivalent material laws in the time domain lead to non-causal expressions, yielding thus to non-physically models. Hysteretic damping must be employed therefore only in the frequency domain. For further details on damping models the reader can refer to Semblat and Pecker [129].

1.2.1 Seismic incident field

The seismic incident displacement field is classically [63] accounted for by a displacement field defined in Ω_s , denoted here by \mathbf{u}^{inc} , that satisfies:

$$\begin{cases} -\nabla \cdot \boldsymbol{\sigma}_s(\mathbf{u}^{inc}) + \rho_s \partial_{tt} \mathbf{u}^{inc} = \mathbf{0} & \text{in } \Omega_s \\ \mathbf{t}_{\mathbf{n}_s}(\mathbf{u}^{inc}) = \mathbf{0} & \text{on } S_0 \end{cases} \quad (1.11)$$

with \mathbf{n}_s , the outward unit normal defined in Fig. 1.3. In particular, the seismic source is assumed to be a far-field source such that \mathbf{u}^{inc} can be approximated by uniform plane waves [30].

The trace of the incident displacement field on Γ will play hereafter the role of an external applied load and therefore, $\mathbf{t}^{inc} = \mathbf{t}_{\mathbf{n}_s}(\mathbf{u}^{inc})$ will rather be considered on Γ interface. Since the incident displacement field is given everywhere within Ω_s , \mathbf{t}^{inc} can be directly evaluated on Γ .

1.2.2 Linear governing equations

In order to state the equations governing the soil, a new auxiliary displacement field \mathbf{u}_{sc} —the diffracted or scattered field—is introduced as the difference between the total displacement field \mathbf{u}_s and the incident field [30, 63]:

$$\mathbf{u}_{sc} = \mathbf{u}_s - \mathbf{u}^{inc} \quad \text{in } \Omega_s. \quad (1.12)$$

The total scattered field can be decomposed as follows:

$$\mathbf{u}_{sc} = \mathbf{u}_{rad}[\boldsymbol{\phi}] + \mathbf{u}_{loc} \quad (1.13)$$

where \mathbf{u}_{loc} corresponds to the local scattered field generated by the incident field \mathbf{u}^{inc} and $\mathbf{u}_{rad}[\boldsymbol{\phi}]$, to the displacement field radiated by the structure into the soil when a displacement field $\boldsymbol{\phi}$ is prescribed on Γ . Remark that \mathbf{u}_{loc} can be interpreted as the radiated (or scattered) displacement field due to the incident displacement field, i.e. $\mathbf{u}_{loc} = \mathbf{u}_{rad}[-\mathbf{u}^{inc}]$ or still, $\mathbf{u}_{sc} = \mathbf{u}_{rad}[\boldsymbol{\phi} - \mathbf{u}^{inc}]$.

Let the trace of the structural displacement field \mathbf{u}_b be prescribed on Γ and hence, let the previously introduced fields $\mathbf{u}_{rad}[\mathbf{u}_b|_\Gamma]$ and \mathbf{u}_{loc} be considered. Together with Sommerfeld's radiation condition at infinity, these fields satisfy respectively:

$$\begin{cases} -\nabla \cdot \boldsymbol{\sigma}_s(\mathbf{u}_{rad}) + \rho_s \partial_{tt} \mathbf{u}_{rad} = \mathbf{0} & \text{in } \Omega_s \\ \mathbf{t}_{\mathbf{n}_s}(\mathbf{u}_{rad}) = \mathbf{0} & \text{on } S_0 \\ \mathbf{u}_{rad} = \mathbf{u}_b & \text{on } \Gamma \end{cases} \quad (1.14)$$

and

$$\begin{cases} -\nabla \cdot \boldsymbol{\sigma}_s(\mathbf{u}_{loc}) + \rho_s \partial_{tt} \mathbf{u}_{loc} = \mathbf{0} & \text{in } \Omega_s \\ \mathbf{t}_{\mathbf{n}_s}(\mathbf{u}_{loc}) = \mathbf{0} & \text{on } S_0 \\ \mathbf{u}_{loc} = -\mathbf{u}^{inc} & \text{on } \Gamma \end{cases} \quad (1.15)$$

where, for simplicity, free-surface boundary conditions have been assumed on S_0 and where notation $\mathbf{u}_{rad}[\mathbf{u}_b|_\Gamma]$ has been omitted for conciseness purposes only. In turn,

displacement field \mathbf{u}_b , which refers to the structural domain Ω_b , verifies:

$$\begin{cases} -\nabla \cdot \boldsymbol{\sigma}_b(\mathbf{u}_b) + \rho_b \partial_{tt} \mathbf{u}_b = \mathbf{f}_b & \text{in } \Omega_b \\ \mathbf{t}_{\mathbf{n}_b}(\mathbf{u}_b) = \mathbf{t}_{b_o} & \text{on } \Gamma_{b_o} \\ \mathbf{t}_{\mathbf{n}_b}(\mathbf{u}_b) + \mathbf{t}_{\mathbf{n}_s}(\mathbf{u}_{rad}) + \mathbf{t}_{\mathbf{n}_s}(\mathbf{u}_{loc}) + \mathbf{t}^{inc} = \mathbf{0} & \text{on } \Gamma \\ \mathbf{u}_b - \mathbf{u}_{rad} - \mathbf{u}_{loc} - \mathbf{u}^{inc} = \mathbf{0} & \text{on } \Gamma \end{cases} \quad (1.16)$$

with \mathbf{f}_b standing for the body forces and \mathbf{t}_{b_o} , for the prescribed tractions over the exterior boundary Γ_{b_o} of Ω_b . It should be noticed that compatibility of the total soil displacement field \mathbf{u}_s and the structure displacement field \mathbf{u}_b is directly ensured by the kinematic conditions considered on Γ .

Moreover, all these fields are assumed to be causal with homogeneous initial conditions:

$$\begin{cases} \mathbf{u}_{rad}(\mathbf{x}, 0) = \partial_t \mathbf{u}_{rad}(\mathbf{x}, 0) = \mathbf{0} & \forall \mathbf{x} \in \Omega_s \\ \mathbf{u}_{loc}(\mathbf{x}, 0) = \partial_t \mathbf{u}_{loc}(\mathbf{x}, 0) = \mathbf{0} & \forall \mathbf{x} \in \Omega_s \\ \mathbf{u}_b(\mathbf{x}, 0) = \partial_t \mathbf{u}_b(\mathbf{x}, 0) = \mathbf{0} & \forall \mathbf{x} \in \Omega_b. \end{cases} \quad (1.17)$$

Provided that these equations are linear, i.e. for the (visco)-elastodynamic problem, the –unilateral– Laplace transform can be applied on the set of equations. In that case, using initial conditions of (1.17) the SSI system of equations becomes:

$$\begin{cases} -\nabla \cdot \hat{\boldsymbol{\sigma}}_b(\hat{\mathbf{u}}_b) + \rho_b s^2 \hat{\mathbf{u}}_b = \hat{\mathbf{f}}_b & \text{in } \Omega_b \\ \hat{\mathbf{t}}_{\mathbf{n}_b}(\hat{\mathbf{u}}_b) = \hat{\mathbf{t}}_{b_o} & \text{on } \Gamma_{b_o} \\ \hat{\mathbf{t}}_{\mathbf{n}_b}(\hat{\mathbf{u}}_b) + \hat{\mathbf{t}}_{\mathbf{n}_s}(\hat{\mathbf{u}}_{rad}) + \hat{\mathbf{t}}_{\mathbf{n}_s}(\hat{\mathbf{u}}_{loc}) + \hat{\mathbf{t}}^{inc} = \mathbf{0} & \text{on } \Gamma \\ \hat{\mathbf{u}}_b - \hat{\mathbf{u}}_{rad} - \hat{\mathbf{u}}_{loc} - \hat{\mathbf{u}}^{inc} = \mathbf{0} & \text{on } \Gamma \end{cases} \quad (1.18)$$

$$\begin{cases} -\nabla \cdot \hat{\boldsymbol{\sigma}}_s(\hat{\mathbf{u}}_{rad}) + \rho_s s^2 \hat{\mathbf{u}}_{rad} = \mathbf{0} & \text{in } \Omega_s \\ \hat{\mathbf{t}}_{\mathbf{n}_s}(\hat{\mathbf{u}}_{rad}) = \mathbf{0} & \text{on } S_0 \\ \hat{\mathbf{u}}_{rad} = \hat{\mathbf{u}}_b & \text{on } \Gamma \end{cases} \quad (1.19)$$

$$\begin{cases} -\nabla \cdot \hat{\boldsymbol{\sigma}}_s(\hat{\mathbf{u}}_{loc}) + \rho_s s^2 \hat{\mathbf{u}}_{loc} = \mathbf{0} & \text{in } \Omega_s \\ \hat{\mathbf{t}}_{\mathbf{n}_s}(\hat{\mathbf{u}}_{loc}) = \mathbf{0} & \text{on } S_0 \\ \hat{\mathbf{u}}_{loc} = -\hat{\mathbf{u}}^{inc} & \text{on } \Gamma \end{cases} \quad (1.20)$$

$$\begin{cases} -\nabla \cdot \hat{\boldsymbol{\sigma}}_s(\hat{\mathbf{u}}^{inc}) + \rho_s s^2 \hat{\mathbf{u}}^{inc} = \mathbf{0} & \text{in } \Omega_s \setminus \Omega_b^b \\ \hat{\mathbf{t}}_{\mathbf{n}_s}(\hat{\mathbf{u}}^{inc}) = \mathbf{0} & \text{on } S_0 \end{cases} \quad (1.21)$$

$s \in \mathbb{C}$ being the Laplace domain variable and the hat symbol $\hat{\cdot}$ denoting the corresponding Laplace-transformed fields. Again, notation $\hat{\mathbf{u}}_{rad}[\hat{\mathbf{u}}_b|_\Gamma]$ has been omitted for the sake of clearness. Note that Fourier domain equations can be straightforwardly obtained by considering $\Re(s) = 0$, $s \in \mathbb{C}$, i.e. $s = i\omega$, $\omega \in \mathbb{R}$.

1.2.3 Variational formulation

Also in the Laplace domain, the solution of the SSI problem $\hat{\mathbf{u}}_b \in \mathbf{H}^1(\Omega_b)$ (see Appx. A) and the different scattered fields have to satisfy the balance equation in the

structure and its set of boundary conditions, all detailed in (1.18). These equations are written in the following paragraphs in a weak sense.

Multiplying the balance equation of (1.18) by any Laplace-transformed virtual displacement field $\delta \hat{\mathbf{v}} \in \mathbf{H}^1(\Omega_b)$, the integration over the whole domain Ω_b results, integrating by parts, in:

$$\begin{aligned} \int_{\Omega_b} \hat{\boldsymbol{\sigma}}_b(\hat{\mathbf{u}}_b) : \hat{\boldsymbol{\epsilon}}_b(\overline{\delta \hat{\mathbf{v}}}) dV + s^2 \int_{\Omega_b} \rho_b \hat{\mathbf{u}}_b \cdot \overline{\delta \hat{\mathbf{v}}} dV &= \int_{\Omega_b} \hat{\mathbf{f}}_b \cdot \overline{\delta \hat{\mathbf{v}}} dV \\ &+ \int_{\Gamma_{bo}} \hat{\mathbf{t}}_{bo} \cdot \overline{\delta \hat{\mathbf{v}}} dS - \int_{\Gamma} \hat{\mathbf{t}}_{nb}(\hat{\mathbf{u}}_b) \cdot \overline{\delta \hat{\mathbf{v}}} dS \end{aligned} \quad (1.22)$$

where the property of symmetry of the strain and stress tensors have been used in the left-hand side of the equation and where $\overline{\diamond}$ denotes the complex conjugate of \diamond . Taking into account the traction boundary condition of (1.18), the following variational formulation of the interaction problem is obtained:

$$\{\mathcal{K} + \mathcal{Z}_V(s) + s^2 \mathcal{M}\}(\hat{\mathbf{u}}_b, \delta \hat{\mathbf{v}}) = \ell_s(\delta \hat{\mathbf{v}}_\Gamma; s) + \ell_b(\delta \hat{\mathbf{v}}) \quad (1.23)$$

where $\delta \hat{\mathbf{v}}_\Gamma = \delta \hat{\mathbf{v}}|_\Gamma \in \mathbf{H}^{\frac{1}{2}}(\Gamma)$ denotes the trace of $\delta \hat{\mathbf{v}}$ on Γ . Thus, the continuous sesquilinear forms of stiffness and mass $\mathcal{K}(\hat{\mathbf{u}}_b, \delta \hat{\mathbf{v}})$ and $\mathcal{M}(\hat{\mathbf{u}}_b, \delta \hat{\mathbf{v}})$ read:

$$\begin{aligned} \mathcal{K}(\hat{\mathbf{u}}_b, \delta \hat{\mathbf{v}}) &= \int_{\Omega_b} \hat{\boldsymbol{\sigma}}_b(\hat{\mathbf{u}}_b) : \hat{\boldsymbol{\epsilon}}_b(\overline{\delta \hat{\mathbf{v}}}) dV \\ \mathcal{M}(\hat{\mathbf{u}}_b, \delta \hat{\mathbf{v}}) &= \int_{\Omega_b} \rho_b \hat{\mathbf{u}}_b \cdot \overline{\delta \hat{\mathbf{v}}} dV \end{aligned} \quad (1.24)$$

In the same way, the linear form $\ell_b(\delta \hat{\mathbf{v}})$ can be written as:

$$\ell_b(\delta \hat{\mathbf{v}}) = \int_{\Omega_b} \hat{\mathbf{f}}_b \cdot \overline{\delta \hat{\mathbf{v}}} dV + \int_{\Gamma_{bo}} \hat{\mathbf{t}}_{bo} \cdot \overline{\delta \hat{\mathbf{v}}} dS \quad (1.25)$$

Finally, the sesquilinear form $\mathcal{Z}_V(\hat{\mathbf{u}}_b, \delta \hat{\mathbf{v}}; s)$, written in terms of the displacement field traces $\delta \hat{\mathbf{v}}_\Gamma$ and $\hat{\mathbf{u}}_b|_\Gamma \in \mathbf{H}^{\frac{1}{2}}(\Gamma)$, leads to the sesquilinear form of the dynamic soil stiffness $\mathcal{Z}(\hat{\mathbf{u}}_b|_\Gamma, \delta \hat{\mathbf{v}}_\Gamma; s)$. The latter form and the linear form of the external seismic load $\ell_s(\delta \hat{\mathbf{v}}_\Gamma; s)$ read as follows:

$$\mathcal{Z}(\hat{\mathbf{u}}_b|_\Gamma, \delta \hat{\mathbf{v}}_\Gamma; s) = \int_{\Gamma} \hat{\mathbf{t}}_{ns}(\hat{\mathbf{u}}_{rad}[\hat{\mathbf{u}}_b|_\Gamma]) \cdot \overline{\delta \hat{\mathbf{v}}_\Gamma} dS \quad (1.26)$$

$$\ell_s(\delta \hat{\mathbf{v}}_\Gamma; s) = - \int_{\Gamma} \hat{\mathbf{t}}_{ns}(\hat{\mathbf{u}}_{loc}) \cdot \overline{\delta \hat{\mathbf{v}}_\Gamma} dS - \int_{\Gamma} \hat{\mathbf{t}}^{inc} \cdot \overline{\delta \hat{\mathbf{v}}_\Gamma} dS. \quad (1.27)$$

As a result of the Betti-Maxwell reciprocity theorem [44] applied on the first integral of the seismic load expression for $\hat{\mathbf{u}}_{loc} = \hat{\mathbf{u}}_{rad}[-\hat{\mathbf{u}}^{inc}]$ and $\hat{\mathbf{u}}_{rad}[\delta \hat{\mathbf{v}}_\Gamma]$:

$$- \int_{\Gamma} \hat{\mathbf{t}}_{ns}(\hat{\mathbf{u}}_{rad}[-\hat{\mathbf{u}}^{inc}]) \cdot \overline{\delta \hat{\mathbf{v}}_\Gamma} dS = \int_{\Gamma} \hat{\mathbf{t}}_{ns}(\hat{\mathbf{u}}_{rad}[\delta \hat{\mathbf{v}}_\Gamma]) \cdot \hat{\mathbf{u}}^{inc} dS, \quad (1.28)$$

the linear form of the seismic force due to the incident displacement field can be reformulated into an expression that is independent of $\hat{\mathbf{u}}_{loc}$, that is:

$$\ell_s(\delta \hat{\mathbf{v}}_\Gamma; s) = \mathcal{Z}(\overline{\delta \hat{\mathbf{v}}_\Gamma}, \hat{\mathbf{u}}^{inc}; s) - \int_{\Gamma} \hat{\mathbf{t}}^{inc} \cdot \overline{\delta \hat{\mathbf{v}}_\Gamma} dS. \quad (1.29)$$

Note that for structures built over shallow or surface foundations, Γ coincides with the free-surface S_0 (where zero traction conditions are imposed) and thus, $\hat{\mathbf{t}}^{inc}$ vanishes. Hence, if by Riesz representation theorem [117] a soil impedance operator $\hat{\mathbb{Z}}(s)$ is introduced, i.e. the sesquilinear form of the soil impedance of Eq. (1.26) can be written in terms of duality pairings $\langle \cdot, \cdot \rangle$ (see Appx. A) as:

$$\mathcal{Z}(\hat{\mathbf{u}}_b|_\Gamma, \delta \hat{\mathbf{v}}_\Gamma; s) = \langle \hat{\mathbb{Z}}(s) \hat{\mathbf{u}}_b|_\Gamma, \delta \hat{\mathbf{v}}_\Gamma \rangle, \quad (1.30)$$

the seismic loading on shallow or surface foundations can be directly obtained only by means of the soil impedance operator and the incident displacement field.

Following a similar reasoning, the traction forces on Γ induced by $\hat{\mathbf{u}}_b|_\Gamma$, which are denoted $\hat{\mathbb{R}}_\Gamma(s)$ hereafter and which can be written as:

$$\hat{\mathbb{R}}_\Gamma(s) = \hat{\mathbb{Z}}(s) \hat{\mathbf{u}}_b|_\Gamma, \quad (1.31)$$

are usually interpreted as the soil-structure interaction (SSI) traction forces. In order to complete this explanation, the definition of the soil impedance operator and its main properties are fully addressed in next section.

1.2.4 The soil impedance operator

In order to introduce the soil impedance operator, let the elastodynamic boundary value problem (BVP) associated to a layered half-space be first considered. In particular, let S_0 be the infinite free-surface of the unbounded domain of soil Ω_s with outward unit normal \mathbf{n}_s and satisfying Lipschitz continuity conditions. Let Ω be a domain that is fully embedded in the soil and whose bounded boundary Γ also satisfies Lipschitz continuity conditions. For the sake of simplicity, it is assumed in the following that only Dirichlet boundary conditions (BC) are applied over Γ and no body forces are considered. It is also assumed that Γ is not included in S_0 , except for a set of points of zero measure (see Fig. 1.4). The corresponding exterior BVP formulated in the Laplace domain for $s \in \mathbb{C}_+ = \{s \in \mathbb{C} : \Re(s) > 0\}$ thus reads:

$$\begin{cases} -\nabla \cdot \hat{\boldsymbol{\sigma}}(\hat{\mathbf{u}}) + s^2 \hat{\mathbf{u}} = \mathbf{0} & \text{in } \Omega_s \\ \hat{\mathbf{u}} = \hat{\boldsymbol{\phi}} & \text{on } \Gamma \\ \hat{\mathbf{t}}_{\mathbf{n}_s}(\hat{\mathbf{u}}) = \mathbf{0} & \text{on } S_0 \end{cases} \quad (1.32)$$

where the trace of $\hat{\mathbf{u}}$ on Γ belongs to the functional space $\mathbf{H}^{\frac{1}{2}}(\Gamma)$ and the associated traction field, to its dual $\tilde{\mathbf{H}}^{-\frac{1}{2}}(\Gamma)$. A tilde is used on the latter functional space in order to highlight that it does not correspond to the classical $\mathbf{H}^{-\frac{1}{2}}(\Gamma)$, since homogeneous Neumann BC of this BVP are applied, in this case, on an infinite boundary [114]. It is interesting to notice that $\hat{\mathbf{u}}$, the unknown of the exterior BVP, corresponds to the displacement field that is radiated into the soil when $\hat{\boldsymbol{\phi}}$ is prescribed on the boundary Γ , that is $\hat{\mathbf{u}} = \hat{\mathbf{u}}_{rad}[\hat{\boldsymbol{\phi}}]$. Moreover, the domain of Ω corresponds to the part of the structural domain Ω_b that is embedded into the soil. Since the *exterior* BVP for the radiated displacement field is considered here, the non-embedded part of Ω_b is thus not necessary to be modelled. Indeed, as it can be seen in the following, Ω_b does not take part in the definition of the boundary integral operators but only on the definition of Γ .

In this framework, traction field $\hat{\mathbf{t}} = \hat{\mathbf{t}}_{n_s}(\hat{\mathbf{u}}) \in \tilde{\mathbf{H}}^{-\frac{1}{2}}(\Gamma)$ satisfies in general the following variational regularized direct integral equation [18, 32] on the boundary Γ :

$$\mathbf{u}(\hat{\mathbf{t}}, \hat{\mathbf{t}}'; s) = \mathcal{T}(\hat{\phi}, \hat{\mathbf{t}}'; s), \quad \forall \hat{\mathbf{t}}' \in \tilde{\mathbf{H}}^{-\frac{1}{2}}(\Gamma), \quad (1.33)$$

where $\mathbf{u}(\hat{\mathbf{t}}, \hat{\mathbf{t}}'; s)$ and $\mathcal{T}(\hat{\phi}, \hat{\mathbf{t}}'; s)$ are continuous bilinear forms defined as:

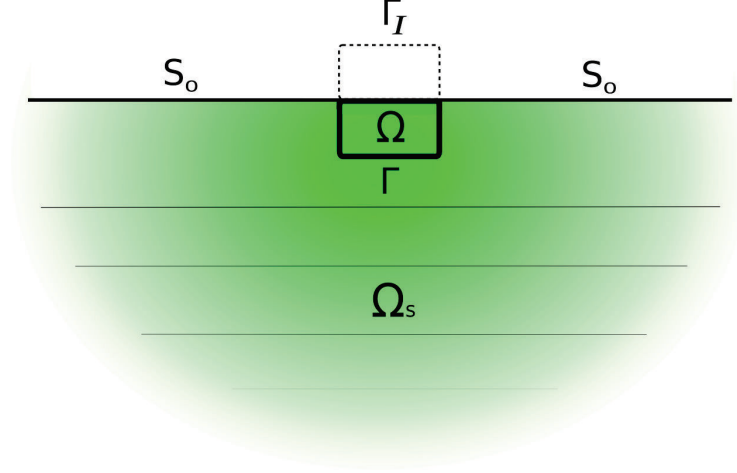


Figure 1.4: Simplified model of the exterior Boundary Value Problem considered. The image boundary represented with dashed lines concerns the regularization approach.

$$\mathbf{u}(\hat{\mathbf{t}}, \hat{\mathbf{t}}'; s) = \int_{\Gamma} \hat{\mathbf{t}}'^T(\mathbf{x}') \int_{\Gamma} \hat{\mathbf{U}}_s^G(\mathbf{x}, \mathbf{x}', s) \hat{\mathbf{t}}(\mathbf{x}) dS_{\mathbf{x}} dS_{\mathbf{x}'} \quad (1.34)$$

$$\begin{aligned} \mathcal{T}(\hat{\phi}, \hat{\mathbf{t}}'; s) = \int_{\Gamma} \hat{\mathbf{t}}'^T(\mathbf{x}') \int_{\Gamma} \left\{ \hat{\mathbf{T}}_s^G(\mathbf{x}, \mathbf{x}', s) \hat{\phi}(\mathbf{x}, s) - \mathbf{T}^0(\mathbf{x}, \mathbf{x}') \hat{\phi}(\mathbf{x}') \right\} dS_{\mathbf{x}} dS_{\mathbf{x}'} \\ + \int_{\Gamma} \hat{\mathbf{t}}'^T(\mathbf{x}') \mathbf{D}(\mathbf{x}') \hat{\phi}(\mathbf{x}') dS_{\mathbf{x}'} \end{aligned} \quad (1.35)$$

\mathbf{v}^T standing for the transpose of any \mathbf{v} . In the latter equations, $\hat{\mathbf{U}}_s^G(\mathbf{x}, \mathbf{x}', s)$ denotes the first Green's tensor of a layered half-space, i.e. for any unitary vectors \mathbf{a} and \mathbf{a}' , a displacement field at any position \mathbf{x} pointing in the direction of \mathbf{a} that is induced by a unit point load along direction \mathbf{a}' applied at \mathbf{x}' can be defined as $\mathbf{a}'^T \hat{\mathbf{U}}_s^G(\mathbf{x}, \mathbf{x}', s) \mathbf{a}$. Analogously, $\mathbf{a}'^T \hat{\mathbf{T}}_s^G(\mathbf{x}, \mathbf{x}', s) \mathbf{a}$ defines the corresponding traction field with $\hat{\mathbf{T}}_s^G(\mathbf{x}, \mathbf{x}', s)$ being the second Green's tensor of a stratified half-space. The regularizing tensor $\mathbf{T}^0(\mathbf{x}, \mathbf{x}')$ [18] is found so that it satisfies:

$$\lim_{r \rightarrow 0} \left(\left| \hat{\mathbf{T}}_s^G(\mathbf{x}, \mathbf{x}', s) - \mathbf{T}^0(\mathbf{x}, \mathbf{x}') \right| \right) < +\infty \quad (1.36)$$

for $r = \|\mathbf{x} - \mathbf{x}'\| \rightarrow 0$. This regularization tensor, which also exists for the particular case of a layered halfspace [30], reads:

$$\mathbf{T}^0(\mathbf{x}, \mathbf{x}') = \frac{\mathbf{G}^0(\mathbf{x}')}{r^2} \quad (1.37)$$

where \mathbf{G}^0 is a second order tensor that can be numerically computed. Finally, $\mathbf{D}(\mathbf{x}')$ is a second order tensor that can be defined, for any unbounded domain of soil, in terms of the regularizing tensor as follows:

$$\mathbf{D}(\mathbf{x}') = \mathbf{I} - \int_{\Gamma_I} \mathbf{T}^0(\mathbf{x}, \mathbf{x}') dS_x \quad (1.38)$$

where Γ_I is the image of Γ with respect to free surface of the half-space (see Fig. 1.4). It is interesting to notice that, as long as \mathbf{x}' remains at a finite distance from the free-boundary, integral in Eq. (1.38) is not singular. In fact, this integral vanishes when Γ is fully included in the definition of the free-boundary (traction fields \mathbf{T}_s^G are zero at free-boundary conditions) and also when Γ is a closed contour that remains entirely at a finite distance from S_0 . Nevertheless, this formulation still holds when \mathbf{x}' belongs to the free-surface since the measure of $\Gamma_I \cap \Gamma$ is equal to zero.

By Riesz representation theorem [117], each bilinear form of Eq. (1.33) admits a unique linear bounded operator mapping two Hilbert spaces. These operators can be defined as follows:

$$\hat{\mathbf{U}}(s) : \tilde{\mathbf{H}}^{-\frac{1}{2}}(\Gamma) \mapsto \mathbf{H}^{\frac{1}{2}}(\Gamma) \quad (1.39)$$

$$\hat{\mathbf{T}}(s) : \mathbf{H}^{\frac{1}{2}}(\Gamma) \mapsto \mathbf{H}^{\frac{1}{2}}(\Gamma) \quad (1.40)$$

Therefore, the soil impedance operator, which corresponds to the Steklov-Poincaré operator [76] of the unbounded soil or to the DtN operator defined over Γ , can be written as the following isomorphism $\hat{\mathbf{Z}}(s) : \mathbf{H}^{\frac{1}{2}}(\Gamma) \mapsto \tilde{\mathbf{H}}^{-\frac{1}{2}}(\Gamma)$:

$$\hat{\mathbf{Z}}(s) = \hat{\mathbf{U}}^{-1}(s)\hat{\mathbf{T}}(s) \quad (1.41)$$

Based on estimates of the Green's function in the Laplace domain, several authors have given different s -depending bounds ($s \in \mathbb{C}_+$) for both layer potentials and integral operators associated to the dissipative Helmholtz equation [75]. Their works are mainly focused on the exterior problems of open bounded domains, which refers basically to infinite domains. However, the SSI problem does not exactly deal with an infinite domain but with a semi-infinite one, i.e. the soil Ω_s . Therefore, a proof within the framework of the Helmholtz equation is provided in the following showing that the impedance operator $s \mapsto \hat{\mathbf{Z}}(s)$, holomorphic in \mathbb{C}_+ , is upper bounded for large s and for $\Re e(s) = \sigma_0 > 0$ so that:

$$\|\hat{\mathbf{Z}}(s)\|_{(\mathbf{H}^{\frac{1}{2}}(\Gamma), \tilde{\mathbf{H}}^{-\frac{1}{2}}(\Gamma))} \leq C(\sigma_0)|s|^2, \quad \text{with } C(\sigma_0) \in \mathbb{R}. \quad (1.42)$$

Proof. Let \mathcal{D} be a continuous extension operator $\mathcal{D} : H^{\frac{1}{2}}(\Gamma) \rightarrow H^1(\Omega)$, satisfying by Lemma 1 of Bamberger and Duong [5] the following:

$$\|\|\mathcal{D}\phi\|\|_{|s|, \Omega} \leq A(\sigma)|s|^{\frac{1}{2}}\|\phi\|_{\frac{1}{2}}, \quad \forall \phi \in H^{\frac{1}{2}}(\Gamma), \Re e(s) > \sigma > 0 \quad (1.43)$$

where $\|\|\cdot\|\|_{|s|, \Omega}$ is defined in Appx. A. Thus the natural norm given in the dual space is defined as:

$$\|\|\partial_n u\|\|_{-\frac{1}{2}} = \sup_{\phi \in H^{\frac{1}{2}}(\Gamma), \phi \neq 0} \frac{|\langle \partial_n u, \phi \rangle|}{\|\phi\|_{\frac{1}{2}}} \leq \sup_{\phi \in H^{\frac{1}{2}}(\Gamma), \phi \neq 0} \frac{\|\|u\|\|_{|s|, \Omega} \|\|\mathcal{D}\phi\|\|_{|s|, \Omega}}{\|\phi\|_{\frac{1}{2}}} \quad (1.44)$$

where Cauchy-Schwarz inequality has been used in last step. The normal derivative is denoted by ∂_n and $\langle \cdot, \cdot \rangle$ correspond to duality pairings (see Appx. A).

The first step of the proof is obtained by using inequality (1.43) in (1.44):

$$\|\partial_n u\|_{-\frac{1}{2}} \leq A(\sigma)|s|^{\frac{1}{2}} \|u\|_{|s|, \Omega} \quad (1.45)$$

which provides a bound¹ for the Neumann data depending on $\|u\|_{|s|, \Omega}$.

The proof of Eq. (1.42) will thus come by proving a bound for $\|u\|_{|s|, \Omega}$. To that aim, let us first obtain the following relation:

$$\Re(s) \|u\|_{|s|, \Omega}^2 = \Re(\langle \partial_n u, su|_{\Gamma} \rangle) \quad (1.46)$$

which comes from the classical variational form $(\nabla u, \nabla v) + s^2(u, v) = \langle \partial_n u, v \rangle$ tested with $v = su|_{\Gamma}$. This can be used to show next inequality for $\Re(s) \neq 0$:

$$\begin{aligned} \|\partial_n u\|_{-\frac{1}{2}}^2 &\leq C'(\sigma)|s| \|u\|_{|s|, \Omega}^2 = C'(\sigma)|s| \frac{\Re(\langle \partial_n u, su|_{\Gamma} \rangle)}{\Re(s)} \\ &\leq C'(\sigma)|s| \frac{|\langle \partial_n u, su|_{\Gamma} \rangle|}{\Re(s)} \leq C'(\sigma) \frac{|s|^2}{\Re(s)} \|\partial_n u\|_{-\frac{1}{2}} \|u|_{\Gamma}\|_{\frac{1}{2}} \end{aligned} \quad (1.47)$$

It follows:

$$\|\partial_n u\|_{-\frac{1}{2}} \leq C(\sigma)|s|^2 \|u|_{\Gamma}\|_{\frac{1}{2}} \quad (1.48)$$

where $C(\sigma)$ is now a new constant depending on $\Re(s) > \sigma > 0$.

Since the impedance operator is a DtN operator that maps $u|_{\Gamma} \mapsto \partial_n u|_{\Gamma}$, the inequality of Eq. (1.48) proves the upper bound of the soil impedance operator with $\mu = 2$. \square

Hereafter, it is assumed that this property of the soil impedance operator is verified not only for the scalar case of the Helmholtz equation but also for the elastodynamic case. In addition, it should be noticed that being $\hat{\mathbb{Z}}(s)$ holomorphic in \mathbb{C}_+ directly ensures the causality of the corresponding operator $t \mapsto \mathbb{Z}(t) = \mathcal{L}^{-1} \hat{\mathbb{Z}}(s)$ in the time domain [108].

1.3 Spatial semi-discretization: the BE-FE coupled equations

The BE-FE coupling can be easily introduced by recalling the expression of the sesquilinear form of dynamic soil impedance of Eq. (1.26) and Eq. (1.30):

$$\mathcal{Z}(\hat{\mathbf{u}}_b|_{\Gamma}, \delta \hat{\mathbf{v}}_{\Gamma}; s) = \int_{\Gamma} \hat{\mathbf{t}}_{\mathbf{n}_s}(\hat{\mathbf{u}}_{rad}[\hat{\mathbf{u}}_b|_{\Gamma}]) \cdot \overline{\delta \hat{\mathbf{v}}_{\Gamma}} dS = \int_{\Gamma} \hat{\mathbb{Z}}(s) \hat{\mathbf{u}}_b|_{\Gamma} \cdot \overline{\delta \hat{\mathbf{v}}_{\Gamma}} dS \quad (1.49)$$

¹Another less restrictive bound can be obtained without using Lemma 1 by just considering the continuity of the operator \mathcal{D} :

$$\|\mathcal{D}\phi\|_1^2 = \|\mathcal{D}\phi\|^2 + \|\nabla(\mathcal{D}\phi)\|^2 \leq C_{\mathcal{D}} \|\phi\|_{\frac{1}{2}}^2, \quad \forall \phi \in H^{\frac{1}{2}}(\Gamma)$$

and identity $\|v\|_{1, |s|} \leq |s| \|v\|_1$.

where the form \mathcal{Z} is discretized using a FE method but the impedance operator $\hat{\mathcal{Z}}$ applied to $\hat{\mathbf{u}}_b|_\Gamma$, and thus $\hat{\mathbf{t}}_{n_s}(\hat{\mathbf{u}}_{rad}[\hat{\mathbf{u}}_b|_\Gamma])$, is obtained from a BE approach. Therefore, the first step towards the FE discretization of \mathcal{Z} is the numerical evaluation of the traction field $\hat{\mathbf{t}}_{n_s}$ of Eq. (1.26) with $\hat{\boldsymbol{\phi}} = \hat{\mathbf{u}}_b|_\Gamma$, which is the trace of the structural displacement field on Γ .

1.3.1 BE discretization

In section 1.2.4, the dynamic soil impedance operator $\hat{\mathcal{Z}}$ has been defined by means of boundary integral operators associated to an exterior BVP. In order to discretize this impedance operator, the Boundary Integral Equation (BIE) of Eq. (1.33) is discretized in the following with a BE method. This numerical technique appears to be quite well-adapted to this problem because of mainly two reasons. First, the BE method is performed entirely on the boundary and, second, in the case of unbounded domains, the radiation conditions are implicitly taken into account.

Let the spatial domain of Γ be approximated by a BE method, i.e. the boundary Γ is divided into N_e boundary elements, whose support is denoted W_E . It thus follows the discretization of the known field $\hat{\boldsymbol{\phi}}(\mathbf{x}; s)$ and the unknown $\hat{\mathbf{t}}_{n_s}(\mathbf{x}; s)$ by means of piecewise-constant shape functions in each \mathbf{e}_j direction of the canonical basis:

$$\hat{\boldsymbol{\phi}}(\mathbf{x}; s) = \sum_{k=1}^{N_e} \sum_{j=1}^3 \mathbf{M}_{jk}(\mathbf{x}) \hat{\phi}_j^k(s) = \mathbf{M}_s \hat{\boldsymbol{\phi}}_s(s) \quad (1.50)$$

$$\hat{\mathbf{t}}_{n_s}(\mathbf{x}; s) = \sum_{k=1}^{N_e} \sum_{j=1}^3 \mathbf{M}_{jk}(\mathbf{x}) \hat{t}_j^k(s) = \mathbf{M}_s \hat{\mathbf{t}}_s(s) \quad (1.51)$$

where \mathbf{M}_{jk} are vectors defined as:

$$\mathbf{M}_{jk} = \begin{cases} \mathbf{e}_j & \text{for } \mathbf{x} \in \Omega_E \\ \mathbf{0} & \text{for } \mathbf{x} \notin \Omega_E \end{cases} \quad (1.52)$$

and $\hat{\boldsymbol{\phi}}_s(s)$ and $\hat{\mathbf{t}}_s(s)$ denote the vectors that respectively collect the displacements and tractions at the center of the elements. Higher order basis functions to approximate displacements, in particular, the use of linear basis functions, would give a more accurate solution [18].

Once Green's solutions are computed, the following algebraic system of equations can be obtained by injecting formulae of Eq. (1.34) and (1.35):

$$\hat{\mathbf{U}}(s) \hat{\mathbf{t}}_s(s) = \hat{\mathbf{T}}(s) \hat{\boldsymbol{\phi}}_s(s) \quad (1.53)$$

where $\hat{\mathbf{U}}$ and $\hat{\mathbf{T}}$ are the BE method system matrices that arise from the double integration over the interface Γ of the traction and displacement fundamental solutions. It is interesting to mention that singular integrals have to be computed and hence special numerical techniques have to be employed [18].

Since $\hat{\boldsymbol{\phi}}(\mathbf{x}; s)$ is discretized using a BE method and $\hat{\mathbf{u}}_b|_\Gamma(\mathbf{x}'; s)$, using a FE method, the kinematic condition stated in Eq. (1.32) must be verified in a variational sense, this is:

$$\int_{\Gamma} \hat{\mathbf{t}}'^T(\mathbf{x}') \hat{\boldsymbol{\phi}}(\mathbf{x}'; s) dS_{\mathbf{x}'} = \int_{\Gamma} \hat{\mathbf{t}}'^T(\mathbf{x}') \hat{\mathbf{u}}_b|_\Gamma(\mathbf{x}'; s) dS_{\mathbf{x}'} \quad (1.54)$$

for any test function $\mathbf{t}'(\mathbf{x}') \in \tilde{\mathbf{H}}^{-\frac{1}{2}}(\Gamma)$. After discretization and testing with the BE shape functions, previous Eq. (1.54) gets to:

$$\mathbf{\Lambda}_s \hat{\boldsymbol{\phi}}_s(s) = \mathbf{T}_q^T \hat{\mathbf{u}}_b|_\Gamma \quad (1.55)$$

with $\mathbf{\Lambda}_s$ being a diagonal matrix containing the surface of the elements and \mathbf{T}_q , the transfer matrix defined as $\mathbf{T}_q = \int_\Gamma \mathbf{N}_b^T \mathbf{M}_s dS$. Recall that \mathbf{M}_s collects the BE shape functions and, as it will be explained in next section 1.3.2, \mathbf{N}_b collects the globally defined FE shape functions of the structure domain. Remark that vector $\hat{\mathbf{u}}_b|_\Gamma$ contains the displacements at FE nodes of the interface Γ and not at BE nodes (the center of the elements).

At this stage, tractions $\hat{\mathbf{t}}_s(s)$ induced by prescribed displacements $\hat{\boldsymbol{\phi}}_s(s)$ on Γ can not only be evaluated by means of the BE discretized equation (1.53):

$$\hat{\mathbf{t}}_s(s) = \hat{\mathbf{U}}^{-1}(s) \hat{\mathbf{T}}(s) \hat{\boldsymbol{\phi}}_s(s) \quad (1.56)$$

but also in terms of displacements expressed in a FE basis:

$$\hat{\mathbf{t}}_s(s) = \hat{\mathbf{U}}^{-1}(s) \hat{\mathbf{T}}(s) \mathbf{\Lambda}_s^{-1} \mathbf{T}_q^T \hat{\mathbf{u}}_b|_\Gamma, \quad (1.57)$$

where Eq. (1.55) has been used in the last step.

Subsequently, the nodal soil-structure interaction forces, denoted by $\hat{\mathbf{R}}_\Gamma(s)$, can be obtained by the FE discretization of the sesquilinear form of Eq. (1.26). Thus, the BE-FE coupling is finally traduced into the following expression:

$$\hat{\mathbf{R}}_\Gamma(s) = \mathbf{T}_q \hat{\mathbf{t}}_s(s) \quad (1.58)$$

Then, using Eq. (1.57), the latter equation derives into:

$$\hat{\mathbf{R}}_\Gamma(s) = \hat{\mathbf{Z}}(s) \hat{\mathbf{u}}_b|_\Gamma, \quad (1.59)$$

where the term of $\hat{\mathbf{Z}}(s) = \mathbf{T}_q \hat{\mathbf{U}}^{-1}(s) \hat{\mathbf{T}}(s) \mathbf{\Lambda}_s^{-1} \mathbf{T}_q^T$ corresponds to the discretized operator of $\hat{\mathbf{Z}}(s)$ and denotes the dynamic soil impedance matrix (or the dynamic soil stiffness matrix) in a FE basis. In this dissertation, this impedance matrix $\hat{\mathbf{Z}}(s)$ is directly computed using the BE code MISS3D [30].

Once the impedance matrix that models the soil domain is obtained, a FE formulation is employed to solve for the structure domain unknowns.

1.3.2 FE discretization

The correspondant variational problem (see Eq. (1.23)) can be discretized by using a FE approach. The displacement field $\hat{\mathbf{u}}_b$ can thus be approximated on a finite dimensional defined on Ω_b as $\hat{\mathbf{u}}_b \approx \mathbf{N}_b \hat{\mathbf{u}}_b$, being \mathbf{N}_b the matrix containing the globally defined shape functions and \mathbf{u}_b the vector of the displacements at FE nodes. A standard Galerkin approach is followed and, using the same basis, the virtual displacement field $\delta \hat{\mathbf{v}} \approx \mathbf{N}_b \delta \hat{\mathbf{v}}$ is also discretized. In the formulation that is employed here, the elements of the symmetrical stress tensor $\hat{\boldsymbol{\sigma}}_b$ are collected in the vector $\hat{\boldsymbol{\sigma}}_b = \{\hat{\sigma}_{xx}, \hat{\sigma}_{yy}, \hat{\sigma}_{zz}, \hat{\sigma}_{xy}, \hat{\sigma}_{yz}, \hat{\sigma}_{zx}\}^T$. Similarly, vector $\hat{\boldsymbol{\epsilon}}_b = \{\hat{\epsilon}_{xx}, \hat{\epsilon}_{yy}, \hat{\epsilon}_{zz}, \hat{\gamma}_{xy}, \hat{\gamma}_{yz}, \hat{\gamma}_{zx}\}^T$

gathers the elements of the symmetrical strain tensor $\hat{\boldsymbol{\epsilon}}_b$, where $\hat{\gamma}_{xy}$, $\hat{\gamma}_{yz}$, $\hat{\gamma}_{zx}$ denote the engineering shear strains. The strain vector $\hat{\boldsymbol{\epsilon}}_b$ can thus be approximated by means of shape functions as $\hat{\boldsymbol{\epsilon}}_b = \mathbf{L}\mathbf{N}_b\hat{\mathbf{u}}_b = \mathbf{B}_b\hat{\mathbf{u}}_b$, where \mathbf{L} denotes the matrix with derivative operators. The stress vector, related to $\hat{\boldsymbol{\epsilon}}_b$ by Hooke's law, is written as $\hat{\boldsymbol{\sigma}}_b = \mathbf{D}_b\mathbf{B}_b\hat{\mathbf{u}}_b$, where \mathbf{D}_b is the constitutive matrix depending on Lamé coefficients for an isotropic homogeneous elastic material. The resulting system of equations reads as follows :

$$(\mathbf{K}_b + s^2\mathbf{M}_b + \hat{\mathbf{Z}}_V)\hat{\mathbf{u}}_b = \hat{\mathbf{f}}_b + \hat{\mathbf{f}}_s \quad (1.60)$$

where $\hat{\mathbf{Z}}_V$ depends on s . Eq. (1.60) can be rewritten by splitting the degrees-of-freedom into those defined on the interface (denoted by subscript Γ) and those belonging to the interior of the building (denoted by subscript b), as follows:

$$\begin{bmatrix} \hat{\mathbf{S}}_{bb}(s) & \hat{\mathbf{S}}_{b\Gamma}(s) \\ (sym.) & \hat{\mathbf{S}}_{\Gamma\Gamma}(s) + \hat{\mathbf{Z}}(s) \end{bmatrix} \begin{bmatrix} \hat{\mathbf{u}}_{bb}(s) \\ \hat{\mathbf{u}}_{b\Gamma}(s) \end{bmatrix} = \begin{bmatrix} \hat{\mathbf{f}}_{bb}(s) \\ \hat{\mathbf{f}}_{b\Gamma}(s) \end{bmatrix} + \begin{bmatrix} \mathbf{0} \\ \hat{\mathbf{f}}_s(s) \end{bmatrix} \quad (1.61)$$

where $\hat{\mathbf{S}}_{\alpha\beta}(s) = s^2\mathbf{M}_{b,\alpha\beta} + \mathbf{K}_{b,\alpha\beta}$ for $\alpha, \beta \in \{b, \Gamma\}$, with $\mathbf{M}_{b,\alpha\beta}$ and $\mathbf{K}_{b,\alpha\beta}$ the matrix blocks of mass and stiffness of domain Ω_b , and where matrix $\hat{\mathbf{Z}}_V(s)$ is non-zero on Γ -DoF's:

$$\hat{\mathbf{Z}}_V(s) = \begin{bmatrix} \mathbf{0} & \mathbf{0} \\ \mathbf{0} & \hat{\mathbf{Z}}(s) \end{bmatrix},$$

$\hat{\mathbf{Z}}(s)$ denoting the soil impedance matrix. The FE stiffness matrix \mathbf{K}_b and the FE mass matrix \mathbf{M}_b are calculated as:

$$\mathbf{K}_b = \int_{\Omega_b} \mathbf{B}_b^T \mathbf{D}_b \mathbf{B}_b dV \quad (1.62)$$

$$\mathbf{M}_b = \int_{\Omega_b} \mathbf{N}_b^T \rho_b \mathbf{N}_b dV \quad (1.63)$$

and the vector of external nodal forces $\hat{\mathbf{f}}_b$ is equal to:

$$\hat{\mathbf{f}}_b = \int_{\Gamma_{bo}} \mathbf{N}_b^T \hat{\mathbf{t}}_{bo} dS + \int_{\Omega_b} \mathbf{N}_b^T \hat{\mathbf{f}}_b dV \quad (1.64)$$

The seismic force vector corresponds to the discretized version of Eq. (1.29):

$$\hat{\mathbf{f}}_s = \hat{\mathbf{Z}}^T \mathbf{u}^{inc} - \mathbf{T}_q^T \underline{\mathbf{t}}^{inc} \quad (1.65)$$

where \mathbf{T}_q has been defined in the previous section.

1.3.3 Extension to the nonlinear case

Since solving nonlinear problems is one of the goals, it is interesting to turn equation (1.61) into the time domain by using the inverse laplace transform. The new obtained system of equations reads:

$$\begin{bmatrix} \mathbf{L}_{t,bb}(\cdot) & \mathbf{L}_{t,b\Gamma}(\cdot) \\ (sym.) & \mathbf{L}_{t,\Gamma\Gamma}(\cdot) \end{bmatrix} \begin{bmatrix} \mathbf{u}_{bb}(t) \\ \mathbf{u}_{b\Gamma}(t) \end{bmatrix} + \begin{bmatrix} \mathbf{0} \\ \mathbf{R}_\Gamma(t) \end{bmatrix} = \begin{bmatrix} \mathbf{F}_b(t) \\ \mathbf{F}_\Gamma(t) + \mathbf{f}_s(t) \end{bmatrix} \quad (1.66)$$

where the time differentiation operator related to $\hat{S}_{\alpha\beta}(s)$ is denoted by $\mathbf{L}_{t,\alpha\beta}(\cdot) = \mathbf{M}_{b,\alpha\beta}\partial_{tt}(\cdot) + \mathbf{K}_{b,\alpha\beta}$ for again $\alpha, \beta \in \{b, \Gamma\}$. Vector $\underline{\mathbf{R}}_{\Gamma}(t)$, called interaction forces, corresponds to a convolution integral coming from the term $\hat{\mathbf{Z}}(s)\hat{\underline{\mathbf{u}}}_{\Gamma}(s)$:

$$\underline{\mathbf{R}}_{\Gamma}(t) = (\mathbf{Z} * \underline{\mathbf{u}}_{\Gamma})(t) = \int_0^t \mathbf{Z}(\tau)\underline{\mathbf{u}}_{\Gamma}(t - \tau) d\tau \quad (1.67)$$

and its numerical treatment is the main motivation of this discussion. Remark that in this convolution, denoted by $*$, soil impedance matrix and displacement field are assumed to vanish for $t < 0$.

When nonlinear phenomena are accounted for, the problem must be formulated in the time domain and thus, $\underline{\mathbf{R}}_{\Gamma}(t)$ also appears in the system of equations. In fact, if nonlinearities are considered in Ω_b , the problem takes the following form:

$$\begin{bmatrix} \mathbf{M}_{b,bb} & \mathbf{M}_{b,b\Gamma} \\ (Sym.) & \mathbf{M}_{b,\Gamma\Gamma} \end{bmatrix} \begin{bmatrix} \underline{\dot{\mathbf{u}}}_b(t) \\ \underline{\dot{\mathbf{u}}}_{\Gamma}(t) \end{bmatrix} + \begin{bmatrix} \underline{\mathbf{F}}_b^{int}(t) \\ \underline{\mathbf{F}}_{\Gamma}^{int}(t) + \underline{\mathbf{R}}_{\Gamma}(t) \end{bmatrix} = \begin{bmatrix} \underline{\mathbf{F}}_b(t) \\ \underline{\mathbf{F}}_{\Gamma}(t) + \underline{\mathbf{f}}_s(t) \end{bmatrix} \quad (1.68)$$

where $\underline{\mathbf{F}}_{\alpha}^{int}(t)$ ($\alpha \in \{b, \Gamma\}$) represents the nonlinear internal efforts in the structure and depend on both displacement and velocity fields. In this case, the stiffness matrix $\mathbf{K}_{b,\alpha\beta}$ of the operator $\mathbf{L}_{t,\alpha\beta}(\cdot)$ introduced in Eq. (1.66) can be interpreted as the tangent matrix of the internal forces.

Nonlinear transient analysis

A classical nonlinear algorithm [66] is used to deal with nonlinearities in the domains. In this section, the main steps of the procedure are briefly introduced.

Let consider the following governing equation:

$$\mathbf{M}_b \underline{\ddot{\mathbf{u}}} + \underline{\mathbf{F}}^{int}(\underline{\mathbf{u}}, \underline{\dot{\mathbf{u}}}, t, \dots) + \underline{\mathbf{R}}(\underline{\mathbf{u}}, t) = \underline{\mathbf{F}}^{ext}(\underline{\mathbf{x}}, t) \quad (1.69)$$

with vanishing initial conditions (simple case) and where matrix \mathbf{M} denotes here the mass matrix of the whole system. Vector $\underline{\mathbf{F}}^{int}$ corresponds to the internal nonlinear forces that possibly depends on multiple variables and vector $\underline{\mathbf{R}}(\underline{\mathbf{u}}, t)$ contains the nodal soil-structure interaction forces. If Eq. (1.69) is rewritten as follows:

$$\mathbf{M}_b \underline{\ddot{\mathbf{u}}} + \underline{\mathbf{f}}^{int}(\underline{\mathbf{u}}, \underline{\dot{\mathbf{u}}}, t, \dots) + \underline{\mathbf{R}}(\underline{\mathbf{u}}, t) - \underline{\mathbf{F}}^{ext}(\underline{\mathbf{x}}, t) = \underline{\mathbf{r}}(\underline{\mathbf{u}}) = \mathbf{0} \quad (1.70)$$

with $\underline{\mathbf{r}}(\underline{\mathbf{u}})$ denoting the residual term, a Newton-Raphson algorithm can be applied to solve the nonlinear problem. This algorithm consists in an iterative process that leads to an approximated numerical solution of Eq. (1.70). This iterative process finishes when convergence criterion is reached, i.e. displacement at iteration $k + 1$, denoted $\underline{\mathbf{u}}^{k+1}$, satisfies Eq. (1.70) for fixed t within a given tolerance ϵ :

$$\|\underline{\mathbf{r}}(\underline{\mathbf{u}}^{k+1})\| < \epsilon \quad (1.71)$$

In more detail, when iteration $k + 1$ is carried out for fixed t , the following expression should be satisfied:

$$\underline{\mathbf{r}}(\underline{\mathbf{u}}^{k+1}) = \underline{\mathbf{r}}(\underline{\mathbf{u}}^k) + \mathbf{S}_T(\underline{\mathbf{u}}^k)(\underline{\mathbf{u}}^{k+1} - \underline{\mathbf{u}}^k) \quad (1.72)$$

where $\mathbf{S}_T(\underline{\mathbf{u}}^k)$ corresponds to the tangent operator on $\underline{\mathbf{r}}(\underline{\mathbf{u}})$ evaluated at $\underline{\mathbf{u}}^k$. In particular, choosing $\underline{\mathbf{u}}^{k+1}$ so that $\underline{\mathbf{r}}(\underline{\mathbf{u}}^{k+1}) = \underline{\mathbf{0}}$ as in Eq. (1.70) gives:

$$\mathbf{S}_T(\underline{\mathbf{u}}^k)\Delta\underline{\mathbf{u}}^{k+1} = -\underline{\mathbf{r}}(\underline{\mathbf{u}}^k) \quad (1.73)$$

where $\Delta\underline{\mathbf{u}}^{k+1} = \underline{\mathbf{u}}^{k+1} - \underline{\mathbf{u}}^k$. Finally, $\underline{\mathbf{u}}^{k+1}$ is computed by means of $\underline{\mathbf{u}}^k$ and $\Delta\underline{\mathbf{u}}^{k+1}$.

Eq. (1.70) shows the dependence on time-varying quantities, such as displacements, velocities and accelerations. In order to compute these terms a time discretization must be done and this is the main issue of next chapter.

1.4 Conclusions

In this chapter the problem of soil-structure interaction has been presented. For the spatial discretization, two main approaches have been briefly reviewed: the direct and the substructure method. Each of them involves the coupling of the FE method with another different numerical technique (absorbing layers, the Infinite Element method, the BE method, the Thin Layer method, the Scaled Boundary-Finite Element method, the method of the hidden state variables, etc.). In addition, both of them aim at overcoming one difficulty, which is modelling the unbounded domain of soil by accounting for Sommerfeld's radiation conditions at infinity. The main difference between these two approaches deals with the fact that substructuring techniques need the construction of an impedance matrix that results in the so-called soil dynamic stiffness matrix, whereas no impedance matrix is required for direct approaches.

In this Ph.D. thesis, a substructuring approach has been adopted. The problem stated in the structure is solved with a Finite Element method. The soil is represented by a soil dynamic stiffness matrix computed using a Laplace domain Boundary Element method.

Within this FE-BE chosen approach, the governing equations of the linear coupled system have been presented in its strong and weak forms. The dynamic soil impedance operator has also been introduced showing that it is a causal operator holomorphic in the complex half-plane $\Re(s) > \sigma_0 > 0$ that satisfies:

$$\|\hat{\mathbb{Z}}(s)\|_{\mathcal{H}} \leq C(\sigma_0)|s|^\mu, \quad \text{with } C(\sigma_0) \in \mathbb{R} \text{ and } \mu = 2.$$

When nonlinear behaviour is accounted for in the FE domain, the problem must be formulated in the time domain. In this case, it has been showed that a time convolution integral between the dynamic soil impedance operator and the trace of the structural displacement field over the SSI-interface appears in the equations. This time convolution corresponds to the so-called SSI forces. In order to evaluate them, a proper time discretization technique has thus to be chosen and this is the main subject of chapter two.

Chapter 2

The Hybrid Laplace-Time Domain Approach

“Entre deux vérités du domaine réel, le chemin le plus facile et le plus court passe bien souvent par le domaine complexe.”

PAUL PAINLEVÉ, 1900

With the resolution of dynamic nonlinear SSI problems being the main issue of this dissertation, the coupled BE-FE equations have to be formulated in the time domain. The problem needs also to be discretized in time and thus, this chapter provides some broad-brush strokes on time integration schemes. In particular, the choice of an adequate integration procedure within a coupled BE-FE approach is briefly discussed.

Special attention has to be given to the time convolution integrals arising at the SSI interface (ie. interaction forces) that must be computed during the resolution of the problem. Indeed, the evaluation of the SSI interaction forces $\mathbf{R}_\Gamma(t)$ relies on the solution of the following integral:

$$\mathbf{R}_\Gamma(t) = (\mathbf{Z} * \mathbf{u}_\Gamma)(t) = \int_0^t \mathbf{Z}(\tau) \mathbf{u}_\Gamma(t - \tau) d\tau, \quad t > 0, \quad (2.1)$$

where the convolution kernel $\mathbf{Z}(t)$, numerically known in the Laplace domain, shows a distributional behaviour. In order to evaluate this convolution, a Hybrid Laplace-Time domain Approach which is based on convolution quadratures is presented. It is first introduced regardless of the problem’s nature and then, it is particularized to dynamic SSI problems.

The coupling of the proposed approach to a Newmark time integration scheme within the BE-FE framework is elaborated and its stability properties discussed. Some features of the proposed approach, as well as those of a Hybrid Frequency-Time domain Approach, are finally analyzed on a simple numerical application.

2.1 State of the art

As stated before, the interaction forces within a BE-FE coupling approach are essentially the representation of the unbounded soil domain. They are thus directly related to the BE system. If the FE model contains some kind of nonlinearities (contact, friction, impact, plasticity, large transformations, etc.), the SSI forces applied on FE domain boundaries must be evaluated in the time domain.

They can be evaluated entirely in the time domain by using a BE method based on time domain Green's functions. However, the main difficulty of this approach is the choice of an adequate time step. Indeed, a very small time step produces an unstable numerical solution, whereas a too large time step introduces numerical damping in the solution. Although, several research works have recently been focused on the improvement of the stability and causality of the transient dynamic BE solutions [112, 155], the fundamental solutions are not always easy to obtain.

To overcome these problems, several approaches based on frequency BE formulations can be found in literature. Hybrid approaches are mainly based on recursive discrete-filtering techniques [146, 147], on Fast Fourier Transform (FFT) algorithms [14] or on balancing approximation techniques [111]. Examples of recursive filtering techniques can also be found in Şafak [37] but these techniques show very high instabilities during the time integration procedure and its application is limited to the analysis of rigid foundations [94]. On the other hand, FFT-based techniques needs the computation of the SSI convolution kernel which usually corresponds to the dynamic impedance matrix of the unbounded soil domain. Nevertheless, Masoumi [94] and Wolf [145] proved that the choice of a flexibility formulation can avoid some numerical difficulties related to Gibbs phenomenon. In this way, François [53] proposed a hybrid frequency-time approach where the SSI convolution to be evaluated was computed by means of a Filon algorithm applied on soil flexibility matrix. This approach can still be combined with the θ -method, which is a dissipative time integration scheme, in order to get more satisfying results.

Even if no SSI convolution has to be evaluated, it might be interesting to recall that hybrid approaches exist also for contact and frictional nonlinearities. One example is the so-called *time-frequency method* recently developed by Obrembski *et al.* [107] or Clouteau and Devésá [31]. The approach, which was recovered from the work of Darbre and Wolf [40], is based on the following strategy. Time solution of the linearized problem is first computed using a frequency based BE method and, afterwards, a time solution is obtained by using a FFT algorithm. It is then corrected by an incremental time stepping procedure in order to reach convergence with the nonlinear solution. Nevertheless this method presents some difficulties of convergence, particularly with 3D modellings.

Alternatively, Schanz and Antes [125, 126] have introduced a new formulation for time domain BEM based on the Convolution Quadrature Method of Lubich [84, 85]. The main difference to usual time-stepping BE formulations is the way to solve the convolution integral appearing in most time-dependent integral equations. In the CQM formulation, this convolution integral is approximated by a quadrature rule whose weights are determined by the Laplace transformed Green's solutions and a multistep method. The combination of CQM with BEM basically improves the stability of the time-stepping procedure and allows to avoid highly complicated fundamental solutions in time domain. In addition, it allows the modelling of viscoelastic

and poroelastic constitutive relations even in quasi-static problems [127]. A comparative study against two other different approaches, both classical transformed Laplace domain and time domain formulations, has been carried out by Gaul and Schanz [55].

Convolution quadrature method has also been combined with Duhamel-BE methods [97, 98, 113] to solve soil-structure interaction and wave propagation problems. But the adoption of the Laplace transform has also been employed without convolution quadratures. In fact, Loureiro and Mansur [83] used a hybrid time-Laplace algorithm based on subsequently numerical Laplace inversion techniques to obtain the time domain solution of the elastodynamic equations of motion and Albuquerque *et al.* [1] applied also a hybrid time-Laplace domain BEM for anisotropic dynamic crack problems.

Even when a stable time integration scheme is used for the BE system, an unstable solution can be obtained within a nonlinear analysis. Lie *et al.* [81], Yu *et al.* [154] pointed out that the FE time discretization scheme may introduce some instabilities. Masoumi [94] thus proposed a coupled θ -method for the BE system and a time stepping scheme developed by Lie and Yu [80] for the FE equations. Time integrations schemes that introduce numerical damping, such as the HHT method [65], can also be used for the FE system of equations.

2.2 Time domain discretization

In order to focus on time domain discretization methods, hereafter, it is assumed that all variables are spatially discretized by means of a FE method. Therefore, and for the sake of conciseness, nodal vectors are no more underlined.

The time stepping procedure involves the division of the whole time interval of calculation into small time increments Δt . This method, which also involves the time discretization of both loadings and unknown fields, assumes that governing equations are only satisfied at some instants $t = n\Delta t$, with $n \in \mathbb{N}$. In addition, other assumptions concerning the variation of the unknown fields (ie. displacements, velocities and accelerations in dynamic problems) within a time step have to be done. In fact, the way that this variation is approximated can constitute a characteristic feature of the time integration scheme and thus, a possible classification. However, time stepping procedures are typically classified as *explicit* or *implicit* depending on the way the current time step (that is at $t = n\Delta t$) is evaluated. For dynamic problems, an explicit algorithm can be defined as:

$$\mathbf{u}_n(\mathbf{x}) = f(\mathbf{u}_{n-1}, \dot{\mathbf{u}}_{n-1}, \ddot{\mathbf{u}}_{n-1}, \mathbf{u}_{n-2}, \dot{\mathbf{u}}_{n-2}, \ddot{\mathbf{u}}_{n-2}, \dots) \quad (2.2)$$

where \mathbf{u}_n approximates the displacement field $\mathbf{u}(n\Delta t)$ and dot denotes time derivative. Remark that in this case, the current time step solution n depends only on past responses. On the contrary, an implicit algorithm, which can be expressed as:

$$\mathbf{u}_n(\mathbf{x}) = f(\dot{\mathbf{u}}_n, \ddot{\mathbf{u}}_n, \mathbf{u}_{n-1}, \dot{\mathbf{u}}_{n-1}, \ddot{\mathbf{u}}_{n-1}, \mathbf{u}_{n-2}, \dot{\mathbf{u}}_{n-2}, \dots) \quad (2.3)$$

exhibits dependency also on the solution of the motion equation evaluated at $t = n\Delta t$ and thus, a coupled algebraic system of equations must be solved. The latter makes implicit schemes more computationally expensive per time step iteration. However, unconditionally stable implicit schemes allows the use of larger time steps to satisfy

the same accuracy requirements. Indeed, explicit schemes are all conditionally stable. That means that the time step size that can be used without getting an unstable solution must be smaller than, or equal to, a critical time step given by the Courant condition [36]. This restriction can lead to the use of a too small time step with respect to the one that would be required to properly represent the physics of the problem. Then, in these cases, an implicit algorithm can be more effective.

Another classification that can be made depends on whether or not the time integration scheme is self-starting. Time stepping procedures where the response at the current time step depends only on the previous time step are self-starting. Otherwise, the time integrator used corresponds to a multistep method (dependency on the responses of the last k time steps).

Moreover, in nonlinear analysis, the choice of the time integration scheme becomes as important as Newton-Raphson equilibrium iterations within each time step. Indeed, even with very tight convergence tolerances for Newton-Raphson iterations (see Sec. 1.3.3), a time integration scheme that is unconditionally stable in a linear analysis may become unstable when nonlinearities are accounted for [11].

In the following, the family of explicit and implicit Newmark time integration schemes will be used for the FE model and the Convolution Quadrature Method, for the BE equations. Therefore, they are briefly addressed in next sections.

2.2.1 Family of Newmark time integration schemes

The family of Newmark time integration schemes [104] are considered as one time step schemes. The reason is because the variables to compute in the current time step depend only on the previous time step, not on several previous time steps (a multi time step scheme). The general Newmark scheme comes from the Taylor expansion of the time function that one wants to compute. In mechanics, the variables to estimate are the displacement $\mathbf{u}(t)$ and the velocity $\dot{\mathbf{u}}(t)$. The general expressions involve two parameters, γ and β , whose value can modify the properties of convergence, stability and consistence of the time integration scheme, e.g. $\beta = 0.25$ and $\gamma = 0.5$ gives an unconditionally stable scheme without numerical dissipation.

The calculation of the displacement and the velocity deals essentially with two phases: one of prediction and the other of correction. The predictors can be directly identified in the Taylor development, they depend only on the previous time step. The two predictors, one for the displacement and the other for the velocity, read:

$$\begin{aligned}\dot{\mathbf{u}}_{n+1}^P &= \dot{\mathbf{u}}_n + \Delta t(1 - \gamma)\ddot{\mathbf{u}}_n \\ \mathbf{u}_{n+1}^P &= \mathbf{u}_n + \Delta t^2\left(\frac{1}{2} - \beta\right)\ddot{\mathbf{u}}_n\end{aligned}\quad (2.4)$$

Therefore, the final expressions of $\mathbf{u}(t)$ and $\dot{\mathbf{u}}(t)$ at the current time step $t = (n + 1)\Delta t$ are:

$$\begin{aligned}\dot{\mathbf{u}}_{n+1} &= \dot{\mathbf{u}}_{n+1}^P + \gamma\Delta t\ddot{\mathbf{u}}_{n+1} \\ \mathbf{u}_{n+1} &= \mathbf{u}_{n+1}^P + \beta\Delta t^2\ddot{\mathbf{u}}_{n+1}\end{aligned}\quad (2.5)$$

In dynamics, the FE equation written at $t = (n + 1)\Delta t$ is generally:

$$\mathbf{M}\ddot{\mathbf{u}}_{n+1} + \mathbf{C}\dot{\mathbf{u}}_{n+1} + \mathbf{K}\mathbf{u}_{n+1} = \mathbf{F}_{n+1}\quad (2.6)$$

Then, it must be chosen for which quantity (displacement, velocity, acceleration) the problem is going to be solved. Depending on which quantity is chosen, Eq. (2.5) must be elaborated and introduced in (2.6) in order to reduce the system to something like:

$$\mathbf{A}\mathbf{x} = \mathbf{B} \quad (2.7)$$

where \mathbf{x} denotes the unknown quantity chosen and \mathbf{A} and \mathbf{B} , the resulting matrix and vectors gathering the predictors and matrices \mathbf{M} , \mathbf{C} , \mathbf{K} . For example, when solving for displacement, which is common in nonlinear problems, matrix \mathbf{A} and vector \mathbf{B} read:

$$\begin{aligned} \mathbf{A} &= \frac{1}{\beta\Delta t^2}\mathbf{M} + \frac{\gamma}{\beta\Delta t}\mathbf{C} + \mathbf{K} \\ \mathbf{B} &= \mathbf{F}_{n+1} + \left(\frac{1}{\beta\Delta t^2}\mathbf{M} + \frac{\gamma}{\beta\Delta t}\mathbf{C}\right)\mathbf{u}_{n+1}^P - \mathbf{C}\dot{\mathbf{u}}_{n+1}^P \end{aligned} \quad (2.8)$$

After predicting and computing the current time step, it follows a phase of correction of the two other quantities. Following the example, they would correspond to the velocity and the acceleration and they would read as:

$$\begin{aligned} \ddot{\mathbf{u}}_{n+1} &= \frac{1}{\beta\Delta t^2}(\mathbf{u}_{n+1} - \mathbf{u}_{n+1}^P) \\ \dot{\mathbf{u}}_{n+1} &= \dot{\mathbf{u}}_{n+1}^P + \gamma\Delta t\ddot{\mathbf{u}}_{n+1} \end{aligned} \quad (2.9)$$

2.2.2 Convolution Quadrature Method

In this section, the Convolution Quadrature Method (CQM) is briefly addressed for the general case of a *sectorial* Laplace transform $F(s)$. For more details, the reader can refer to Lubich [84].

In the framework of a *sectorial* Laplace transform, $F(s)$ is analytic in Σ_φ , which is defined as:

$$\Sigma_\varphi = \left\{s \in \mathbb{C} : |\arg(s - \sigma_0)| < \pi - \varphi, \varphi < \frac{\pi}{2}, \sigma_0 \in \mathbb{R}\right\} \quad (2.10)$$

and, also in Σ_φ , $F(s)$ verifies:

$$|F(s)| \leq M|s|^{-\nu} \quad \text{for some } M, \nu \in \mathbb{R} \quad (2.11)$$

The case of a *non-sectorial* Laplace transform can be easily particularized for $\varphi = \frac{\pi}{2}$. The analyticity domain of $F(s)$ is thus bounded in a half-plane $\operatorname{Re}(s) > \sigma_0 > 0$.

The inverse Laplace transform is then given by

$$f(t) = \frac{1}{2\pi i} \int_{\Gamma} F(s)e^{st} ds, \quad t > 0 \quad (2.12)$$

with Γ a contour in the sector of analyticity, going to infinity with an acute angle to the negative real half-axis and oriented with increasing imaginary part¹. The function $f(t)$ is analytic in $t > 0$ and satisfies:

$$|f(t)| \leq Ct^{\nu-1}e^{\sigma_0 t}, \quad t > 0 \quad (2.13)$$

¹Numerical evaluation of the inverse Laplace transform can be obtained using other (even more performing) integration contours such as Talbot contours or hyperbolas [52, 138].

and is therefore locally integrable if $\nu > 0$ (and absolutely convergent). When $\nu < 0$, the problem is conveniently formulated as in Lubich [86], that is in terms of $F(s) = s^m F_m(s)$ with $m \geq |\nu|$. In that article, the case of convolutions with non-integrable kernel is also addressed.

Under these assumptions, the approximation of a continuous convolution (possibly matrix \times vector²):

$$(f * g)(t) := \int_0^t f(t - \tau)g(\tau) d\tau, \quad 0 \leq t \leq T \quad (2.14)$$

can be evaluated at $t = n\Delta t$, with $n = 0, 1, \dots, N$ and time step $\Delta t > 0$, by using a convolution quadrature, that is:

$$(f * g)(n\Delta t) \approx \sum_{k=0}^n w_{n-k}(\Delta t)g(k\Delta t) \quad (2.15)$$

where the quadrature weights w_n are the coefficients of the generating power series³:

$$\sum_{n=0}^{\infty} w_n(\Delta t)z^n = F\left(\frac{r(z)}{\Delta t}\right) \quad z \in \mathbb{C}, |z| \leq 1. \quad (2.16)$$

Here $r(z)$ is a given rational function, chosen as the quotient of the generating polynomials of a linear multistep method verifying the following assumptions:

1. strongly zero-stability and stability in a neighbourhood of infinity: $r(z)$ is analytic and without zeros in a neighbourhood of the closed unit disk $|z| \leq 1$, with the exception of a zero at $z = 1$;
2. $A(\alpha)$ -stability with $\alpha > \varphi$ of (2.10): $|\arg r(z)| \leq \pi - \alpha$ for $|z| < 1$;
3. consistency of order $P \geq 1$: $\frac{1}{\Delta t}r(e^{-\Delta t}) = 1 + O(\Delta t^P)$ as $\Delta t \rightarrow 0$.

It can be noticed that (2.16) is well-defined if $\frac{r_0}{\Delta t}$ is in the domain of analyticity of $F(s)$, where r_0 denotes $r(z)$ evaluated at $z = 0$. Since $r_0 > 0$ by the conditions on $r(z)$, this is satisfied at least for sufficiently small $\Delta t > 0$. The use of convolution quadrature formulas based on implicit Runge-Kutta methods (such as the Radau IIA schemes) instead of multistep methods is not common for engineering applications [6, 88] and remains a perspective of the present work.

Proof. For the sake of simplicity, the same reasoning of [84] and a similar notation is used in here⁴. Replacing $f(t)$ with expression (2.12) within Eq. (2.14) and exchanging integrals leads to:

$$y(t) = \int_0^t f(t - \tau)g(\tau) d\tau = \frac{1}{2\pi i} \int_{\Gamma} F(s) \underbrace{\int_0^t e^{s(t-\tau)} g(\tau) d\tau}_{x(t;s)} ds \quad (2.17)$$

with Γ the same contour as in (2.12). The inner integral, abbreviated with $x(t; s)$ is a solution of the differential equation of first order:

$$\partial_t x(t; s) = sx(t; s) + g(t) \quad (2.18)$$

²The absolute values on the left-hand sides of the bounds (2.12) and (2.11) are to be interpreted as matrix norms for matrix-valued convolution kernels.

³Quadrature weights w_n can also be interpreted as the inverse Z-transform [67] of $W(z) = F\left(\frac{r(z)}{\Delta t}\right)$, where $z \in \mathbb{C}$ denotes the Z-transform variable.

⁴The same proof can be done by means of the Z-transform theory.

with vanishing initial conditions. Therefore, $\partial_t x(t; s)$ can be approximated at $t = n\Delta t$, $n \geq 0$, by a linear k -step method:

$$\partial_t x(t; s)|_{t=n\Delta t} \approx \frac{\sum_{j=0}^k \alpha_j x_{n+j-k}}{\Delta t} = \sum_{j=0}^k \beta_j (s x_{n+j-k} + g((n+j-k)\Delta t)) \quad (2.19)$$

with equal time steps Δt , the starting values $x_{-k} = \dots = x_{-1} = 0$ and $g \in C[0, \infty)$ extended by 0 to the negative real axis. Coefficients α_j and β_j correspond to the multistep constants. Recall that a linear multistep method applied on a ordinary differential equation of first order, this is for instance $\dot{x}(t) = h(t, x)$, can be generally written at $t = n\Delta t$ as:

$$\sum_{j=0}^k \alpha_j x_{n+j-k} = \Delta t \sum_{j=0}^k \beta_j h(n\Delta t, x_{n+j-k}). \quad (2.20)$$

Unfortunately, this representation of the multistep method does not allow to extract the discrete values x_n which shall be used in (2.17). Multiplying (2.19) by z^n and summing over n from 0 to ∞ we obtain:

$$(\alpha_0 z^k + \dots + \alpha_k) X(z) = (\beta_0 z^k + \dots + \beta_k) \cdot (\Delta t \cdot s X(z) + \Delta t G(z)) \quad (2.21)$$

with the generating (formal) power series

$$X(z) = \sum_{n=0}^{\infty} x_n z^n, \quad G(z) = \sum_{n=0}^{\infty} g(n\Delta t) z^n.$$

Solving this equation for $X(z)$ we find that x_n is the n -th coefficient of the power series $\left(\frac{r(z)}{\Delta t} - s\right)^{-1} G(z)$ where:

$$r(z) = \frac{(\alpha_0 z^k + \dots + \alpha_{k-1} z + \alpha_k)}{(\beta_0 z^k + \dots + \beta_{k-1} z + \beta_k)} \quad (2.22)$$

verifies condition 3. Therefore, the approximation in (2.17) at $t = n\Delta t$ is the n -th coefficient of:

$$\sum_{n=0}^{\infty} y(n\Delta t) z^n = \frac{1}{2\pi i} \int_{\Gamma} F(s) \left(\frac{r(z)}{\Delta t} - s\right)^{-1} G(z) ds = F\left(\frac{r(z)}{\Delta t}\right) G(z) \quad (2.23)$$

where the equality holds by Cauchy's integral formula. By using (2.16) we finally obtain that:

$$y(n\Delta t) = \sum_{k=0}^n w_{n-k}(\Delta t) g(k\Delta t), \quad n = 0, 1, \dots, N \quad (2.24)$$

which corresponds to (2.15). \square

Following notation of Eq. (2.22), some examples of linear multistep methods can be found in Tab. 2.1. Particularly interesting are the backward differentiation formulas (BDF) of order $P \leq 6$, given by $r(z) = \sum_{m=1}^P \frac{1}{m} (1-z)^m$, which correspond to a linear multistep method of Eq. (2.20) with $\beta_j = 0$. In Fig. 2.1 some examples are

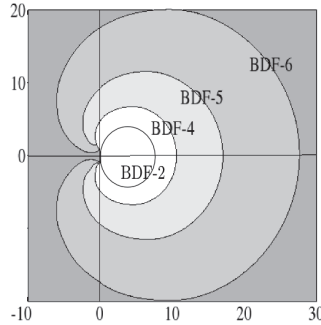


Figure 2.1: Backward differentiation formulas of order P on the complex plane.

Table 2.1: Generating polynomials of some well-known k -step methods of order P .

| Method | Type | $\alpha(z)$ | $\beta(z)$ | k | P |
|------------------------|----------|-------------------------------------|------------------------------|---|---|
| Forward Euler | explicit | $1 - z$ | z | 1 | 1 |
| Trapezoidal Rule | implicit | $1 - z$ | $\frac{1}{2} + \frac{1}{2}z$ | 1 | 2 |
| Backward Euler or BDF1 | implicit | $1 - z$ | 1 | 1 | 1 |
| BDF2 | implicit | $\frac{3}{2} - 2z + \frac{1}{2}z^2$ | 1 | 2 | 2 |

plotted on the complex plane for $|z| = 1$. BDF show, respectively for $P = 1, \dots, 6$, $A(\alpha)$ -stability with $\alpha = 90^\circ, 90^\circ, 88^\circ, 73^\circ, 51^\circ, 18^\circ$. As this dissertation is focused on causal operators (i.e. operators satisfying (2.11) on Σ_φ with $\varphi = \frac{\pi}{2}$) only multistep methods that verify the $A(\alpha)$ -stability condition for $\alpha \leq \varphi = \frac{\pi}{2}$ are considered, that is only multistep methods of order $P \leq 2$ [39].

Therefore, the CQM with an underlying BDF2 method will be considered hereafter for the evaluation of the interaction forces. This method is, in some way, the time discretization method used for the BE system. But the reason of choosing CQM might be found by analyzing its numerical characteristics. Among its main attractive features, one can highlight that they work well for singular kernels and they are specially useful when the Laplace transform of the convolution kernel can be evaluated. They also show excellent stability properties when used for the discretization of integral equations or integro-differential equations of convolution type. This is mainly due to the fact that the stability of a discrete convolution equation depends on the range of the generating function of the weights for $|z| < 1$ [123]. In fact, in Eq. (2.16), the generating function is directly related to the Laplace transform, which somehow determines the stability properties of the continuous convolution equation.

2.3 The Hybrid Laplace-Time Domain Approach

The transient solution of the dynamic equations is obtained by using a time integration scheme. In FE analysis, this time integration scheme is usually based on a single solution procedure, such as the Newmark time integration scheme. On the other hand, in a BE analysis, the system response at each time step depends not only on the response at the previous time step (as classically done in a FE analysis) but also on

all previous states of the system. Therefore, different types of time integration schemes may be used for each type of analysis so that a stable⁵ solution could be guaranteed. Unfortunately, as mentioned on the introduction of this chapter, the stability of either or both BE and FE solutions does not ensure the stability of the coupled BE-FE solution. In order to stabilize the BE-FE coupled time stepping solution, the hybrid Laplace-time approach –denoted hereafter as HLTA– is proposed.

Following the strategy of Lubich [86] to show numerical properties of convolution quadratures, the HLTA is based on the factorisation of the polynomial part of the impedance function $\hat{\mathbf{Z}}(s)$. The formulation of a general mathematical framework is first addressed. It is then particularized to the case of dynamic interaction problems, where the HLTA allows to introduce inertial, damping and stiffness terms in the formulation. The reason to introduce these terms comes from the fact that the unknowns of our problem are not only displacements but also velocities and accelerations (see for instance Newmark’s time integration scheme in Sec. 2.2.1).

In the case of a dynamic soil-structure interaction, it seems convenient to express the interaction forces $t \mapsto \mathcal{L}^{-1}(\hat{\mathbf{Z}}\hat{\mathbf{u}})(t)$ as a linear combination of inertial, damping and stiffness terms instead of hiding all the inertial and damping effects behind the time impedance function. This approach is already used in other kind of dynamic problems, such as fluid-structure interaction (FSI) problems. In fact, in FSI problems, literature proposes similar approaches to compute the aerodynamic forces. They are mostly based on the decomposition of the impedance function defined in the Laplace domain into a second order polynomial and a regular function. This yields in time domain to a linear combination of inertial, damping and stiffness terms [68, 156].

2.3.1 General formulation

Let Ω be a bounded subset of \mathbb{R}^3 with a smooth boundary $\partial\Omega$. Let homogeneous boundary conditions be considered on $\partial\Omega$, except for $\Gamma \subset \partial\Omega$ which represents the interface between Ω and the unbounded subdomain Ω_s . Let an impedance function $s \mapsto \hat{\mathbf{Z}}(s)$, defined on Γ and with inverse Laplace transform $t \mapsto \mathbf{Z}(t)$, $t \in \mathbb{R}$, be analytic on the complex half-plane $\Re(s) > \sigma_0$ and bounded for large s :

$$\|\hat{\mathbf{Z}}(s)\|_{\mathcal{H}} \leq C(\sigma_0) |s|^\mu, \quad \text{with } C(\sigma_0), \mu \in \mathbb{R} \quad (2.25)$$

where $s \in \mathbb{C}$ denotes the Laplace variable and $\|\cdot\|_{\mathcal{H}}$ the norm of an appropriate Hilbert space \mathcal{H} . Remark that μ corresponds to $-\nu$ of Lubich’s notation of Eq. (2.11).

In this framework, the problem to be considered is the evaluation of a convolution integral between two causal functions like:

$$(\mathbf{Z} * \mathbf{u})(t) = \int_0^t \mathbf{Z}(t - \tau) \mathbf{u}(\tau) d\tau, \quad 0 \leq t \leq T \quad (2.26)$$

where the impedance $\mathbf{Z}(t)$ is the kernel of the convolution and $\mathbf{u}(t)$ denotes a sufficiently time-differentiable field on Γ . Recall that a causal function is zero for $t < 0$. Hereafter, continuous fields are assumed to be discretized in the space domain.

⁵An integration scheme is said to be stable if the numerical solution, under any initial conditions, does not grow without bound (Bathe, 1996).

Let $\hat{\mathbf{Z}}(s) = \hat{\mathbf{Z}}_m(s)\hat{\mathbf{P}}(s)$ with $\hat{\mathbf{P}}(s)$ a s -polynomial function of degree $m \geq \mu > 0$ with matrix-valued coefficients of dimension n_Γ , the number of degrees-of-freedom on the interface Γ (for $\mu \leq 0$, polynomial $\hat{\mathbf{P}}(s)$ can be chosen as the identity matrix):

$$\hat{\mathbf{P}}(s) = \sum_{p=0}^m \mathbf{\Lambda}_p s^p \quad (2.27)$$

where $\mathbf{\Lambda}_p \in \mathbb{M}_{n_\Gamma}^+(\mathbb{R})$.

Following this polynomial decomposition, the distributional convolution kernel $\mathbf{Z}(t)$ is thus written as the product of a sum of p -order derivatives ($0 \leq p \leq m$), which are weighted by the matrix-valued coefficients $\mathbf{\Lambda}_p$, and a continuous exponentially bounded function $\mathbf{Z}_m(t) = \mathcal{L}^{-1}(\hat{\mathbf{Z}}_m(s))$, i.e.

$$\mathbf{Z}(t) = \left(\mathbf{Z}_m * \sum_{p=0}^m \mathbf{\Lambda}_p \frac{d^p \delta}{dt^p} \right) (t) \quad (2.28)$$

where $\delta(t)$ denotes Dirac's delta distribution. Remark that, by Cauchy's integral theorem, $\mathbf{Z}_m(t)$ is a causal function [86]. Thus:

$$(\mathbf{Z} * \mathbf{u})(t) = \sum_{p=0}^m \left(\int_0^t \mathbf{Z}_m(\tau) \mathbf{\Lambda}_p \mathbf{u}^{(p)}(t - \tau) d\tau \right) \quad (2.29)$$

with $\mathbf{u}(t)$ a smooth causal function.

Therefore, if $\Delta t > 0$ denotes the time step, the Convolution Quadrature Method [84] approximates the convolution integral in Eq. (2.29) by a discrete convolution as:

$$(\mathbf{Z} * \mathbf{u})(n\Delta t) = \sum_{k=1}^n \left(\Psi_0^{n-k+1} \mathbf{u}_k + \dots + \Psi_m^{n-k+1} \mathbf{u}_k^{(m)} \right) \quad (2.30)$$

where $\mathbf{u}_k^{(p)}$ approximates the p -derivative of displacement at $t = k\Delta t$, $\mathbf{u}^{(p)}(k\Delta t)$, and coefficients $\{\Psi_j^i\} \in \mathbb{M}_{n_\Gamma}^+(\mathbb{R})$ ($i = 1..n$, $j = 1..m$) correspond to the weights of the generating power series:

$$\sum_{k=0}^{+\infty} \Psi_j^k z^k = \hat{\mathbf{Z}}_m(s_{\Delta t}) \mathbf{\Lambda}_j \quad (2.31)$$

The complex sampled values $s_{\Delta t}$ of impedance are given by a rational function of a linear multistep method of order P satisfying strong A -stability conditions. In this dissertation, let $s_{\Delta t}$ be $\frac{r(z)}{\Delta t}$ where $r(z)$ is the backward differentiation formula of $P = 2$ reading $r(z) = \frac{3}{2} - 2z + \frac{1}{2}z^2$.

2.3.2 Application to SSI problems: *MKC formulation*

The soil impedance matrix, i.e. the discretized version of the impedance operator, maps any displacement vector of the soil-structure interface to its corresponding force vector on the same boundary. Recall that all continuous fields are discretized in space and thus the problem is addressed in terms of matrices and vectors.

The dynamic soil impedance matrix, assumed analytic in the half-plane $\Re(s) > \sigma_0$ for causality purposes, will be considered in the following form:

$$\hat{\mathbf{Z}}(s) = \hat{\mathbf{Z}}_{sin}(s) + \hat{\mathbf{Z}}_{nsin}(s) \quad (2.32)$$

where $\hat{\mathbf{Z}}_{sin}(s)$ denotes the *singular* part of the impedance and $\hat{\mathbf{Z}}_{nsin}(s)$ denotes a regular function whose inverse Laplace transform:

$$\mathbf{Z}_{nsin}(t) = \frac{1}{2\pi i} \int_{\sigma_0 + i\mathbb{R}} e^{st} \hat{\mathbf{Z}}_{nsin}(s) ds \quad (2.33)$$

defines a continuous, exponentially bounded function which vanishes for $t < 0$. A *singular* impedance is assumed hereafter to be an impedance that is not bounded in the high frequency range. On the contrary, a non-singular impedance would tend to zero for high values of the frequency and thus, its inverse Laplace transform exists in the classical sense.

For the case of an impedance matrix coming from a FE formulation, Cottureau [35] showed that the singular part can be written as:

$$\hat{\mathbf{Z}}_{sin}(s) = \mathbf{M}_\Gamma s^2 + \mathbf{C}_\Gamma s + \mathbf{K}_\Gamma \quad (2.34)$$

where \mathbf{K}_Γ , \mathbf{C}_Γ and \mathbf{M}_Γ are the matrices modelling the soil inertial, damping and stiffness effects. Note that this expression explicitly satisfy condition stated in Eq. (2.25). By using some of the well-known properties of the Laplace transform, it can be verified that the inverse Laplace transform of $\hat{\mathbf{Z}}_{sin}(s)$ is defined in terms of distributions, particularly, it involves the first and second time derivatives of Dirac's delta function:

$$\mathbf{Z}_{sin}(t) = \mathbf{M}_\Gamma \ddot{\delta}(t) + \mathbf{C}_\Gamma \dot{\delta}(t) + \mathbf{K}_\Gamma \delta(t) \quad (2.35)$$

Recall that $\mathbf{Z}_{sin}(t)$ corresponds to the time convolution kernel of the interaction forces. The evaluation of this kind of –distributional– convolution integrals involving such a singular behaviour is not trivial and thus, a CQM-based time discretization seems to be a well-adapted strategy for this type of problem.

Nevertheless, paying attention to the physical units of Eq. (2.26) which are actually those of a force (Newtons), it seems natural to express the convolution not only in terms of displacements, but also in terms of accelerations and velocities. To that end, the polynomial part $\hat{\mathbf{P}}(s)$ of the impedance is factorized yielding to:

$$\hat{\mathbf{Z}}(s) = \hat{\mathbf{Z}}_m(s) \hat{\mathbf{P}}(s) = \hat{\mathbf{Z}}_m(s) \left(\tilde{\mathbf{M}}_\Gamma s^2 + \tilde{\mathbf{C}}_\Gamma s + \tilde{\mathbf{K}}_\Gamma \right) \quad (2.36)$$

where $\tilde{\mathbf{K}}_\Gamma$, $\tilde{\mathbf{C}}_\Gamma$ and $\tilde{\mathbf{M}}_\Gamma$ are respectively some estimates of the matrices \mathbf{K}_Γ , \mathbf{C}_Γ and \mathbf{M}_Γ presented in Eq. (2.34). Some procedures to determine these estimates are described in Sec. 2.3.3.

Therefore, the convolution can be written in terms of the Laplace transform as follows:

$$(\mathbf{Z} * \mathbf{u})(t) = \frac{1}{2\pi i} \int_{\sigma_0 + i\mathbb{R}} \hat{\mathbf{Z}}_m(s) \hat{\mathbf{P}}(s) \hat{\mathbf{u}}(s) e^{st} ds \quad (2.37)$$

The polynomial function $\hat{\mathbf{P}}(s)$ acts thus over the displacement as a differential operator and Eq. (2.26) finally reads:

$$(\mathbf{Z} * \mathbf{u})(t) = (\mathbf{Z}_m * \tilde{\mathbf{M}}_\Gamma \ddot{\mathbf{u}})(t) + (\mathbf{Z}_m * \tilde{\mathbf{C}}_\Gamma \dot{\mathbf{u}})(t) + (\mathbf{Z}_m * \tilde{\mathbf{K}}_\Gamma \mathbf{u})(t) \quad (2.38)$$

where the interaction force vector (denoted hereafter by $\mathbf{R}_\Gamma(t)$) involves in its calculation the evaluation of displacement, velocity and acceleration convolutions.

If a time step $\Delta t > 0$ is chosen, the convolution integral can be discretized again as in Eq. (2.30) leading to:

$$\mathbf{R}_{\Gamma,n} = \sum_{k=1}^n \left(\Psi_2^{n-k+1} \ddot{\mathbf{u}}_k + \Psi_1^{n-k+1} \dot{\mathbf{u}}_k + \Psi_0^{n-k+1} \mathbf{u}_k \right) \quad (2.39)$$

where matrices multiplying displacement vectors \mathbf{u}_k , velocity vectors $\dot{\mathbf{u}}_k$ and acceleration vectors $\ddot{\mathbf{u}}_k$ are given by:

$$\begin{aligned} \Psi_0^k &= \mathbf{Z}_m^k \tilde{\mathbf{K}}_\Gamma \\ \Psi_1^k &= \mathbf{Z}_m^k \tilde{\mathbf{C}}_\Gamma \\ \Psi_2^k &= \mathbf{Z}_m^k \tilde{\mathbf{M}}_\Gamma \end{aligned} \quad (2.40)$$

From a numerical point of view, these three convolutions (see Eq. (2.39)) are just unknown at $t = n\Delta t$, since all previous time steps have already been computed. Therefore, Eq. (2.39) can be written by isolating instant n as:

$$\mathbf{R}_{\Gamma,n} = \Psi_2^1 \ddot{\mathbf{u}}_n + \Psi_1^1 \dot{\mathbf{u}}_n + \Psi_0^1 \mathbf{u}_n + \mathbf{R}_{\Sigma(n-1)} \quad (2.41)$$

Consequently, coefficients $\Psi_i^1 (i = 0, 1, 2)$ are respectively related to instantaneous stiffness, damping and inertia terms and $\mathbf{R}_{\Sigma(n-1)}$ depends only on previous time steps:

$$\mathbf{R}_{\Sigma(n-1)} = \sum_{k=1}^{n-1} \left(\Psi_2^{n-k+1} \ddot{\mathbf{u}}_k + \Psi_1^{n-k+1} \dot{\mathbf{u}}_k + \Psi_0^{n-k+1} \mathbf{u}_k \right) \quad (2.42)$$

Eigenmode decomposition

In order to reduce the computational cost, the kinematics of the SSI interface can be approximated by the linear combination of N eigenmodes ϕ_j , $j = 1, \dots, N$. That is, the nodal displacement vector corresponding to degrees-of-freedom on Γ can be written as:

$$\mathbf{u}_\Gamma(t) = \sum_{j=1}^N \alpha_j(t) \phi_j \quad (2.43)$$

where $\alpha_j(t)$ correspond to the so-called generalized or modal coordinates. If ϕ_j (also known as Ritz vectors) are collected in a matrix Φ_Γ and the modal coordinates are collected in a vector $\alpha_\Gamma(t)$, Eq. (2.43) reads:

$$\mathbf{u}_\Gamma(t) = \Phi_\Gamma \alpha_\Gamma(t) \quad (2.44)$$

If the nodal displacement vector is expressed in this Ritz basis, the interaction forces should be projected in the same basis, that is:

$$\mathbf{f}_\Gamma(t) = \Phi_\Gamma^T \mathbf{R}_\Gamma(t) \quad (2.45)$$

where $\mathbf{f}_\Gamma(t)$ stands for the modal SSI interaction forces.

Once the problem is discretized in the time domain, Eq. (2.44) and Eq. (2.39) can be combined and thus, Eq. (2.44) can be written at $t = n\Delta t$:

$$\mathbf{f}_{\Gamma,n} = \sum_{k=1}^n \left(\Phi_{\Gamma}^T \Psi_2^{n-k+1} \Phi_{\Gamma} \ddot{\alpha}_{\Gamma,k} + \Phi_{\Gamma}^T \Psi_1^{n-k+1} \Phi_{\Gamma} \dot{\alpha}_{\Gamma,k} + \Phi_{\Gamma}^T \Psi_0^{n-k+1} \Phi_{\Gamma} \alpha_{\Gamma,k} \right) \quad (2.46)$$

By taking $\check{\Psi}_i^k = \Phi_{\Gamma}^T \Psi_i^k \Phi_{\Gamma}$ ($i = 0, 1, 2$) previous equation becomes:

$$\mathbf{f}_{\Gamma,n} = \sum_{k=1}^n \left(\check{\Psi}_2^{n-k+1} \ddot{\alpha}_{\Gamma,k} + \check{\Psi}_1^{n-k+1} \dot{\alpha}_{\Gamma,k} + \check{\Psi}_0^{n-k+1} \alpha_{\Gamma,k} \right) \quad (2.47)$$

where $\check{\Psi}_0^0$, $\check{\Psi}_1^0$ and $\check{\Psi}_2^0$ corresponds, respectively, to the generalized (or modal) instantaneous matrices of stiffness, damping and mass associated to the soil. In fact, this eigenmode decomposition allows the computation of the soil modal impedance matrix with a reduced computational effort.

Flexibility formulation

Instead of evaluating $\mathbf{R}_{\Gamma}(t)$ as a function of $\mathbf{Z}(t)$, interaction forces can be written as a function of $\mathbf{F}(t)$ which is the inverse Laplace transform of $\hat{\mathbf{Z}}^{-1}(s)$. Such a formulation will be called a *flexibility formulation*, otherwise, it will be referred to as *stiffness formulation* [144, 145, 148].

When a flexibility formulation is adopted, the convolution integral to evaluate is not the one in Eq. (2.39) but the following one:

$$\mathbf{u}_n = (\mathbf{F} * \mathbf{Q})(n\Delta t) = \sum_{k=1}^n \Theta^{n-k+1} \mathbf{Q}_k \quad (2.48)$$

where $\mathbf{F}(t)$ is the flexibility matrix (the inverse of the impedance matrix $\mathbf{Z}(t)$) and $\mathbf{Q}(t)$ ⁶ are the interaction forces. Assuming that $\hat{\mathbf{Z}}(s)$ is as Eq. (2.34), it can be verified that the flexibility matrix also satisfies the condition of Eq. (1.42). In fact, for $\mu < 0$ (for $\mu = -2$ indeed) the CQM can be straightforwardly applied without using a polynomial factorisation. Therefore, if $\hat{\mathbf{F}}(s)$ denotes the Laplace transform of $\mathbf{F}(t)$, the matrix coefficients Θ^k correspond to the coefficients of the power series:

$$\sum_{n=0}^{\infty} \Theta_n(\Delta t) z^n = \hat{\mathbf{F}} \left(\frac{r(z)}{\Delta t} \right) \quad z \in \mathbb{C}, |z| \leq 1. \quad (2.49)$$

In order to compute the interaction forces vector \mathbf{Q}_n at time $t = n\Delta t$, equation (2.48) is rearranged as follows:

$$\mathbf{Q}_n = (\Theta^1)^{-1} \mathbf{u}_n - (\Theta^1)^{-1} \sum_{k=1}^{n-1} \Theta^{n-k+1} \mathbf{Q}_k \quad (2.50)$$

where $(\Theta^1)^{-1}$ is the instantaneous stiffness term.

⁶In order to avoid confusions, the interaction forces will be denoted either $\mathbf{Q}(t)$ or $\mathbf{R}(t)$ when either a flexibility or a stiffness formulation is respectively adopted.

Equation (2.50) shows that interaction forces can be calculated in terms of displacements and the interaction forces at previous time steps. If one wants inertia and damping terms to appear, an other formulation has to be proposed:

$$\mathbf{Q}_n = \left(\tilde{\Theta}^1\right)^{-1} \left(\mathbf{M}_\Gamma \ddot{\mathbf{u}}_n + \mathbf{C}_\Gamma \dot{\mathbf{u}}_n + \mathbf{K}_\Gamma \mathbf{u}_n\right) - \left(\tilde{\Theta}^1\right)^{-1} \sum_{k=1}^{n-1} \tilde{\Theta}^{n-k+1} \mathbf{Q}_k \quad (2.51)$$

where the matrix coefficients $\tilde{\Theta}_k$ are now the coefficients of the power series:

$$\sum_{n=0}^{\infty} \tilde{\Theta}_n(\Delta t) z^n = \hat{\mathbf{F}}_* \left(\frac{r(z)}{\Delta t} \right) \quad z \in \mathbb{C}, |z| \leq 1. \quad (2.52)$$

with $\hat{\mathbf{F}}_*(s)$ denoting the Laplace transform of:

$$\hat{\mathbf{F}}_*(s) = \left(\mathbf{M}_\Gamma s^2 + \mathbf{C}_\Gamma s + \mathbf{K}_\Gamma\right) \hat{\mathbf{F}}(s) \quad (2.53)$$

Remark that in Eq. (2.51) $(\tilde{\Theta}^1)^{-1} \mathbf{M}_\Gamma$, $(\tilde{\Theta}^1)^{-1} \mathbf{C}_\Gamma$, $(\tilde{\Theta}^1)^{-1} \mathbf{K}_\Gamma$ are thus the instantaneous inertia, damping and stiffness matrix of the unbounded soil domain.

2.3.3 MKC identification

As seen before, $\tilde{\mathbf{K}}_\Gamma$, $\tilde{\mathbf{C}}_\Gamma$ and $\tilde{\mathbf{M}}_\Gamma$ correspond to some estimates of the real \mathbf{K}_Γ , \mathbf{C}_Γ and \mathbf{M}_Γ matrices associated to the soil impedance matrix within a FE formulation. However, in the present case, only the BE soil impedance matrix is provided at some complex frequencies. Assuming that the soil impedance matrix should be the same either within a FE formulation or a BE one, the FE matrices $\tilde{\mathbf{K}}_\Gamma$, $\tilde{\mathbf{C}}_\Gamma$ and $\tilde{\mathbf{M}}_\Gamma$ can be approximated by means of the BE soil impedance samples by using identification techniques that can be found in the literature.

All identification methods start with the assumption on the form of the soil impedance operator and, in general, the use of an equivalent lumped-parameter model is recommended [110]. Indeed, the SSI convolution appearing in dynamic SSI problems, is no more necessary to be computed. However, stiffness and damping terms are not enough to get accurate results, and a virtual mass should also be considered [103]. These parameters depend on the type of foundation and soil profile. The works of Nakamura [99, 100] were for instance focused on rigid foundations with homogeneous or layered soils. They were afterwards extended for the case of hysteretic damped soil impedance functions [62, 102], where the Hilbert transform can be used to deal with causality problems.

Other common methods assume that the soil impedance matrix can be expressed as a rational function, such as:

$$\hat{\mathbf{Z}}(i\omega) = \frac{\hat{\mathbf{N}}(i\omega)}{\hat{\mathbf{q}}(i\omega)} \quad (2.54)$$

with $\hat{\mathbf{q}}$ being a polynomial of degree P and with $\hat{\mathbf{N}}$ being a matrix-valued polynomial of $(i\omega)$ of degree $P+2$. The rational approximation is obtained by means of available samples of the soil impedance operator at some (complex) frequencies and an optimization algorithm. The most employed optimization techniques include nonlinear

least-squares [101] and the hybrid genetic-simplex algorithm [45]. However, as the impedance constitutes a stable system, zeros and poles of the rational function are enforced to lie on the left-half complex s plane. Some other constraints that have to be taken into account are, for instance, the positive-definiteness of matrices and the causality. Among these methods, there is the hidden state variable method [35]. It is based on the approximation of the soil impedance to a lumped-parameter model by considering a set of hidden degrees-of-freedom defined on the interior of the soil domain.

2.4 Coupling to the time integration scheme used for the FE system

As seen before, a Newmark time integration scheme is used for the FE equations. For the BE system, a CQM with an underlying linear multistep method is employed. The dynamic SSI problem is then solved by coupling both FE and BE systems. This BE-FE coupling is actually materialized in the form of SSI forces, i.e. a convolution integral that has to be evaluated in the time domain. In the following, the way how this coupling is implemented and some numerical stability issues are discussed.

In this section the coupled scheme is presented for both explicit and implicit schemes of Newmark integration method. A brief explanation on stability properties is also provided.

2.4.1 Stability properties

As seen before, a time integration procedure is stable when the integration solution does not increase artificially after some time steps (the number of time steps is related to the fundamental period of the system). But stability can also be defined in terms of perturbations: any undesired initial condition at time step n (due for instance to a computer error of precision), does not grow during the next time steps of integration.

In order to study the stability of a single time step⁷ integration scheme, time discretized equations have to be elaborated to obtain a system of equations expressed as:

$$\mathbf{U}_n = \mathbf{G}\mathbf{U}_{n-1} + \mathbf{L}_{n-1} \quad (2.55)$$

where matrix \mathbf{G} denotes the growth matrix and vector \mathbf{U}_n , the state vector collecting, for dynamic problems, the nodal displacements and velocities $[\mathbf{U}_n^T, \dot{\mathbf{U}}_n^T]^T$. Vector \mathbf{L}_{n-1} depends on the excitation at both $t = (n-1)\Delta t$ and $t = n\Delta t$. The corresponding time integration procedure is said to be stable if the modulus of all the eigenvalues of \mathbf{G} is less than, or equal to, one. Indeed, if a perturbation $\delta\mathbf{U}_0$ on initial conditions is considered, the error will be damped during the time integration:

$$\delta\mathbf{U}_n = \mathbf{G}\delta\mathbf{U}_{n-1} = \mathbf{G}^n \delta\mathbf{U}_0. \quad (2.56)$$

Nevertheless, the stability analysis of the HLTA is much more complicated. In this case, the time integration scheme used for the FE set of equations is coupled to a

⁷For multistep methods, stability analyses in the time domain can be done using the similar approach of Romero [121].

linear multistep method. Since the linear multistep method is somehow hidden behind the CQM, an equivalent time scheme must be found to obtain a system like the one in Eq. (2.55). Thus, the convolution integral that corresponds to the SSI interaction forces should be written in terms of responses at previous time steps. To illustrate this point, let interaction forces $\mathbf{R}_{\Gamma,n}$ on Γ be written analogously to Eq. (2.17) as:

$$\mathbf{R}_{\Gamma,n} = \frac{1}{2\pi i} \int_{\Gamma} \hat{\mathbf{Z}}(s) \mathbf{x}_n(s) ds \quad (2.57)$$

where $\hat{\mathbf{Z}}(s)$ stands for soil impedance matrix in the Laplace domain ($s \in \mathbb{C}$). If, for the sake of simplicity, a BDF of first order is used for the CQM discretization, Eq. (2.18) can be expressed as:

$$\frac{\mathbf{x}_n(s) - \mathbf{x}_{n-1}(s)}{\Delta t} = s \mathbf{x}_n(s) + \mathbf{g}_n \quad (2.58)$$

where \mathbf{g}_n corresponds to the nodal displacement at the SSI interface. By combining Eq. (2.57) and Eq. (2.58), one gets to the following:

$$\mathbf{R}_{\Gamma,n} = \frac{1}{2\pi i} \int_{\Gamma} \frac{\hat{\mathbf{Z}}(s)}{1 - s\Delta t} \mathbf{x}_{n-1}(s) ds + \frac{1}{2\pi i} \int_{\Gamma} \frac{\hat{\mathbf{Z}}(s)}{1 - s\Delta t} \mathbf{g}_n ds \quad (2.59)$$

which, by Cauchy's integral formula, finally results in:

$$\mathbf{R}_{\Gamma,n} = \frac{1}{\Delta t} \hat{\mathbf{Z}}(\Delta t^{-1}) \mathbf{x}_{n-1}(\Delta t^{-1}) + \hat{\mathbf{Z}}(\Delta t^{-1}) \mathbf{g}_n \quad (2.60)$$

Such an equation can be easily introduced in the equation of motion and, after obtaining the corresponding equation (2.55), the eigenvalue problem associated with \mathbf{G} should be worked out. However, $\mathbf{x}_{n-1}(\Delta t^{-1})$ is not defined at $s = \Delta t^{-1}$ and thus stability analysis becomes unfeasible in this way. Further research should be done on this subject, which could actually be an entire topic of dissertation. In particular, it would be interesting to explore other approaches such as energy-based techniques.

Although numerical stability has not been possible to be proved, this property will be investigated throughout several numerical examples.

2.4.2 Implicit algorithm

Let the degrees-of-freedom of the structure be denoted by the subindex 1 and those of the interface, by 2. If $\mathbf{u}_n = [\mathbf{u}_{1,n}^T \mathbf{u}_{2,n}^T]^T$ is the displacement vector at $t = n\Delta t$, then:

$$\begin{bmatrix} \mathbf{M}_{11} & \mathbf{M}_{12} \\ \mathbf{M}_{21} & \mathbf{M}_{22} \end{bmatrix} \ddot{\mathbf{u}}_n + \begin{bmatrix} \mathbf{C}_{11} & \mathbf{C}_{12} \\ \mathbf{C}_{21} & \mathbf{C}_{22} \end{bmatrix} \dot{\mathbf{u}}_n + \begin{bmatrix} \mathbf{K}_{11} & \mathbf{K}_{12} \\ \mathbf{K}_{21} & \mathbf{K}_{22} \end{bmatrix} \mathbf{u}_n + \begin{bmatrix} \mathbf{0} \\ \mathbf{R}_n \end{bmatrix} = \mathbf{F}_n^{ext} \quad (2.61)$$

where \mathbf{R}_n denotes the numerical approximation of the interaction forces at instant $t = n\Delta t$.

Introducing Eq. (2.41) into (2.61) and solving for the displacement by means of a Newmark scheme, the following equation is obtained:

$$\begin{bmatrix} \mathbf{A}_{11} & \mathbf{A}_{12} \\ \mathbf{A}_{21} & \tilde{\mathbf{A}}_{22} \end{bmatrix} \mathbf{u}_n = \tilde{\mathbf{B}}_n = \mathbf{B}_n - \begin{bmatrix} \mathbf{0} \\ \mathbf{R}_{\Sigma(n-1)} \end{bmatrix} \quad (2.62)$$

where \mathbf{A} and \mathbf{B}_n denote the same Newmark equations defined in Sec. 2.2.1, except for \mathbf{A}_{22} which has to be modified as follows:

$$\mathbf{A}_{22} = \frac{1}{\beta\Delta t^2} (\mathbf{M}_{22} + \Psi_2^1) + \frac{\gamma}{\beta\Delta t} (\mathbf{C}_{22} + \Psi_1^1) + (\mathbf{K}_{22} + \Psi_0^1) \quad (2.63)$$

The terms Ψ_2^1 , Ψ_1^1 , Ψ_0^1 in equation (2.63) modify the condition number of the equivalent stiffness matrix \mathbf{A} and therefore, their value have an impact on the convergence of the solution. Contrary to the Newmark forces $\tilde{\mathbf{B}}_n$, which have to be updated at each time step, \mathbf{A} is constant and can be computed once for all.

When the HLTA is considered with a flexibility formulation, interaction forces are denoted for clarity by \mathbf{Q}_n instead of \mathbf{R}_n . In this case, it is not Eq. (2.41) but Eq. (2.50) which has to be introduced in Eq. (2.61). Following the same kind of reasoning, the following equations are finally obtained:

$$\mathbf{A}_{22} = \frac{1}{\beta\Delta t^2} \mathbf{M}_{22} + \frac{\gamma}{\beta\Delta t} \mathbf{C}_{22} + \left(\mathbf{K}_{22} + (\Theta^1)^{-1} \right) \quad (2.64)$$

$$\tilde{\mathbf{B}}_n = \mathbf{B}_n + \begin{bmatrix} \mathbf{0} \\ \mathbf{Q}_{\Sigma(n-1)} \end{bmatrix} \quad (2.65)$$

Remark that when a flexibility formulation is considered, all the interaction forces $\{\mathbf{R}_i\}$ ($i = 1, \dots, n-1$) must be stored during all the analysis.

2.4.3 Explicit algorithm

The explicit algorithm corresponds to the case where $\beta = 0$, i.e. the predicted displacements are the final ones. It is important to notice that an explicit algorithm is interesting for diagonal matrices and therefore, \mathbf{A}_{12} and \mathbf{A}_{21} are assumed to be zero. Solving for the acceleration, one obtains:

$$\begin{bmatrix} \mathbf{A}_{11} & \mathbf{A}_{12} \\ \mathbf{A}_{21} & \mathbf{A}_{22} \end{bmatrix} \ddot{\mathbf{u}}_n = \mathbf{B}_n - \begin{bmatrix} \mathbf{0} \\ \Psi_1^1 \dot{\mathbf{u}}_{2,n}^P + \Psi_0^1 \mathbf{u}_{2,n}^P + \mathbf{R}_{\Sigma(n-1)} \end{bmatrix} \quad (2.66)$$

where \mathbf{B}_n is the Newmark equivalent vector of forces associated to the explicit scheme. The Newmark operator applying on the acceleration is different than the one applying on the displacement and because of \mathbf{R}_n , the term \mathbf{A}_{22} must also be modified:

$$\mathbf{A}_{22} = \mathbf{M}_{22} + \Psi_2^1 + \gamma\Delta t (\mathbf{C}_{22} + \Psi_1^1) \quad (2.67)$$

It is interesting to notice that, as for an implicit algorithm, the Newmark operator remains constant during all the resolution procedure while the right-hand side of the equation has to be computed for each time step.

2.5 Comparison with the Hybrid Frequency-Time domain Approach

As in the previous section, the problem here remains essentially the same, i.e. *solving a convolution integral in the time domain in order to deal with nonlinear SSI problems*. However, the main difference from the previous section is that, in this case, the convolution kernel is not computed in the Laplace domain but in the frequency domain. Such an approach will thus be called hereafter a hybrid frequency-time domain approach (HFTA), in contrast with the Hybrid Laplace-Time domain Approach (HLTA).

When a hybrid frequency-time domain procedure is adopted, the CQM is no more well-adapted. Indeed, the CQM needs the convolution kernel $\mathbf{Z}(t)$ to be known in the complex plane, that is its Laplace transform $\mathcal{L}\mathbf{Z}(t) : \mathbb{C} \rightarrow \mathbb{C}$, and, in the Fourier domain, the support of the impedance is the real axis ($\mathcal{F}\mathbf{Z}(t) : \mathbb{R} \rightarrow \mathbb{C}$, where \mathcal{F} denotes the Fourier transform operator). Moreover, the use of a HFTA involves the choice of time interpolation functions for the interaction forces.

In the frequency domain, real and imaginary parts of the dynamic stiffness matrix tend to infinity for large ω . A stiffness formulation thus results in numerical difficulties when evaluating its inverse Fourier transform at time $t = 0$. Therefore, a flexibility formulation should be rather employed in the frequency domain [94]. In fact, real and imaginary parts of the flexibility matrix tend to zero at infinity. But, even if it performs better than the stiffness formulation, the non-zero value of the flexibility at high frequencies (Gibbs phenomenon) has sometimes non-causal effects on the time domain function. Fortunately, this problem can be overcome with the extrapolation of the flexibility up to higher frequencies or by using low-pass time interpolation functions [94]. Hence, the main inconvenients of working with a flexibility formulation are the resulting computational cost and the possible inversion problems due to a singular stiffness matrix (particularly in the case of a modal basis analysis). To avoid this formulation, one may expect to attenuate the instabilities of a stiffness formulation by using an approach close to the HLTA, that is:

$$\hat{\mathbf{Z}}(i\omega) = \hat{\mathbf{Z}}_m(i\omega)\hat{\mathbf{P}}(i\omega) = \hat{\mathbf{Z}}_m(i\omega) \left(-\omega^2\tilde{\mathbf{M}}_\Gamma + i\omega\tilde{\mathbf{C}}_\Gamma + \tilde{\mathbf{K}}_\Gamma \right) \quad (2.68)$$

Since $\hat{\mathbf{Z}}_m(i\omega)$, which is the function to be integrated over all the frequencies, tends to zero at infinity, no numerical difficulties should appear at $t = 0$ (except for the Gibbs phenomenon). However, the distributional behaviour $\hat{\mathbf{Z}}_m(i\omega)$ is still present in the formulation in most of cases and thus, numerical instabilities cannot be removed from the calculation. CQM properties seem to be what actually smoothes these numerical problems and what also reduces the sensitivity to the size of the time step. Certainly, the use of closed contours of integration is one of the reasons.

In order to illustrate what is stated above, the Hybrid Frequency-Time domain Approach proposed by François [53] has been chosen as a frequency-based approach. This approach relies on a flexibility formulation that is first addressed in the following subsection. Both approaches, HLTA and François' HFTA, are then tested on a spring-dashpot-mass lumped-parameter model. The main goal of the present discussion is to provide some insight on their advantages and inconvenients when the interaction forces must be evaluated in the time domain. The model considered is thus as simple as possible and shows a fully linear behaviour.

2.5.1 Frequency-based formulation for the time evaluation of the SSI forces

When a flexibility formulation is taken into account, the convolution integral to solve becomes:

$$\mathbf{u}(t) = \int_0^t \mathbf{F}(\tau) \mathbf{Q}(t - \tau) d\tau \quad (2.69)$$

where $\mathbf{Q}(t)$ denotes the interaction forces between the soil and the structure.

The interaction forces $\mathbf{Q}(t)$ are discretized in the time domain:

$$\mathbf{Q}(t) = \sum_{k=1}^{+\infty} \phi(t - k\Delta t) \mathbf{Q}_k \quad (2.70)$$

The approach developed in François [53] is followed here. As a result, for the time interpolation function $\phi(t)$, the linear time interpolation function used commonly in time domain boundary element discretization has been chosen:

$$\phi(t) = \begin{cases} 1 - \frac{|t|}{\Delta t} & \text{if } -\Delta t \leq t \leq \Delta t \\ 0 & t \geq \Delta t \text{ or } t \leq -\Delta t \end{cases},$$

Substituting expression of Eq. (2.70) into Eq. (2.69), the displacement $\mathbf{u}(t)$ reads:

$$\mathbf{u}(t) = \int_0^t \mathbf{F}(\tau) \left(\sum_{k=1}^{+\infty} \phi(t - \tau - k\Delta t) \mathbf{Q}_k \right) d\tau \quad (2.71)$$

Changing the order of integration and summation yields:

$$\mathbf{u}(t) = \sum_{k=1}^{+\infty} \left(\int_0^t \mathbf{F}(\tau) \phi(t - \tau - k\Delta t) d\tau \right) \mathbf{Q}_k \quad (2.72)$$

Then, the displacement \mathbf{u}_n at time $t = n\Delta t$ is obtained as:

$$\mathbf{u}_n = \sum_{k=1}^{+\infty} \left(\int_0^{n\Delta t} \mathbf{F}(\tau) \phi((n - k)\Delta t - \tau) d\tau \right) \mathbf{Q}_k \quad (2.73)$$

Due to causality, the summation $\sum_{k=1}^{+\infty}$ is limited up to $k = n$, since the displacement solution at time $t = n\Delta t$ is only influenced by the interaction forces \mathbf{Q}_k with $k \leq n$. Eq. (2.73) is then rearranged as follows:

$$\mathbf{u}_n = \sum_{k=1}^n \left(\int_0^{(n-k+1)\Delta t} \mathbf{F}(\tau) \phi((n - k)\Delta t - \tau) d\tau \right) \mathbf{Q}_k \quad (2.74)$$

where the integration is performed from 0 to $(n - k + 1)\Delta t$ due to the bounded support of the interpolation function $\phi(t)$. The displacement vector \mathbf{u}_n corresponding to the motion at the interface nodes finally reads:

$$\mathbf{u}_n = \sum_{k=1}^n \mathbf{F}^{n-k+1} \mathbf{Q}_k \quad (2.75)$$

where

$$\mathbf{F}^k = \int_0^{k\Delta t} \mathbf{F}(\tau) \phi((k-1)\Delta t - \tau) d\tau \quad (2.76)$$

From Eq. (2.75), the interaction forces vector \mathbf{Q}_n at the time $t = n\Delta t$ reads as follows:

$$\mathbf{Q}_n = (\mathbf{F}^1)^{-1} \mathbf{u}_n - (\mathbf{F}^1)^{-1} \sum_{k=1}^{n-1} \mathbf{F}^{n-k+1} \mathbf{Q}_k \quad (2.77)$$

where $(\mathbf{F}^1)^{-1}$ is the instantaneous dynamic stiffness matrix of the unbounded soil domain. Note that $(\mathbf{F}^1)^{-1}$ plays here the same role of $(\mathbf{\Theta}^1)^{-1}$ in Eq. (2.50).

In order to calculate the dynamic flexibility matrices \mathbf{F}^k in Eq. (2.76), a distinction is made between the case $k = 1$ and $k \geq 2$.

The first dynamic flexibility matrix \mathbf{F}^1 reads:

$$\mathbf{F}^1 = \int_0^{\Delta t} \mathbf{F}(\tau) \phi(-\tau) d\tau \quad (2.78)$$

or, alternatively:

$$\mathbf{F}^1 = \int_{-\infty}^{+\infty} \mathbf{F}(\tau) \phi(-\tau) H(\tau) d\tau \quad (2.79)$$

where $H(t)$ is the Heaviside function.

Using the Convolution Theorem, Eq. (2.79) is finally written as:

$$\mathbf{F}^1 = \frac{1}{2\pi} \int_{-\infty}^{+\infty} \hat{\mathbf{F}}(i\omega) \hat{\varphi}(\omega) d\omega \quad (2.80)$$

being $\hat{\varphi}(\omega)$ the Fourier transform of $\varphi(t) = \phi(t)H(-t)$ equals to:

$$\hat{\varphi}(\omega) = \frac{1 - e^{i\omega\Delta t} + i\omega\Delta t}{\omega^2\Delta t} \quad (2.81)$$

Following the same principle, the flexibility matrix \mathbf{F}^k ($k \geq 2$) is written as:

$$\mathbf{F}^k = \frac{1}{2\pi} \int_{-\infty}^{+\infty} \hat{\mathbf{F}}(i\omega) \hat{\phi}(\omega) e^{i\omega(k-1)\Delta t} d\omega \quad (2.82)$$

where $\hat{\phi}(\omega)$, which is the Fourier transform of $\phi(t)$, is equal to:

$$\hat{\phi}(\omega) = \frac{2 - 2 \cos(\omega\Delta t)}{\omega^2\Delta t} \quad (2.83)$$

Figs. 2.2 and 2.3 show the Fourier transform of both time interpolation functions $\varphi(t)$ and $\phi(t)$, which have a filtering effect on the flexibility function. Therefore, the time domain function of the flexibility is never actually computed, only its convolution with the interpolation function is evaluated.

The first flexibility matrix of Eq. (2.80) \mathbf{F}^1 is computed by means of a trapezoidal rule, which is the only A-stable time integration scheme (see conditons listed in

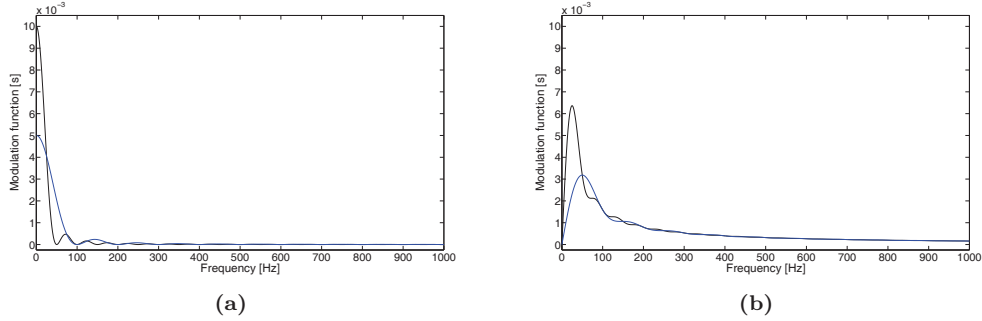


Figure 2.2: (a) Real and (b) imaginary parts of the time interpolation function $\hat{\phi}(\omega)$ in the frequency domain for $\Delta t = 0.02$ s (black line) and $\Delta t = 0.01$ s (blue line).

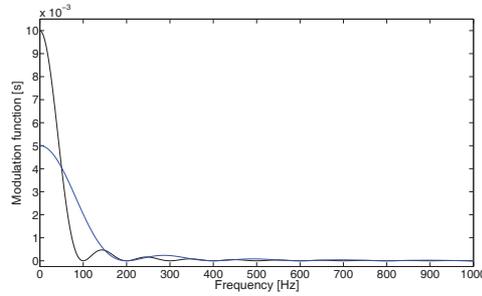


Figure 2.3: Real part (imaginary part is zero) of the time interpolation function $\hat{\phi}(\omega)$ in the frequency domain for $\Delta t = 0.01$ s (black line) and $\Delta t = 0.005$ s (blue line).

Sec. 2.2.2) that does not introduce numerical dissipation. On the contrary, the other flexibility matrices \mathbf{F}^k ($k > 1$) of Eq. (2.82) are calculated using a Filon integration algorithm with an oscillatory kernel function. Due to the unbounded support of the integrals involved in these calculations, an asymptotic development of the flexibility coefficients in the infinity should be taken into account [54, 145]. However, high frequency components are filtered by the shape functions (see Fig. 2.2 and 2.3) and thus, this development is optimal.

2.5.2 Illustrative numerical example

The numerical model chosen (Fig. 2.4) is one that allows to represent soil-structure interaction problems. It consists of three masses m_1 , m_2 , m_3 that correspond respectively to the structure, the foundation and the unbounded soil. At the same time, the foundation m_2 is split into $m_{2,1}$ which considers the inertial effects due to the base of the structure and $m_{2,2}$, which takes into account those coming from the soil. Mass m_3 represents one internal degree-of-freedom of the soil. Dashpot d_2 and d_3 model radiation damping in the soil and d_1 is related to the energy dissipation within the structure. Before stating the SSI system of equations to solve, the soil impedance has to be calculated and to do that, a domain decomposition approach has to be adopted.

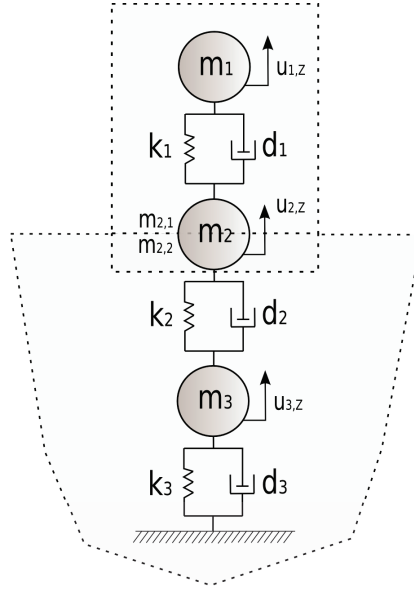


Figure 2.4: Lumped-parameter model of the soil-foundation-structure system.

The domain decomposition considered here is the following:

- the superstructure: $m_1, m_{2,1}$;
- the soil: $m_{2,2}, m_3$;

and therefore, the soil impedance $\hat{Z}(s)$ that has to be calculated corresponds to the impedance seen from $m_{2,1}$. The impedance matrix associated to a dynamic set of FE matrices can be generalized in the vectorial form of:

$$\hat{Z}(s) = \hat{S}_\Gamma(s) - \hat{S}_c(s) \hat{S}_{in}^{-1}(s) \hat{S}_c^T(s) \quad (2.84)$$

where $\hat{S}_\Gamma(s)$, $\hat{S}_c(s)$, \hat{S}_{in} are the block matrices of the FE system of the soil, denoted by $\hat{S}(s)$ and defined as follows:

$$\hat{S} = \begin{bmatrix} \hat{S}_\Gamma & \hat{S}_c \\ \hat{S}_c^T & \hat{S}_{in} \end{bmatrix} = \begin{bmatrix} \mathbf{M}_\Gamma & \mathbf{M}_c \\ \mathbf{M}_c^T & \mathbf{M}_{in} \end{bmatrix} s^2 + \begin{bmatrix} \mathbf{C}_\Gamma & \mathbf{C}_c \\ \mathbf{C}_c^T & \mathbf{C}_{in} \end{bmatrix} s + \begin{bmatrix} \mathbf{K}_\Gamma & \mathbf{K}_c \\ \mathbf{K}_c^T & \mathbf{K}_{in} \end{bmatrix}, \quad (2.85)$$

the subindex Γ , c and in denote respectively the degrees-of-freedom contained on the soil-structure interface, those which are coupled and the soil internal ones.

Considering the impedance in the form of Eq. (2.32), a non-singular and a singular part have to be identified. Taking the SSI model of Fig. 2.4 and the same notation of Eq. (2.34), the following association can be written for the singular part:

$$\begin{aligned} K_\Gamma &= k_2 - \frac{d_2^2}{m_3}, \\ C_\Gamma &= d_2, \\ M_\Gamma &= m_{2,2} \end{aligned} \quad (2.86)$$

and for the non-singular one:

$$\hat{Z}_{nsin} = -\frac{1}{m_3} \frac{(2d_2k_2m_3 - (d_2 + d_3)d_2^2)s + m_3k_2^2 - (k_2 + k_3)d_2^2}{m_3s^2 + (d_2 + d_3)s + k_2 + k_3} \quad (2.87)$$

which vanishes for large values of s .

Table 2.2: Properties of the structure-foundation system.

| $m_1[kg]$ | $m_{2,1}[kg]$ | $k_1[N.m^{-1}]$ | $c_1[N.s.m^{-1}]$ |
|------------------|------------------|---------------------|-------------------|
| $1.8 \cdot 10^7$ | $3.6 \cdot 10^6$ | $2.1 \cdot 10^{10}$ | $1.23 \cdot 10^7$ |

Table 2.3: Properties of the soil modelled by a lumped-parameter impedance.

| $m_{2,2}[kg]$ | $k_2[N.m^{-1}]$ | $c_2[N.s.m^{-1}]$ | $m_3[kg]$ | $k_3[N.m^{-1}]$ | $c_3[N.s.m^{-1}]$ |
|------------------|------------------|-------------------|-----------|-------------------|-------------------|
| $6.5 \cdot 10^5$ | $3.6 \cdot 10^6$ | $1.59 \cdot 10^9$ | 1.0 | $1.59 \cdot 10^9$ | $1.59 \cdot 10^5$ |

The time history of the load applied in z-direction at the bottom of the structure, m_2 , is considered to be a Ricker wavelet whose frequency content is centered at $f_0 = 5$ Hz:

$$F_z(t) = (1 - 2\lambda^2)e^{-\lambda^2} \quad (2.88)$$

with $\lambda = \pi f_0(t - t_D)$ and $t_D = 1$ s the time delay.

Once the soil impedance can be numerically evaluated with values of Tab. 2.2 and 2.3, the equations of the SSI system can be discretized in time (e.g. with a time step $\Delta t = 10^{-3}$ s) yielding to:

$$\mathbf{M}\ddot{\mathbf{u}}_n + \mathbf{C}\dot{\mathbf{u}}_n + \mathbf{K}\mathbf{u}_n + \mathbf{R}_n = \mathbf{F}_n \quad (2.89)$$

where vectors $\mathbf{u}_n = [u_{n,1,z}^T, u_{n,2,z}^T]^T$, $\mathbf{R}_n = [0, R_{n,\Gamma}^T]^T$, $\mathbf{F}_n = [0, F_{n,z}^T]^T$ and matrices:

$$\begin{aligned} \mathbf{M} &= \begin{bmatrix} m_1 & 0 \\ 0 & m_{2,1} \end{bmatrix} \\ \mathbf{C} &= \begin{bmatrix} d_1 & -d_1 \\ -d_1 & d_1 \end{bmatrix} \\ \mathbf{K} &= \begin{bmatrix} k_1 & -k_1 \\ -k_1 & k_1 \end{bmatrix} \end{aligned} \quad (2.90)$$

Eq. (2.89) is solved for the displacement using a classical unconditionally stable Newmark time integration scheme ($\beta = 0.25$, $\gamma = 0.5$). No numerical damping is considered. It should be noticed that the instantaneous coefficient $(\mathbf{F}^1)^{-1}$ (see Eq. (2.77)) or the equivalent of Ψ_0^1 in Eq. (2.41) can be assembled into the Newmark operator at the beginning of the calculation. In addition, when a flexibility formulation is adopted the interaction force vector has to be saved and updated at each time step.

Concerning the numerical values of all these parameters: they are chosen so that a P-wave velocity of $C_P = 845 \text{ m.s}^{-1}$ is given for the soil and a pumping eigenfrequency of 5.4 Hz is given for the structure clamped at its base. For the CQM, parameters are tuned according to literature [113] and for the cut-off frequency in the Hybrid Frequency-Time domain Approach, the double of the time sampling frequency $2.0 \cdot 10^3 \text{ Hz}$ has been chosen.

In order to compare both approaches a reference solution is first computed considering the whole system in the time domain.

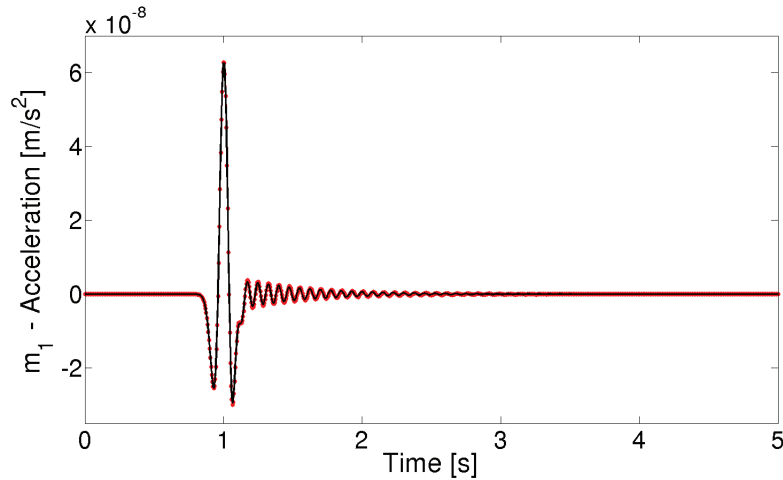


Figure 2.5: Acceleration at m_1 computed with the Hybrid Frequency-Time domain Approach (red points) compared to the reference solution (black) for $M_\Gamma = m_{2,2}$.

For the case of the HLTA with an underlying BDF2, satisfactory results are obtained for all values tested. However, although Hybrid Frequency-Time domain Approach (HFTA) shows also good results for some values, numerical problems arise for larger values of parameters. For instance, when the inertial effects M_Γ in the impedance matrix become too large, the obtained solution disagrees with the reference one. In Fig. 2.5 the acceleration measured at m_1 for $M_\Gamma = m_{2,2}$ is plotted. Alternatively, Fig. 2.6 presents the acceleration at the same point for an $M_\Gamma = 10 m_{2,2}$, also computed using the HFTA. The ratio between the flexibility functions obtained by the HFTA and HLTA is plotted in Fig. 2.7 where greater coefficients are observed for the HFTA.

However, if a BDF1 multistep method is used for the HLTA, similar results are obtained with respect to the HFTA (see Fig. 2.7). Since artificial dissipation increases with the order of BDF method, one may think that numerical damping is necessary to get an accurated solution. Indeed, François [53] recommends the combination of the Hybrid Frequency-Time domain Approach with a θ -method, which is also a dissipative time integrator of second order. As for this comparison the θ -method has not been implemented, a Newmark's modified average acceleration method (numerical dissipation can be adjusted by a parameter α_d) could straightforwardly be used instead. However, even if the latter integrator should preserve the same properties as the HHT integrator, its order of accuracy is actually reduced to one [60] and thus, integrators with different orders of accuracy would be again being compared.

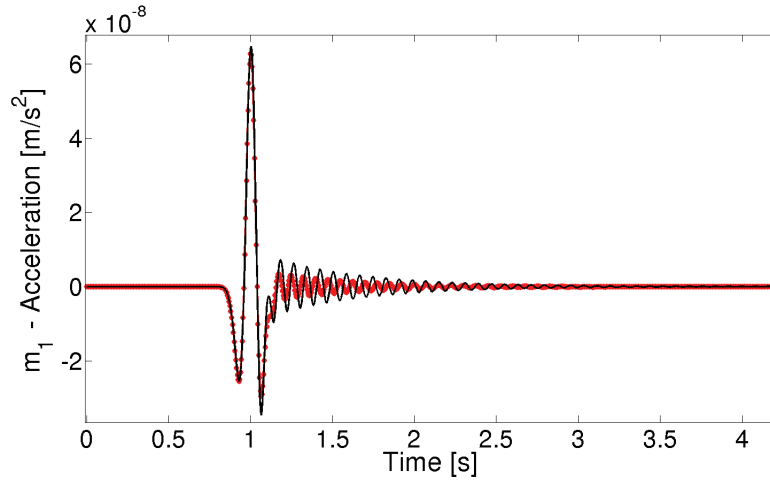


Figure 2.6: Acceleration at m_1 computed with the Hybrid Frequency-Time domain Approach (red points) compared to the reference solution (black) for $M_\Gamma = 10 m_{2,2}$.

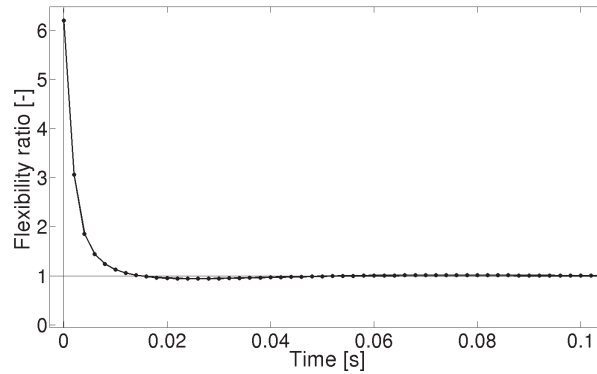


Figure 2.7: Ratio between time flexibility functions calculated by both approaches: the BDF2-based HLTA and the HFTA.

If the stiffness formulation considered in Eq. (2.41) is adopted, the convolution is computed in terms of the acceleration vector. Therefore, as the impedance does not need to be inverted a gain in computation time can be observed. However, it gives very similar results. Table 2.4 shows the Root Mean Square (RMS) error of the acceleration measured at m_1 relative to the maximum recorded during 5 s.

Table 2.4: RMS errors of the acceleration response computed at m_1 with both Hybrid Laplace-Time domain Approach (HLTA) and the Hybrid Frequency-Time domain Approach (HFTA) for different type of formulations.

| | Flexibility | Stiffness |
|------|-------------|-----------|
| HLTA | 0.0152% | 0.00046% |
| HFTA | 2.47% | - |

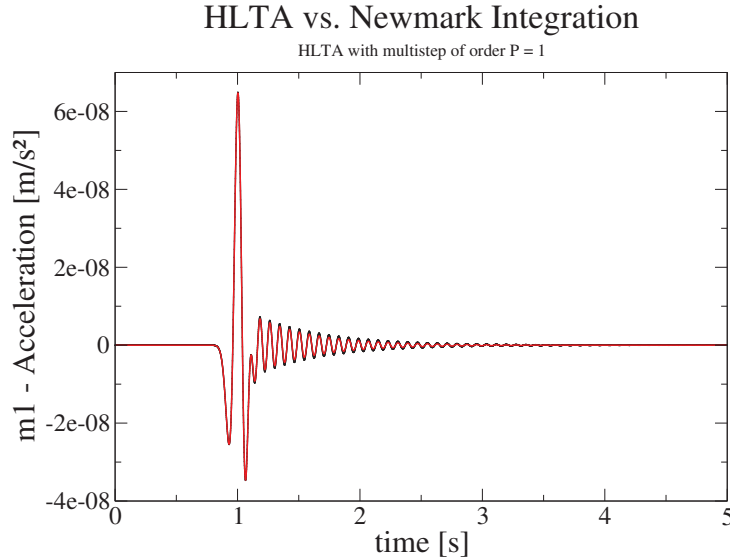


Figure 2.8: Acceleration at m_1 computed with the multistep BDF1-based Hybrid Laplace-Time domain Approach (red) compared to the reference solution (black).

2.6 Conclusions

Dynamic SSI equations are discretized in the time domain within a BE-FE coupled approach. Different time integrators are used for the BE and FE systems. In particular, a Convolution Quadrature Method based on a BDF2 is used for the BE equations whereas a classical Newmark scheme is used in the FE subdomain.

The use of convolution quadratures requires the evaluation of the soil impedance operator in the Laplace domain instead of the Fourier domain. However, the latter does not cause an inconvenience but the contrary, since some advantages can be observed with respect to other frequency-based approaches. First of all, within a CQ Method, the Cauchy's integral formula has to be evaluated and therefore, a closed contour is considered. The latter avoids difficulties related to cut-off frequencies and Gibbs phenomenon. Moreover, as CQM is well-adapted to singular convolution kernels, smaller time steps can be used without getting unstable solutions. The use of an implicit dissipative time integration scheme (BDF2) is also useful for the stability of the solution, particularly for nonlinear analyses.

Another important point is that the HLTA allows the explicit introduction of inertial, damping and stiffness terms during the evaluation of the SSI forces. Indeed, these terms are not explicit but hidden behind the dynamic behaviour of the soil impedance matrix and some of the approaches proposed in the literature to identify them are briefly reviewed.

The HLTA seems to be compatible with the use of either implicit or explicit time integration schemes of the FE equations. In particular, in the present chapter, the coupling with an implicit unconditionally stable Newmark procedure has been addressed. However, it seems that theoretical stability properties of such a coupled BE-FE time scheme are not easy to prove and energetic approaches may be explored.

Chapter 3

Numerical experiments and validation

“In theory, there is no difference between theory and practice. But, in practice, there is.”

JAN L. A. VAN DE SNEPSCHEUT

This chapter aims to experiment with the HLTA and to understand not only how it performs but also its limitations. Therefore, the computation of soil impedances in the time domain is tested in different linear cases: surface or embedded rigid and flexible foundations lying on homogeneous or stratified soils. The HLTA is next investigated within the case of nonlinear material constitutive laws.

3.1 Preliminaries

This section addresses different aspects that are common to all numerical simulations: the computation of the CQM weights, the time impedance functions and the identification of the MKC matrices. Problems related to the damping model and the implementation of the HLTA within *Code_Aster* environment are also detailed.

3.1.1 Numerical implementation of the CQ Method

In this section, the numerical evaluation of the CQM weights $w_n(\Delta t)$ (see Eq. (2.16)) is discussed. In fact, they can be obtained using different techniques [85]:

1. Power series expansion which is an efficient approach when $F(s)$ is a simple expression such as a rational function.
2. Trapezoidal rule approximation of the Cauchy integral for $w_n(\Delta t)$ with contour $|z| = \rho$:

$$w_n(\Delta t) = \frac{1}{2\pi i} \int_{|z|=\rho} F\left(\frac{r(z)}{\Delta t}\right) z^{-n-1} dz \quad (3.1)$$

In the second approach, which is actually the one used in this dissertation, Cauchy's integral can be rewritten in terms of polar coordinates $z = \rho e^{i\theta}$. The trapezoidal rule approximation can thus also be applied using L equal angle steps $\Delta\theta = \frac{2\pi}{L}$ as follows:

$$\tilde{w}_n(\Delta t) = \frac{\rho^{-n}}{L} \sum_{l=0}^{L-1} F(s_l) e^{-i \frac{2\pi l}{L} n}, \quad n = 0, 1, \dots, N \quad (3.2)$$

where $s_l = \frac{r(\rho e^{i \frac{2\pi l}{L}})}{\Delta t}$ with $r(z)$ the polynomial of the underlying linear multistep method. Assuming that $F(s_l)$ are computed with precision ϵ_{CQM} , coefficients $\tilde{w}_n(\Delta t)$ can thus be obtained with accuracy $O(\sqrt{\epsilon_{CQM}})$ when $L = N$ and $\rho^N = \sqrt{\epsilon_{CQM}}$. In addition, for these values of L and ρ , Fast Fourier Transform (FFT) algorithm can be applied to compute the weights, yielding to $O(L \log L)$ operations instead of $O(L^2)$. However, the value to be assigned to ϵ_{CQM} is not obvious. In fact, too small values of ϵ_{CQM} , such as 10^{-20} or 10^{-30} , yield to very small radii $|z| = \rho$ of integration in Cauchy's integral and, since the integrand involves a singularity at $z = 0$, a too small radius can result in an inappropriate evaluation of the integral. Indeed, coefficients $\tilde{w}_n(\Delta t)$ depends on ρ^{-n} and thus, for large n , they can give inaccurate values. This problem remains present even if higher accuracy integration techniques, such as Simpson's rule of integration, are used [124].

Therefore, after testing on different values of ϵ_{CQM} one realizes that a good compromise for the computation of the soil impedance matrix-valued coefficients Z_n , $n \geq 0$ is $\epsilon_{CQM} = 10^{-10}$. However, even in the case of this given precision, Z_n become inaccurate in most of the cases for $n > n_{70\%} = 0.7 \frac{T}{\Delta t}$, where T stands for the last instant of calculation and Δt , for the time step. Hereafter, time impedance functions are thus computed for a time window sufficiently large to satisfy accuracy requirements of $\epsilon_{CQM} = 10^{-10}$ also for $n_{70\%} < n < \frac{T}{\Delta t}$.

3.1.2 The soil impedance in the time domain

As mentioned in Chap. 2, the evaluation of the interaction forces on the SSI-interface involves the computation of a convolution integral over the whole continuous time domain. In order to understand the role of an impedance function in the time domain two examples are studied.

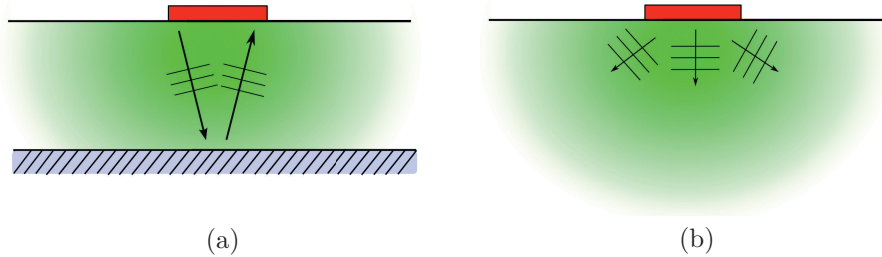


Figure 3.1: (a) Simplified model of one-layer soil overlying a bedrock. (b) Simplified model of a homogeneous soil.

Let us first consider the case of a square surface foundation lying over an elastic soil consisting of a homogenous layer and the bedrock (see Fig. 3.1a). In this configuration,

if one suddenly applies a vertical load over the foundation, the generated wavefront will travel towards the bedrock. Reasoning in terms of discrete time, after some time steps, the wave will be reflected on the bedrock and so, it will propagate backwards to the free surface. If the interaction forces were computed just by means of the last previous state –which is actually the case of a Newmark scheme– this incident field coming from the bedrock would never be accounted for. The latter evidences that not only the last previous step is necessary but the whole time history must be considered when computing the interaction forces and therefore, solving the convolution integrale becomes in most cases compulsory or unavoidable. We can conclude then that the interaction forces have some kind of dependency on the soil profile because of the wave propagation phenomena taking place inside. The same applies for the time impedance function. In fact, the time impedance function can be interpreted as the time evolution of the interaction forces induced by unitary displacements.

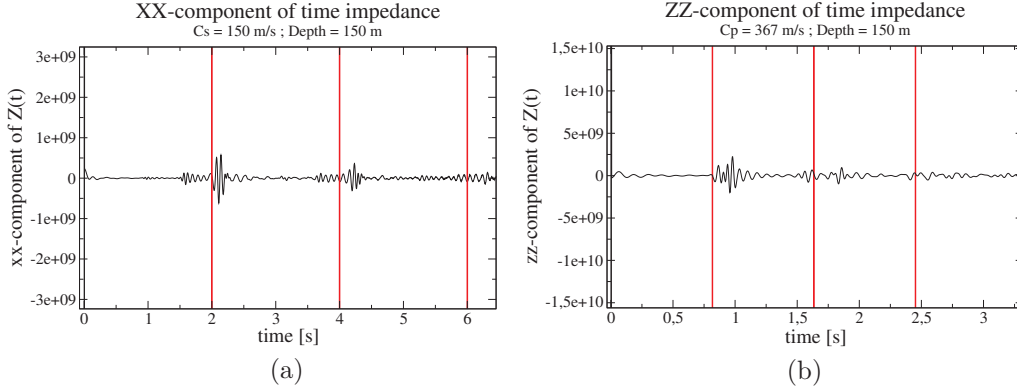


Figure 3.2: (a) Horizontal and (b) vertical components of the time impedance evolution for a soil consisting of a 150-m-layer.

These conclusions can be observed in Fig. 3.2a and Fig. 3.2b where time impedance function has been computed using a time step of $\Delta t = 2.5 \cdot 10^{-3} \text{ s}$ for a 150 m-soil layer with a shear wave velocity of $C_S = 150 \text{ m.s}^{-1}$ and P-wave velocity of $C_P = 367 \text{ m.s}^{-1}$ respectively. The results presented here certainly correspond to a very soft soil, but similar results can be obtained for either medium or hard soils. Fig. 3.2a which corresponds to the horizontal component of the impedance highlights the propagation of the shear wave velocity (every $2 t_{prop,S} = 2 \text{ s}$). Analogously, Fig. 3.2b which corresponds to the vertical component shows the instants of arrival of the P-wave (every $2 t_{prop,P} = 0.8174 \text{ s}$).

The high amplitude at $t = 0$ is related to the distributional character of the impedance function in the time domain, which has been verified in Sec. 2.3.2. The ideal impedance function in the Laplace domain, which corresponds to $\mathbf{M}s^2 + \mathbf{C}s + \mathbf{K}$ (\mathbf{M} , \mathbf{C} , \mathbf{K} being respectively mass, damping and stiffness FE matrices), can be simply expressed in the time domain as: $\mathbf{M}\ddot{\delta}(t) + \mathbf{C}\dot{\delta}(t) + \mathbf{K}\delta(t)$. Notice that oscillations amplitude decays as time goes, which proves the fact that some energy is lost in the soil, at least in the form of geometric or radiation damping. It is also interesting to notice that the sum of the time impedance coefficients tend to the static value of soil

stiffness. Indeed, unilateral Laplace transform formula gives:

$$\hat{\mathbf{Z}}(s=0) = \int_0^{+\infty} \mathbf{Z}(t) dt \quad (3.3)$$

expression which, after time discretization, becomes:

$$\hat{\mathbf{Z}}(s=0) \approx \sum_{n=0}^N \mathbf{Z}_n \quad (3.4)$$

The second example deals with a squared surface foundation over an elastic homogeneous half-space (see Fig. 3.1b). In this case, no reflection on the bedrock is expected. In fact, it is well-known that this kind of system can be modelled by a lumped-parameter model consisting of a mass, a dash-pot and a spring. Regarding the fact that mass involves acceleration terms, it may be appropriate to think that the interaction forces –that is the convolution– should be expressed, somehow, in terms of the displacement vector at time step n and also at time step $n-1$ and $n-2$. In that case, the time impedance evolution should be zero after the first three coefficients. This is actually what it is obtained in Fig. 3.3 when the time impedance is computed for example for $\Delta t = 2.5 \cdot 10^{-3}$ and with a soil having a shear wave velocity of $C_S = 150 \text{ m.s}^{-1}$. It is interesting to notice that this analysis can also be done in the opposite way: if the time impedance evolution of a given soil tends quickly to zero, then it might be possible to find a simple equivalent lumped-parameter system that could avoid the computation of the convolution. This is actually the topic of next section.

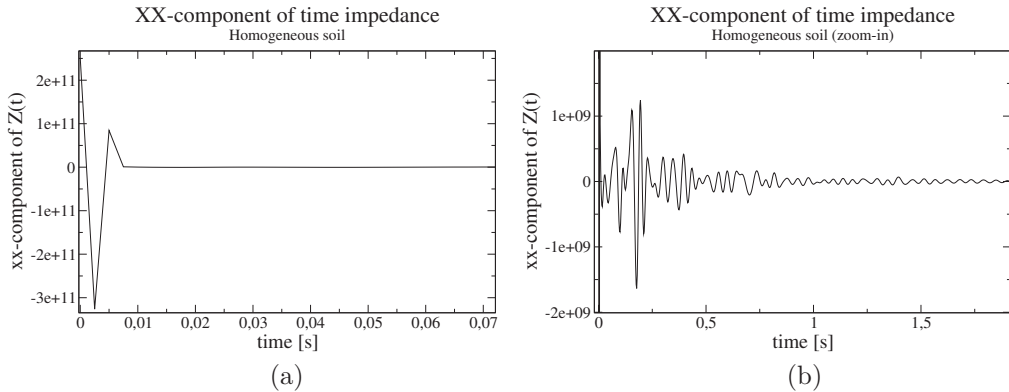


Figure 3.3: (a) Horizontal component of the time impedance function for a homogeneous soil. (b) Idem with different y -axis limits.

3.1.3 Hysteretic damping model

The BE method developed in MISS3D allows the computation of the soil impedance matrix for hysteretic damping. The use of this damping model yields to frequency

impedance functions that satisfy the form of a s -polynomial with complex coefficients. Causality, which is a property that should be verified when using convolution quadratures, is thus lost in the time domain.

As a result, spurious oscillations appear in the time impedance waveform (see Fig. 3.4). Although these oscillations do not perturb the calculation of the structural response, they do not give a clear picture in the way to understand the role of the time impedance function. Because of this, the time history of the plotted impedances in this section do not contain hysteretic damping.

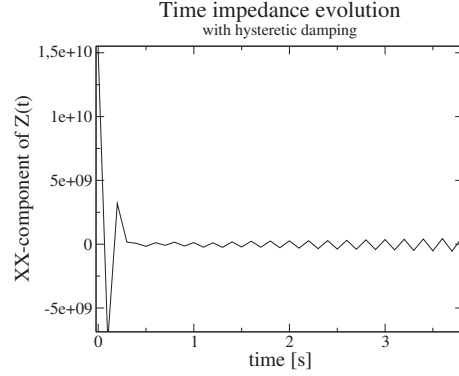


Figure 3.4: Time impedance function containing hysteretic damping.

3.1.4 Soil matrices identification approach

In order to estimate the $\tilde{\mathbf{M}}$, $\tilde{\mathbf{C}}$ and $\tilde{\mathbf{K}}$ a very simple approach is followed in this chapter. First of all, the soil impedance is computed by MISS3D (in-house BE code at École Centrale Paris) in the frequency domain. The computed impedance soil $\hat{\mathbf{Z}}_s(\omega)$ is assumed in the form of:

$$\hat{\mathbf{Z}}_s(\omega) \approx -\omega^2 \mathbf{M} + i\omega \mathbf{C} + \mathbf{K}(1 + i\beta_s) \quad (3.5)$$

where ω denotes the angular frequency and β_s , the hysteretic damping coefficient. This assumption seems to be accurate enough for surface foundations lying either on homogeneous soils or *regular* soil. Expression *regular* means here that velocity-depth trend of the soil increases with depth, ie. there is no inversion of velocities between layers of soil from the free-surface to the bedrock.

Equation (3.5) is then evaluated at two frequencies: one chosen very close to zero (eg. $\omega_1 = 2\pi f_1 = 2\pi \cdot 0.3 \text{ rad.s}^{-1}$) and the other, ω_2 , chosen at the first eigenfrequency of the structure satisfying homogeneous Dirichlet boundary conditions on the SSI interface. As a result, stiffness $\tilde{\mathbf{K}}$ is estimated as:

$$\tilde{\mathbf{K}} = \Re(\hat{\mathbf{Z}}_s(\omega_1)) \quad (3.6)$$

and the soil mass matrix, $\tilde{\mathbf{M}}$, as:

$$\tilde{\mathbf{M}} = \frac{\Re(\hat{\mathbf{Z}}_s(\omega_2)) - \tilde{\mathbf{K}}}{-\omega_2^2} \quad (3.7)$$

More comments have to be done on the choice of the soil damping matrix $\tilde{\mathbf{C}}$. Indeed, it actually corresponds to a viscous damping and it could be thus approximated as follows:

$$\tilde{\mathbf{C}} = \frac{\Im(\hat{\mathbf{Z}}_s(\omega_2)) - \Im(\hat{\mathbf{Z}}_s(\omega_1))}{\omega_2} \quad (3.8)$$

Note that the component $\Im(\hat{\mathbf{Z}}_s(\omega_1))$ accounts for hysteretic damping and thus, for the static solution (i.e. at $f = f_1$). Therefore, removing this component results

in larger amplitudes of the structural response. To avoid this problem, unless the contrary is explicitly stated, the next expression is considered in the following analyses:

$$\tilde{\mathbf{C}} = \frac{\Im m(\hat{\mathbf{Z}}_s(\omega_2))}{\omega_2} \quad (3.9)$$

Impedance matrix symmetrization

The soil impedance matrix is a fully populated matrix derived from the use of a BE method. As already mentioned, the BE method used in this dissertation corresponds to the one implemented in code MISS3D, which corresponds to a Galerkin BE approach. However, due to numerical errors of integration, the obtained BE matrices are not always symmetric. In order to use the standard functionalities of the FE in-house code (*Code_Aster*) and avoid the use of fully-populated matrices, the matrices associated to the soil domain (ie. $\hat{\mathbf{Z}}_s(\omega)$, $\tilde{\mathbf{M}}$, $\tilde{\mathbf{C}}$ and $\tilde{\mathbf{K}}$) are symmetrized as usual:

$$\mathbf{A}_{sym} = \frac{\mathbf{A} + \mathbf{A}^T}{2} \quad (3.10)$$

where \mathbf{A} represents here any soil nonsymmetric matrix.

3.1.5 Interpolation of the interaction forces in the time domain

Numerical difficulties of convergence can arise when nonlinear phenomena are accounted for. In some cases, reducing the time step from Δt to $\gamma\Delta t$ ($0 \leq \gamma \leq 1$) may help to reach convergence. However, if the discretization of the time impedance –by means of the CQM– has been done with a time step Δt , an interpolation technique has to be implemented to overcome the problems of convergence related to the non-linear analysis. In this framework, SSI forces as well as the new unknowns to solve for have to be evaluated at time $t = (n + \gamma)\Delta t$. In terms of numerical approximations, the linearized problem reads:

$$\mathbf{M}\ddot{\mathbf{u}}_{n+\gamma} + \mathbf{C}\dot{\mathbf{u}}_{n+\gamma} + \mathbf{K}\mathbf{u}_{n+\gamma} + \mathbf{R}_{n+\gamma} = \mathbf{F}_{n+\gamma} \quad (3.11)$$

Then, since SSI forces depend on the unknowns of the problem, the vector of interaction forces $\mathbf{R}_{n+\gamma}$ in Eq. (3.11) should be rewritten as a function of $\mathbf{u}_{n+\gamma}$ and $\mathbf{Z}_{n+\gamma}$. In order to avoid the computation of \mathbf{Z}_k for the new time step $\gamma\Delta t$ one may think of an interpolation procedure for the time impedance evolution. However, this is not possible. The convolution quadrature method works only for fixed time step and then, the number of terms in the convolution is fixed from the beginning. By interpolating the time impedance matrix evolution, the number of these terms changes and so does the global value of the interaction forces. In order to avoid this problem, the present section addresses an interpolation procedure not of the time impedance function but of the global interaction forces vector.

Following François [53], let a linear temporal variation be assumed for the soil-structure interaction forces within a time step ($0 \leq \tau' \leq \Delta t$), which can be written as:

$$\mathbf{R}(n\Delta t + \tau') \approx \frac{\tau'}{\Delta t}\mathbf{R}_{n+1} + \left(1 - \frac{\tau'}{\Delta t}\right)\mathbf{R}_n, \quad n = 0, \dots, N \quad (3.12)$$

or, denoting $\frac{\tau'}{\Delta t}$ by γ and the approximation of $\mathbf{R}(n\Delta t + \tau')$ by $\mathbf{R}_{n+\gamma}$, as:

$$\mathbf{R}_{n+\gamma} = \gamma \mathbf{R}_{n+1} + (1 - \gamma) \mathbf{R}_n, \quad n = 0, \dots, N \quad (3.13)$$

It should be noted that an *implicit* scheme of interpolation has been chosen, since only \mathbf{R}_n is known in Eq. (3.13). Thus, one may prefer the expression of *extrapolation* rather than *interpolation* for the computation of $\mathbf{R}_{n+\gamma}$. However, \mathbf{R}_{n+1} does not require to be computed since, as shown in Eq. (3.11), the real unknowns are $\mathbf{u}_{n+\gamma}$, $\dot{\mathbf{u}}_{n+\gamma}$, $\ddot{\mathbf{u}}_{n+\gamma}$. If \mathbf{R}_n and \mathbf{R}_{n+1} are replaced in Eq. (3.13) by their corresponding expression of Eq. (2.39), one gets to:

$$\mathbf{R}_{n+\gamma} = \mathbf{Z}_0 \mathbf{u}_{n+\gamma} + \sum_{k=1}^n \mathbf{Z}_k \mathbf{u}_{n+\gamma-k} + \gamma \mathbf{Z}_{n+1} \mathbf{u}_0, \quad n = 0, \dots, N \quad (3.14)$$

where $\mathbf{u}_{n+\gamma}$ denotes the numerical approximation of $\mathbf{u}(n\Delta t + \gamma\Delta t)$ given by:

$$\mathbf{u}_{n+\gamma} = \gamma \mathbf{u}_{n+1} + (1 - \gamma) \mathbf{u}_n \quad (3.15)$$

Recall that the matrix-valued coefficients of the time impedance evolution are already computed for the whole time interval of calculation (so \mathbf{Z}_{n+1} in Eq. (3.14) is known) and \mathbf{u}_k for $0 < k < n + 1$ are also known from the previous time steps calculations.

Moreover, if initial vanishing conditions are considered for the displacement field, i.e. $\mathbf{u}_0 = \mathbf{0}$, Eq. (3.14) finally yields to:

$$\mathbf{R}_{n+\gamma} = \mathbf{Z}_0 \mathbf{u}_{n+\gamma} + \sum_{k=1}^n \mathbf{Z}_k \left(\gamma \mathbf{u}_{n+1-k} + (1 - \gamma) \mathbf{u}_{n-k} \right), \quad n = 0, \dots, N \quad (3.16)$$

Therefore, Eq. (3.16) shows indeed that the displacement field vector at $t = (n + 1)\Delta t$ is never computed since the algebraic system of Eq. (3.11) is directly solved for $\mathbf{u}_{n+\gamma}$.

The same *implicit* interpolation scheme can be used when the soil impedance matrix is decomposed into inertial, damping and stiffness terms. In this case, Eq. (3.14) reads for $n = 0, \dots, N$:

$$\begin{aligned} \mathbf{R}_{n+\gamma} = & \mathbf{Z}_0^M \ddot{\mathbf{u}}_{n+\gamma} + \mathbf{Z}_0^C \dot{\mathbf{u}}_{n+\gamma} + \mathbf{Z}_0^K \mathbf{u}_{n+\gamma} \\ & + \sum_{k=1}^n \left(\mathbf{Z}_k^M \ddot{\mathbf{u}}_{n+\gamma-k} + \mathbf{Z}_k^C \dot{\mathbf{u}}_{n+\gamma-k} + \mathbf{Z}_k^K \mathbf{u}_{n+\gamma-k} \right) \end{aligned} \quad (3.17)$$

where displacement, velocity and acceleration initial vanishing conditions have been assumed for simplicity.

It should be remarked that during the whole calculation ($n = 0, \dots, N$), even if the time step is modified, the contribution of the instantaneous impedance terms to the operator that has to be inverted at every time step remains constant. For example, in Eq. (3.16), the term \mathbf{Z}_0 is always multiplying the displacement field vector that must be evaluated, regardless that it corresponds to time step $n\Delta t$ or $(n + \gamma)\Delta t$. The same happens when the soil impedance operator is decomposed into inertial, damping and stiffness terms: \mathbf{Z}_0^K , \mathbf{Z}_0^C , \mathbf{Z}_0^M remain always in the left hand-side of the equation.

If a flexibility formulation is adopted the same interpolation procedure can be used. In this case and using the same notation as in Sec. 2.3.2, Eq. (3.14) becomes

for $n = 0, \dots, N$:

$$\mathbf{Q}_{n+\gamma} = (\mathbf{F}_0)^{-1} \mathbf{u}_{n+\gamma} - (\mathbf{F}_0)^{-1} \left(\gamma \mathbf{F}_{n+1} \mathbf{Q}_0 + \sum_{k=1}^n \mathbf{F}_k \mathbf{Q}_{n+\gamma-k} \right) \quad (3.18)$$

where $\mathbf{Q}_{n+\gamma} = \gamma \mathbf{Q}_{n+1} + (1 - \gamma) \mathbf{Q}_n$ and \mathbf{F}_k correspond respectively to the vector of interaction forces at time step $n + \gamma$ and the time flexibility matrix-valued coefficient at time step k . Recall that for flexibility formulations the whole time evolution of the interaction forces have to be saved during the calculation.

3.2 Linear analysis

This section aims to find out how HFTA performs within different linear numerical analyses: surface or embedded foundations, rigid or flexible foundations, homogeneous or stratified soils.

3.2.1 Reference solution

To obtain a reference solution, the equilibrium of the coupled SSI system is solved in the frequency domain:

$$\left(\begin{bmatrix} \mathbf{K}_{bb} & \mathbf{K}_{b\Gamma} \\ \mathbf{K}_{\Gamma b} & \mathbf{K}_{\Gamma\Gamma} + \hat{\mathbf{Z}}_s(\omega) \end{bmatrix} - \omega^2 \begin{bmatrix} \mathbf{M}_{bb} & \mathbf{M}_{b\Gamma} \\ \mathbf{M}_{\Gamma b} & \mathbf{M}_{\Gamma\Gamma} \end{bmatrix} \right) \begin{bmatrix} \hat{\mathbf{u}}_b(\omega) \\ \hat{\mathbf{u}}_\Gamma(\omega) \end{bmatrix} = \begin{bmatrix} \hat{\mathbf{f}}_b(\omega) \\ \hat{\mathbf{f}}_\Gamma(\omega) + \hat{\mathbf{f}}_s(\omega) \end{bmatrix} \quad (3.19)$$

where $\mathbf{M}_{\alpha\beta}$ and $\mathbf{K}_{\alpha\beta}$, $\alpha, \beta \in \{b, \Gamma\}$, respectively correspond to the FE mass and stiffness matrices. Recall that b stands for building internal degrees-of-freedom and Γ , for those on the SSI-interface. Again, $\hat{\mathbf{Z}}_s(\omega)$ denotes the soil impedance matrix in the frequency domain, $\hat{\mathbf{f}}_s(\omega)$, the equivalent seismic force.

In order to solve for the structural response, a classic generalized Craig-Bampton decomposition method is used. Thus, the total displacement field can be expressed by means of Q vibration modes:

$$\mathbf{u}_b = \begin{bmatrix} \hat{\mathbf{u}}_b(\omega) \\ \hat{\mathbf{u}}_\Gamma(\omega) \end{bmatrix} = \begin{bmatrix} \boldsymbol{\psi}_b & \boldsymbol{\psi}_b^s \\ \mathbf{0} & \boldsymbol{\psi}_\Gamma \end{bmatrix} \begin{bmatrix} \hat{\boldsymbol{\alpha}}_b(\omega) \\ \hat{\boldsymbol{\alpha}}_\Gamma(\omega) \end{bmatrix} = \boldsymbol{\Psi}_{CB} \hat{\boldsymbol{\alpha}}_b(\omega) \quad (3.20)$$

where vector $\hat{\boldsymbol{\alpha}}_b(\omega)$ collects the modal coordinates. After building global FE matrices of mass and stiffness, matrices $\boldsymbol{\psi}_b$, $\boldsymbol{\psi}_b^s$ and $\boldsymbol{\psi}_\Gamma$ can be computed in *Code_Aster*. Indeed, eigenmodes $\boldsymbol{\psi}_b$ corresponding to the structure clamped at its base are obtained by solving:

$$(\mathbf{K}_{bb} - \omega^2 \mathbf{M}_{bb}) \boldsymbol{\psi}_b = 0 \quad (3.21)$$

and the quasi-static transmission $\boldsymbol{\psi}_b^s$ of the interface modes into the structure is given by:

$$\boldsymbol{\psi}_b^s = -\mathbf{K}_{bb}^{-1} \mathbf{K}_{b\Gamma} \boldsymbol{\psi}_\Gamma \quad (3.22)$$

Matrix ψ_Γ is usually the unit matrix, however, in order to reduce the computational effort, a reduction technique can be employed to account for flexible foundation (see Sec. 2.3.2). Hence, the corresponding eigenvalue problem reads:

$$(\mathbf{K}'_{\Gamma\Gamma} - \omega^2 \mathbf{M}'_{\Gamma\Gamma})\psi_\Gamma = 0 \quad (3.23)$$

where $\mathbf{K}'_{\Gamma\Gamma}$ and $\mathbf{M}'_{\Gamma\Gamma}$ are respectively the stiffness and mass matrices resulting of the concentration of the mass on the foundation that lies on a set of springs. Mass is concentrated on the foundation. Note that these matrices are not the same as $\mathbf{K}_{\Gamma\Gamma}$ and $\mathbf{M}_{\Gamma\Gamma}$ and require thus a supplementary FE assembly.

Once Ψ_{CB} calculated in *Code_Aster* and the soil impedance and the equivalent seismic force computed with a BE method in MISS3D, the following problem can thus be solved:

$$\begin{aligned} & \left(\begin{bmatrix} \mathbf{\Lambda}_{QQ} & \mathbf{0} \\ \mathbf{0} & \psi_\Gamma^T (\mathbf{K}_{\Gamma\Gamma} - \mathbf{K}_{\Gamma b} \mathbf{K}_{bb}^{-1} \mathbf{K}_{b\Gamma}) \psi_\Gamma \end{bmatrix} \right. \\ & - \omega^2 \left[\begin{array}{cc} \mathbf{I}_{QQ} & \psi_b^T [\mathbf{M}_{bb} \quad \mathbf{M}_{b\Gamma}] \begin{bmatrix} \psi_b^s \\ \psi_\Gamma^s \end{bmatrix} \\ \begin{bmatrix} \psi_b^T & \psi_\Gamma^T \end{bmatrix} \begin{bmatrix} \mathbf{M}_{bb} \\ \mathbf{M}_{\Gamma b} \end{bmatrix} \psi_b & \begin{bmatrix} \psi_b^T & \psi_\Gamma^T \end{bmatrix} \begin{bmatrix} \mathbf{M}_{bb} & \mathbf{M}_{b\Gamma} \\ \mathbf{M}_{\Gamma b} & \mathbf{M}_{\Gamma\Gamma} \end{bmatrix} \begin{bmatrix} \psi_b^s \\ \psi_\Gamma^s \end{bmatrix} \end{array} \right] \\ & \quad \left. + \begin{bmatrix} \mathbf{0} & \mathbf{0} \\ \mathbf{0} & \psi_\Gamma^T \hat{\mathbf{Z}}_s(\omega) \psi_\Gamma \end{bmatrix} \right) \begin{Bmatrix} \hat{\alpha}_b(\omega) \\ \hat{\alpha}_\Gamma(\omega) \end{Bmatrix} \\ & = \begin{bmatrix} \psi_b^T \hat{\mathbf{f}}_b(\omega) \\ \psi_b^{sT} \hat{\mathbf{f}}_b(\omega) + \psi_\Gamma^T \hat{\mathbf{f}}_\Gamma(\omega) \end{bmatrix} + \begin{bmatrix} \mathbf{0} \\ \psi_\Gamma^T \hat{\mathbf{f}}_s(\omega) \end{bmatrix} \quad (3.24) \end{aligned}$$

where $\mathbf{\Lambda}_{QQ} = \text{diag}(\omega_i^2)$ is a diagonal matrix of size $Q \times Q$ containing the square of the eigenfrequencies ω_i ($i = 1 \dots Q$) of the structure satisfying fixed-base boundary conditions. Matrix \mathbf{I}_{QQ} corresponds to the identity matrix coming from the orthogonality of modes ψ_b with respect to mass matrix \mathbf{M}_{bb} .

All post-processing tasks are also carried out in *Code_Aster*. Particularly, the transient reference solution is obtained by using an FFT.

3.2.2 Lumped-parameter model

The first numerical model considered in this linear analysis consists of two masses, m_1 and m_2 , which respectively represent the structure and its foundations. Both masses are linked by a spring of stiffness k and a dashpot c that accounts for viscous dissipation in the structure. A rigid body constraint exists between mass m_2 and the surface foundation modelled with shell FE (see Fig. 3.5) in *Code_Aster*. The base-slab lies over an elastic homogeneous unbounded soil and, as mentioned before, the soil is modelled with MISS3D, which allows the computation of the soil impedance matrix in the Laplace domain. The properties of the model are listed in Tab. 3.1.

The load applied to m_2 in the x -direction e_x corresponds to the earthquake giving the free-field accelerogram $\gamma_f(t)$ shown in Fig. 3.6, whose maximal acceleration is around $0.3g$. A time step of 0.01 s and a precision of $\epsilon_{CQM} = 10^{-10}$ for the Convolution Quadrature Method (CQM) give sufficiently accurate results.

Solving for displacement by means of an unconditionally stable Newmark time integration scheme ($\beta = 0.25$, $\gamma = 0.5$), the transient response shown in Fig. 3.7 is

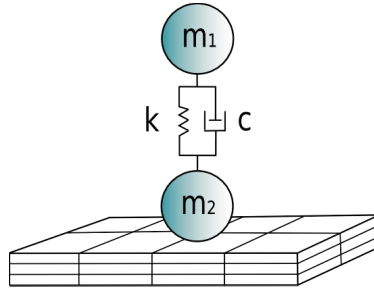


Figure 3.5: Simplified model of a structure on a square surface foundation.

Table 3.1: Properties of the structure (m_1 , m_2 , k and c) and the soil (ρ , E , ν and β_s).

| m_1 [kg] | m_2 [kg] | k [N.m ⁻¹] | c [N.s.m ⁻¹] | ρ [kg.m ⁻³] | E [MPa] | ν [-] | β_s (%) |
|------------------|------------------|--------------------------|----------------------------|------------------------------|-----------|-----------|---------------|
| $1.8 \cdot 10^7$ | $3.6 \cdot 10^6$ | $2.1 \cdot 10^{10}$ | $1.23 \cdot 10^7$ | 2 100 | 1 500 | 0.4 | 5 |

obtained. It corresponds to the acceleration of m_1 evaluated with the Hybrid Laplace-Time domain Approach (involving only displacement convolution) and compared with its reference solution. The root mean square error over the maximale acceleration in a 20 s-interval regarding the reference is about $\epsilon = 0.53\%$. Results get better when not only stiffness convolution but also damping convolution is used, the error reduces to 0.50%. Still, it drops down to 0.43% if inertia terms are also introduced in the evaluation of the interaction forces. As mentioned, the polynomial factorisation is done with \mathbf{K}_Γ , \mathbf{C}_Γ and \mathbf{M}_Γ estimated by means of the first fundamental frequency of the clamped structure. Maybe because the low number of degrees-of-freedom in this model (actually twelve), the HLTA shows robustness with respect to the values of \mathbf{K}_Γ , \mathbf{C}_Γ and \mathbf{M}_Γ .

3.2.3 Large-scale FE model

The next model corresponds to a FE structure modelling the reactor building of a nuclear power plant. The structure is supposed to have a deformable slab lying on a –soft/medium– homogeneous soil. The main difficulty of this analysis is the number of degrees-of-freedom modelling the SSI interface, which stands close to 1 100 degrees-of-freedom. In order to cut down on computational effort, a reduction technique has to be applied for the interface.

The FE model of the building consists of shell elements, also for the base slab (see Fig. 3.8). The first fundamental frequency arises at $f_1 = 3$ Hz. The loading, in x -direction, is chosen so that the main frequency content of the building is excited. Fig. 3.9 shows the transient excitation as well as its spectral content. The baseline of the accelerogram has been removed (see Appx. B). For the computation of the time impedance matrix, a time step $\Delta t = 0.008$ s and a precision of $\epsilon_{CQM} = 10^{-10}$ is employed. For the transient calculation, again, an unconditionally stable time integration scheme ($\beta = 0.25$, $\gamma = 0.5$) is adopted.

As mentioned before, it is too costly to account for exact kinematics of the interface. Two possibilities can be adopted: to expand structural response on a Ritz basis or to simplify the model by considering rigid foundations. In this case, because of the

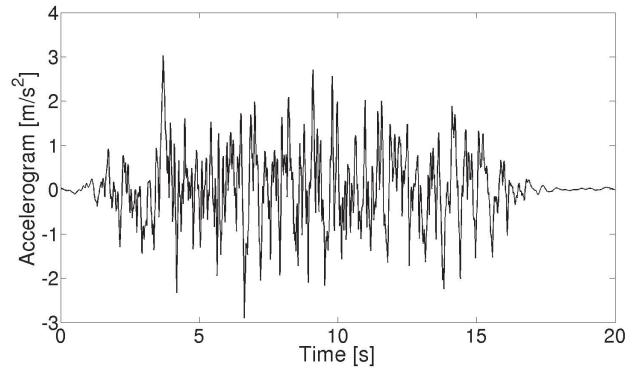


Figure 3.6: Free-field accelerogram applied to m_2 .

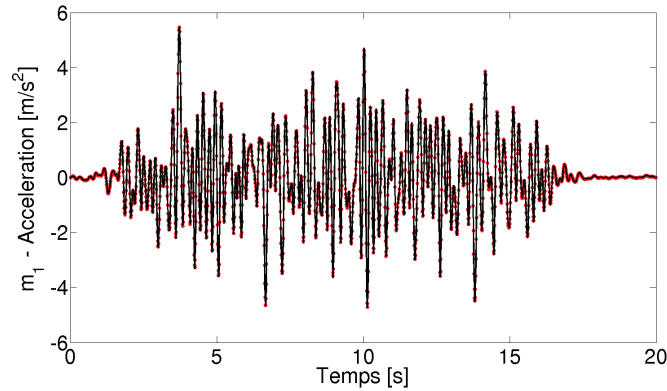


Figure 3.7: Displacement at m_1 in the x -direction computed with the HLTA (black line) and compared to the reference solution (red markers).

soil properties and of the surface foundation dimensions, no significant difference is observed between both cases, as proves reference base-slab responses shown in Fig. 3.10. Here, 60 modes (up to 121.496 Hz) are retained for the case of flexible foundation and, of course, the 6 rigid body modes for the case of non-deformable foundation. The number of modes is chosen so that the dynamic response does not differ from the exact one. In fact, for this model, 30 modes (up to 77.407 Hz) might have been enough but, from a numerical point of view, larger matrix dimensions were preferred to be tested.

According to Fig. 3.12 and Fig. 3.13, similar results are obtained when the HLTA is respectively used either in the case of a direct convolution $(\mathbf{Z} * \mathbf{u})(t)$ or in the case of a decomposed convolution $(\mathbf{Z} * \mathbf{u})(t) = (\mathbf{Z}_M * \mathbf{u})(t) + (\mathbf{Z}_C * \mathbf{u})(t) + (\mathbf{Z}_K * \mathbf{u})(t)$. Whereas displacement responses are very close to each other, accelerations show slight differences between rigid and flexible solutions. These discrepancies become smaller when a decomposed convolution is considered. In fact, in this case, an MKC formulation performs better because of homogeneous soil characteristics. As Fig. 3.11 shows, \mathbf{Z}_K and \mathbf{Z}_M are homothetic functions whose scaling factors correspond respectively to \mathbf{K}_Γ and \mathbf{M}_Γ . In addition, as these time evolutions are quickly attenuated, the mass, damping and stiffness matrices of the soil can be easily identified. Recall that

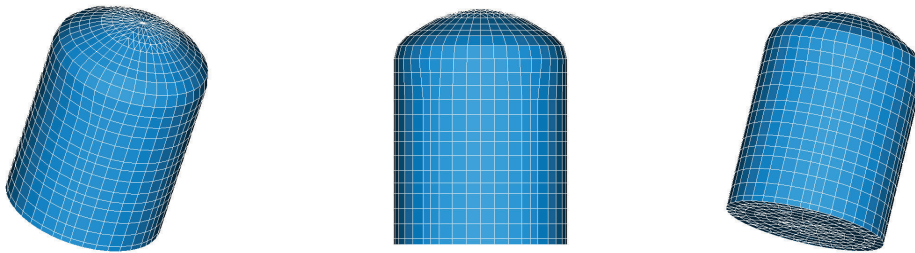


Figure 3.8: Different views of the FE model of reactor building considered in this study.

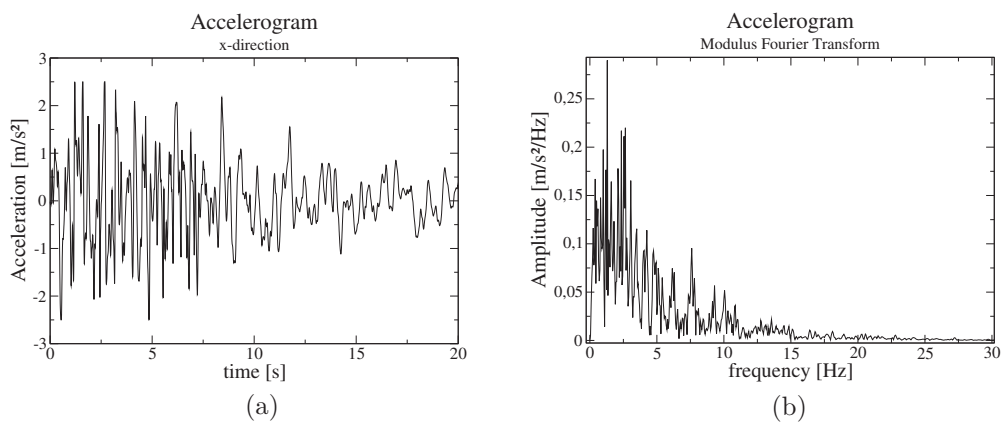


Figure 3.9: Free-field acceleration applied on x -direction (a) in time domain and (b) in frequency domain.

these time impedances evolutions contain the effect of the hysteretic damping.

However, in comparison with the reference solution, it seems that HLTA solution with rigid foundation results in higher amplitudes than for the case of flexible foundation. In addition, Fig. 3.14 shows that better results are obtained when an MKC formulation is used.

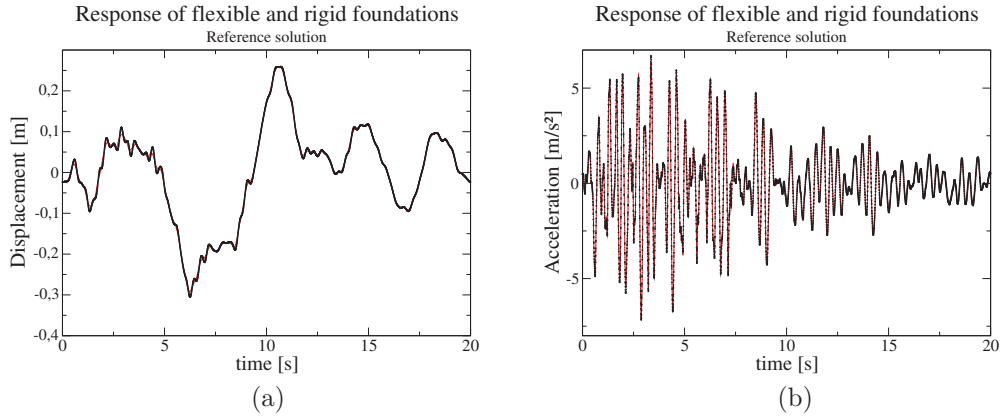


Figure 3.10: Comparison between rigid (red) and flexible (black) foundation responses in (a) displacement and (b) in acceleration at the top of the building for the reference solution.

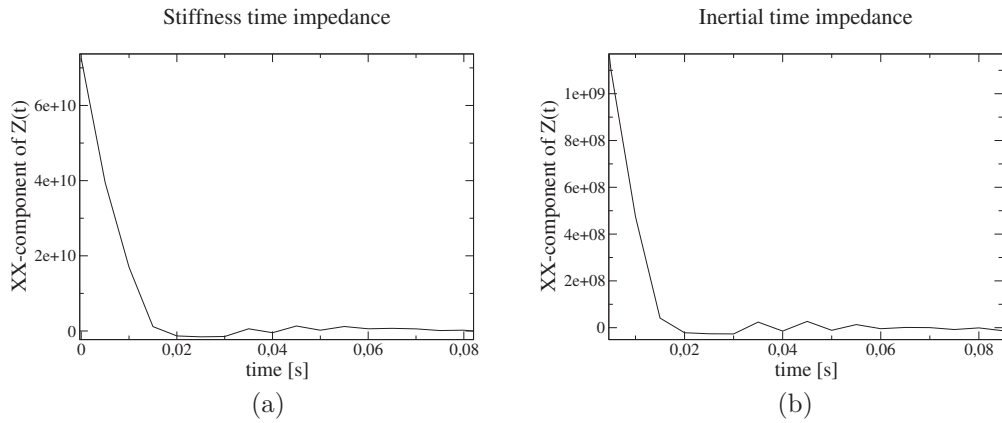


Figure 3.11: (a) Time-history of impedance $Z_K(t)$ and (b) of impedance $Z_M(t)$.

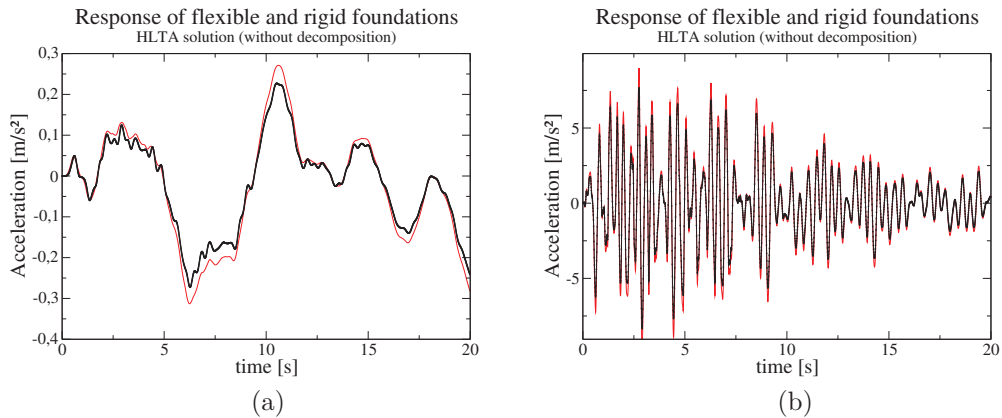


Figure 3.12: Comparison between rigid (red) and flexible (black) responses in (a) displacement and (b) in acceleration at the top of the building for HLTA without MKC formulation.

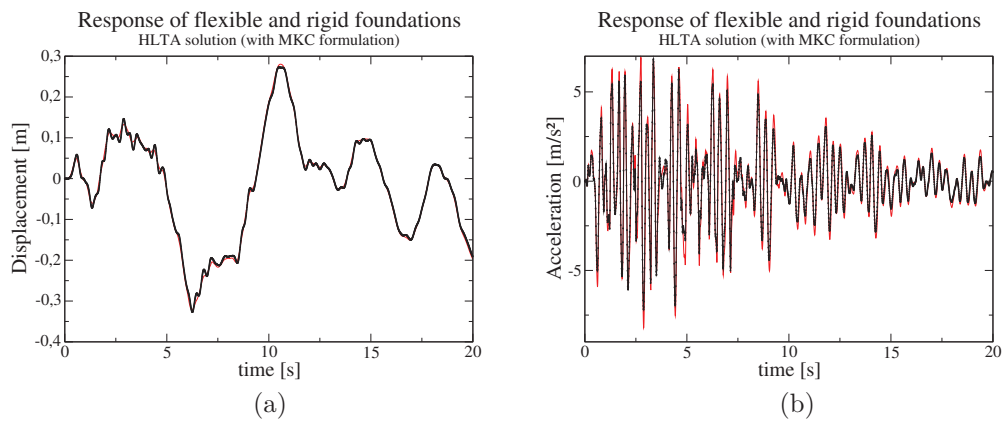


Figure 3.13: Comparison between rigid (red) and flexible (black) foundation responses in (a) displacement and (b) in acceleration at the top of the building for HLTA with MKC formulation.

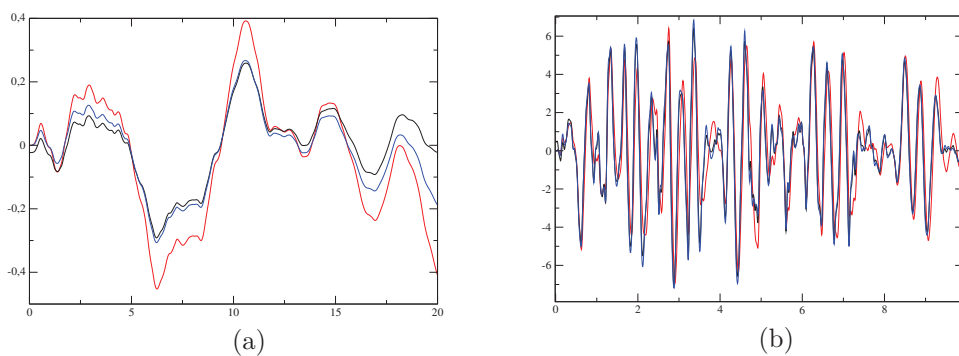


Figure 3.14: Comparison between HLTA using an MKC formulation (black), without MKC decomposition (red) and the reference solution (blue) for (a) displacement and (b) acceleration in the time domain at the top of the building.

3.2.4 Structure-soil-structure interaction model

The next numerical experiment deals with a case of structure-soil-structure interaction (3SI), which involves the interaction between two structures throughout the soil. The numerical model chosen for this study corresponds to the one used for the “Soil-Structure Interaction NUPEC” workshop, which was organized by the Nuclear Power Electric Corporation (NUPEC) in Japan during the mid-1990s. This workshop was based on some experimental data obtained under real seismic loading conditions [33, 74]. Fig. 3.15 shows indeed the real buildings where the experimental tests were carried out.

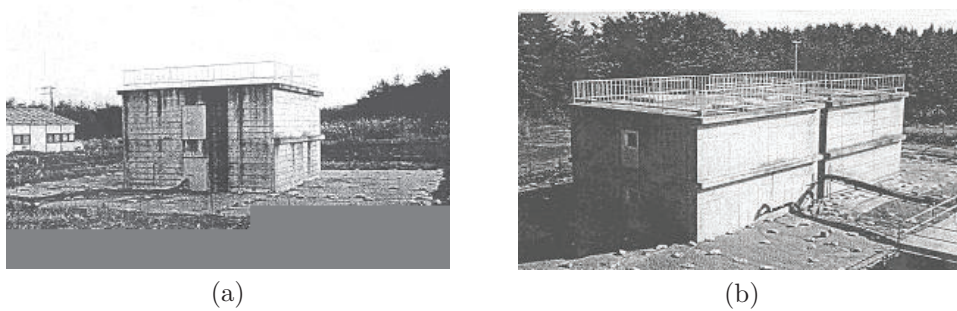


Figure 3.15: (a) Real view of the single embedded building as well (b) of two identical closely spaced embedded buildings used within the NUPEC benchmark.

The numerical model used for this study is presented in Fig. 3.16. It consists of two stick models, which are based on the real geometry of NUPEC buildings, made up of four masses and twelve massless beams of five different types. Reinforced concrete is assumed for material properties, that is a Young’s modulus of $E = 31\,000\text{ MPa}$, a Poisson’s ratio of $\nu = 0.16$ and a density of $\rho = 2\,028\text{ kg}\cdot\text{m}^{-3}$. The foundations, which constitute the SSI-interface, are embedded into the soil (about 5 m) and modelled using shell elements. For more details on the characteristics of the model please refer to the work of Clouteau *et al.* [33].

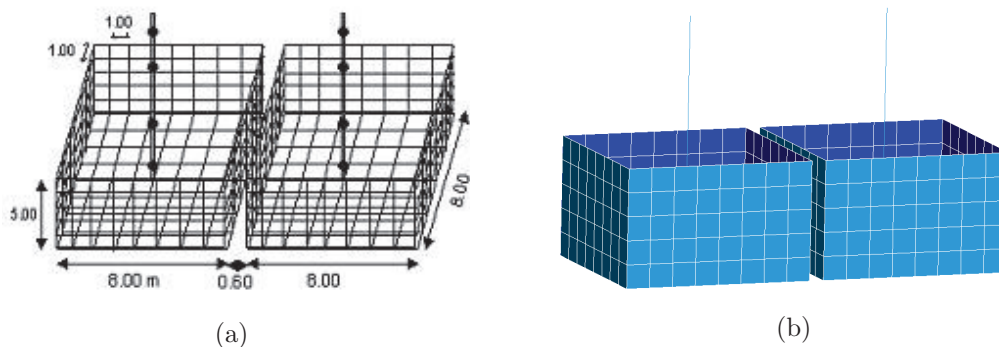


Figure 3.16: Simplified model of the NUPEC 3SI application: (a) diagram of dimensions and a (b) view of the FE model.

The loading applied on the embedded foundation corresponds to free-field accelerograms based on earthquake recordings, in both x -direction and y -direction.

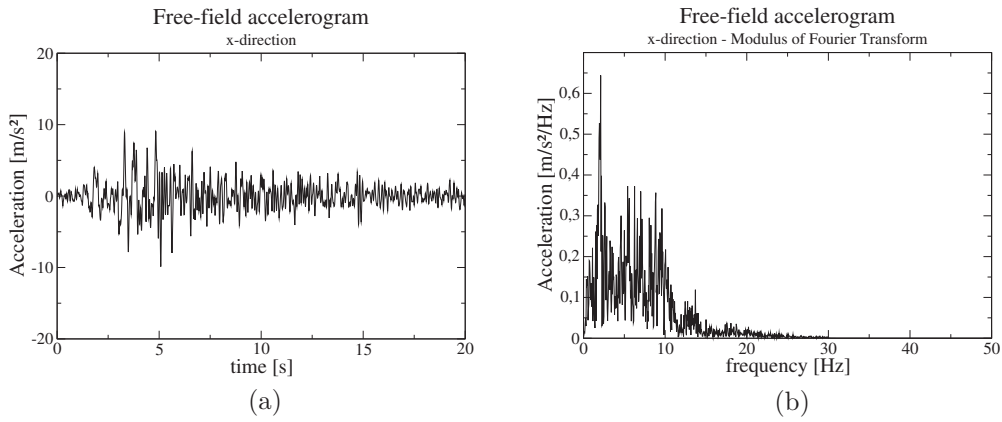


Figure 3.17: (a) Transient free-field accelerogram applied on the x -direction and (b) the modulus of its Fourier transform (FFT).

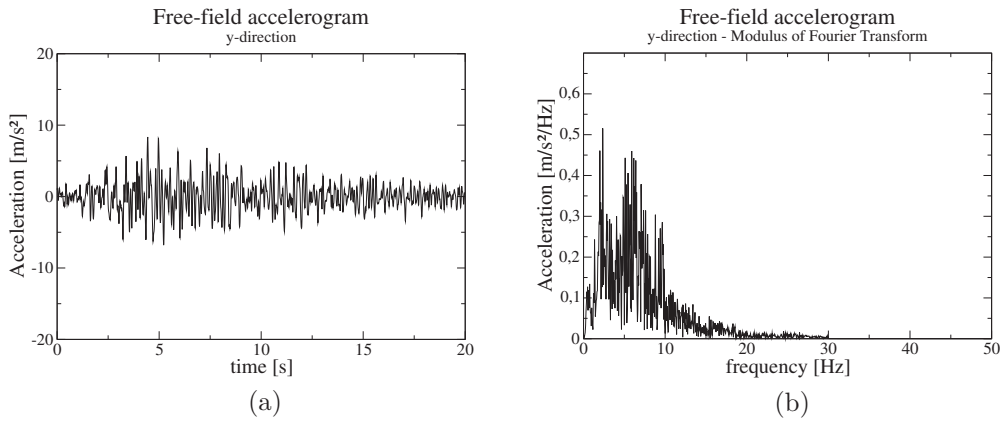


Figure 3.18: (a) Transient free-field accelerogram applied on the y -direction and (b) the modulus of its Fourier transform (FFT).

Regarding the soil, Fig. 3.19 and Tab. 3.2 show its profile which consists of ten different layers, including the bedrock. This complex soil profile should not be a problem since wave propagation velocities increase with depth, i.e. the soil has a *regular* profile. However, the combination of such a soil with the fact that the SSI-interface is embedded into the soil arises as the main difficulty of this study. Indeed, fictitious eigenfrequencies occur when the boundary integral equation is used for exterior problems, since it has nonunique solution at frequencies corresponding to the eigenfrequencies of the excavated part—the interior domain—with Dirichlet boundary

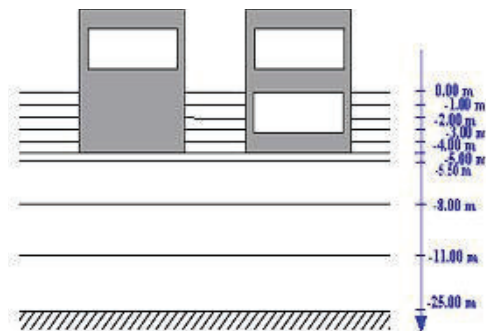


Figure 3.19: Soil profile with the thickness of each soil layer and its relative position respect to the buildings.

conditions on the SSI-interface [115]. This problem should be corrected when the boundary equation is formulated in the Laplace domain, as the use of complex frequencies ensures a unique solution. It is thus interesting to study how HLTA performs in such a case.

Table 3.2: Properties of the soil layers ranged by depth: the first layer corresponds to the free-surface layer and the tenth one to the substratum. Hysteretic damping β_s is given in percentage.

| Layer | Thickness [m] | $\rho[kg.m^{-3}]$ | $E[MPa]$ | $\nu[-]$ | β_s (%) |
|-------|---------------|-------------------|------------|----------|---------------|
| 1 | 1.00 | 1 770 | 117.880 | 0.386 | 10 |
| 2 | 1.00 | 1 770 | 190.270 | 0.279 | 10 |
| 3 | 1.00 | 1 770 | 207.000 | 0.265 | 10 |
| 4 | 1.00 | 1 770 | 224.190 | 0.251 | 10 |
| 5 | 1.00 | 1 770 | 248.670 | 0.272 | 10 |
| 6 | 0.50 | 1 940 | 97.776 | 0.120 | 10 |
| 7 | 2.50 | 1 940 | 614.930 | 0.371 | 10 |
| 8 | 3.00 | 1 940 | 10 151.000 | 0.415 | 4 |
| 9 | 14.00 | 2 210 | 10 190.000 | 0.386 | 4 |
| 10 | 27.75 | 2 210 | 15 010.000 | 0.343 | 4 |

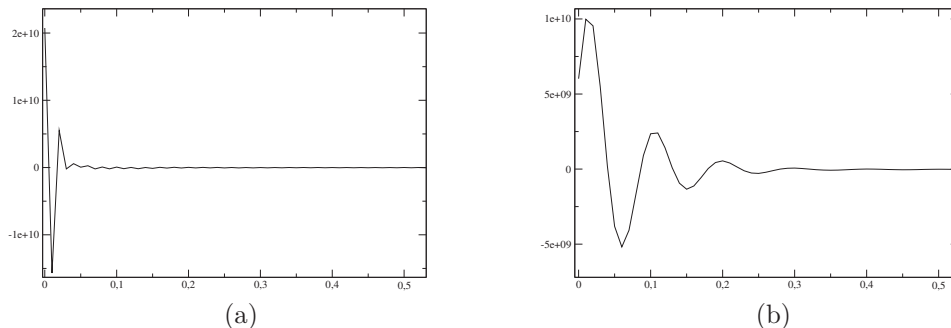


Figure 3.20: (a) Time impedance $Z(t)$ and (b) the $Z_K(t)$ coming from an MKC formulation.

As mentioned in the preliminaries, the soil impedance matrix in the frequency domain can be computed by MISS3D in order to estimate the soil matrices. However, in this case, the real part of the impedance function is difficult to be approximated by a polynomial of second order. Therefore, the MKC formulation yields to time impedance evolutions that globally differ from an approximation of the Dirac's delta distribution. This can be appreciated in Fig. 3.20 where time impedances computed with and without MKC decomposition are plotted.

In fact, for this case, if the soil matrices are not correctly identified the calculation fails to converge. Other decompositions have also been tested, such as KC, MC and MK, but none of them yielded to convergence. Therefore, all calculations have been carried out without any kind of impedance decomposition. The obtained acceleration response at the top of one of the buildings, in the x -direction and y -direction, is compared with the reference solution in Fig. 3.21.

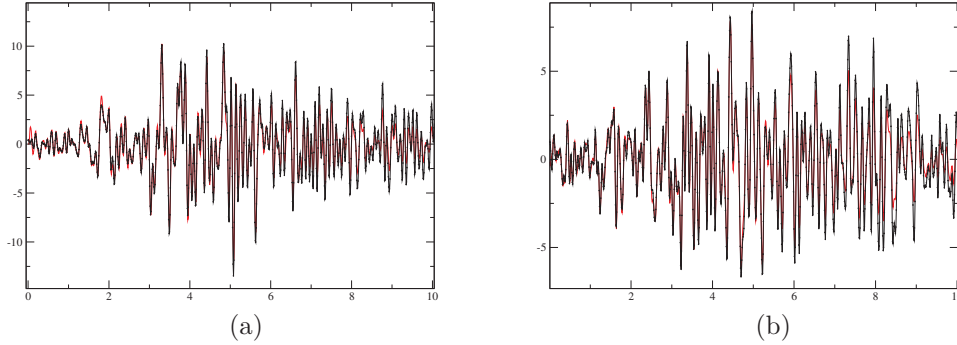


Figure 3.21: Transient accelerations at the top of one of the buildings in the (a) x -direction and (b) y -direction respect to the reference solutions.

3.3 Nonlinear framework

The two numerical applications allowing an MKC formulation are considered in this section. The reason is that, in such cases, a transient referent solution can be obtained in a straightforward way. Indeed, the soil can be replaced by a lumped-parameter impedance and assembled to the FE model as sketched in Fig. 3.22.

Lumped-parameter model

The nonlinear behaviour is introduced by an elastoplastic spring with one end attached to the upper mass m_1 and the other, to a smaller mass m_2 . Analogously to the linear numerical application, a square surface foundation layering on a homogeneous half-space is connected to mass m_2 by means of a rigid body constraint (see Fig. 3.23) and the loading of Fig. 3.6 is considered. The soil impedance seen from the foundation is again computed with a boundary element method in the Laplace domain. The same properties are considered for the structure and the soil, except of the fact that no viscous dissipation is considered for this case. The elastoplastic behaviour of the spring is modeled with the linear kinematic work hardening law sketched in Fig. 3.23. The elastic deformation is characterized here by the elastic stiffness matrix \mathbf{K}_e which, after reaching the yield load \mathbf{F}_y , becomes $\mathbf{K}_p = 0.1\mathbf{K}_e$.

The governing equations of this numerical model from the non-inertial reference frame of the structure –which is undergoing the free-field acceleration $\gamma_f(t)$ of Fig. 3.6– can be written at $t = n\Delta t$ as follows:

$$\begin{bmatrix} \mathbf{M}_{11} & \mathbf{0} \\ \mathbf{0} & \mathbf{M}_{22} + \Psi_2^1 \end{bmatrix} \begin{bmatrix} \ddot{\mathbf{u}}_{1,n} \\ \ddot{\mathbf{u}}_{2,n} \end{bmatrix} + \begin{bmatrix} \mathbf{F}_{1,n}^{int} \\ \mathbf{F}_{2,n}^{int} \end{bmatrix} = \begin{bmatrix} -\mathbf{M}_1 \mathbf{e}_x \gamma_{f,n} \\ -\mathbf{M}_2 \mathbf{e}_x \gamma_{f,n} \end{bmatrix} + \begin{bmatrix} \mathbf{0} \\ -\mathbf{R}_{\Sigma(n-1)} \end{bmatrix} \quad (3.25)$$

where $\mathbf{F}_\alpha^{int}(t)$ ($\alpha \in \{1, 2\}$) denote the nonlinear internal efforts in the structure and depend on both displacement and velocity vectors. The interaction forces $\mathbf{R}_{\Gamma,n}$ have been directly substituted by Eq. (2.41). It has to be noticed that the application

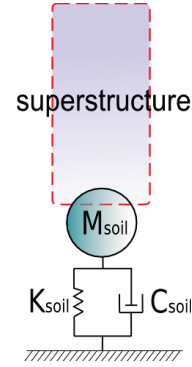


Figure 3.22: Model for the nonlinear reference solution.

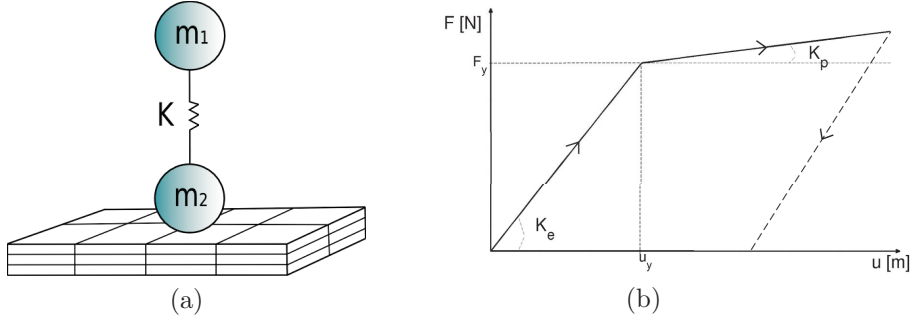


Figure 3.23: (a) Simplified model of a structure on a square surface foundation. (b) Linear kinematic work hardening law of the nonlinear spring K .

considered here is particularized to the case where $\tilde{\mathbf{K}}_\Gamma = \tilde{\mathbf{C}}_\Gamma = \mathbf{0}$, that is the case where only inertial terms are taken into account for the computation of the convolution integral:

$$\mathbf{R}_{\Gamma,n} = \sum_{k=1}^n \Psi_2^{n-k+1} \ddot{\mathbf{u}}_{2,k} = \Psi_2^1 \ddot{\mathbf{u}}_{2,n} + \sum_{k=1}^{n-1} \Psi_2^{n-k+1} \ddot{\mathbf{u}}_{2,k} \quad (3.26)$$

where $\Psi_2^k = \mathbf{Z}_m^k \tilde{\mathbf{M}}_\Gamma$. As mentioned at the beginning of the chapter, coefficients \mathbf{Z}_m^k can be efficiently computed by using FFT algorithms.

The governing equations are finally solved for displacement by using the modified average acceleration time integration scheme of the Newmark family ($\beta = 0.25$, $\gamma = 0.5$). This time integration scheme allows to introduce numerical damping by means of the parameter α_d . Hence, if numerical damping is introduced ($\alpha_d = 0.1$) for the reference solution computed with \mathbf{F}_y , the measured relative error reduces to $e_{10} = 1.59\%$. This artificial damping that is introduced is directly related to the iterative Newton procedure. The fact of considering only inertial terms for the convolution decomposition may also have an influence. Otherwise, the stiffness terms coming from the soil impedance would have to be assembled to the tangent matrix within each nonlinear iteration and thus, modify the final response.

It should be noted that if yield load is chosen sufficiently large, the entire calculation remains linear. Therefore, linear and nonlinear responses can easily be compared using a fixed precision, for example $\epsilon_{CQM} = 10^{-10}$. Fig. 3.24 shows that the displacement at m_1 in the x -direction compared to the reference solution and also to the linear solution for \mathbf{F}_y . It is then observed that the amplitude of displacements is increased as expected. In addition, when the elastoplastic effects are taken into account, the structural response is clearly shifted to the low frequencies because of the reduction in stiffness ($\mathbf{K}_e > \mathbf{K}_p$). However, only one fundamental frequency seems to stand out in the response as if just one equivalent stiffness were present in the system. Hence, the effects of both stiffness \mathbf{K}_e and \mathbf{K}_p on the response can be highlighted by increasing the yield load (see Fig. 3.25).

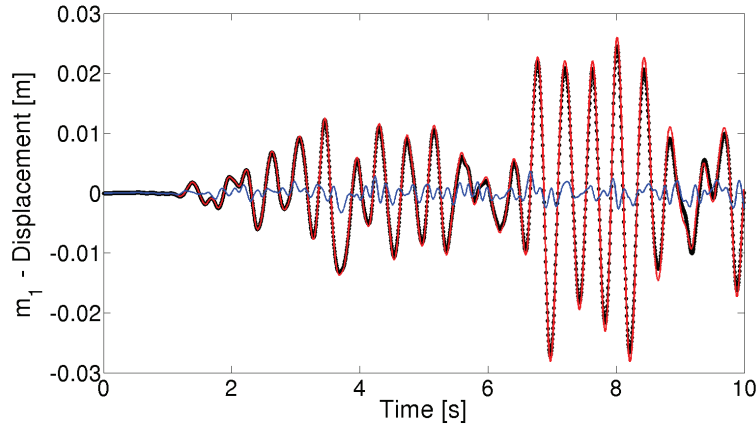


Figure 3.24: Displacement at m_1 in the x -direction computed with the hybrid time-Laplace domain approach (black markers) and compared to the reference solution (red line) and to the linear response (blue line) for a yield load F_y .

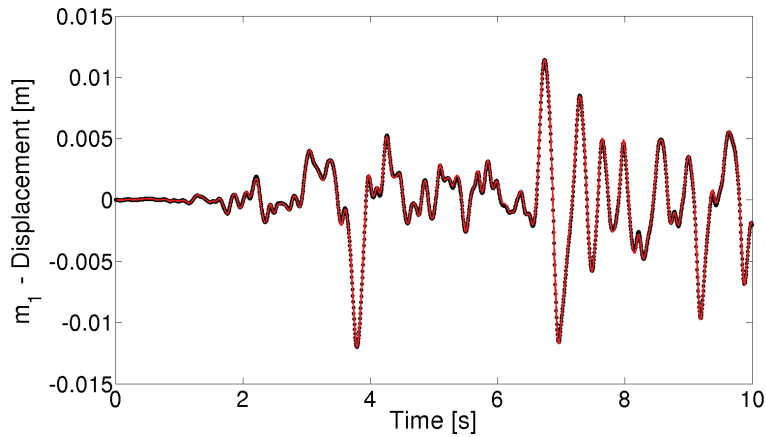


Figure 3.25: Displacement at m_1 in the x -direction computed with the hybrid time-Laplace domain approach (black markers) and compared to the reference solution (red line) for a yield load of $6.5F_y$.

Large-scale FE model

The same FE model used in Sec. 3.2.3 is here extended to a nonlinear analysis, but only for a rigid surface foundation. As for the lumped-parameter model, a constitutive law of plasticity is globally spread in all the building. The influence of this nonlinear material behaviour on both acceleration and displacement responses can be appreciated in Fig. 3.26 for the case of the reference solution.

Nonlinear analysis has been done for different yield loads and for different types of decomposition within a MKC formulation. Problems of convergence have been encountered when an incomplete MKC formulation is used, such as MK, MC or even KC. On the contrary, if a full MKC decomposition is adopted not only better results

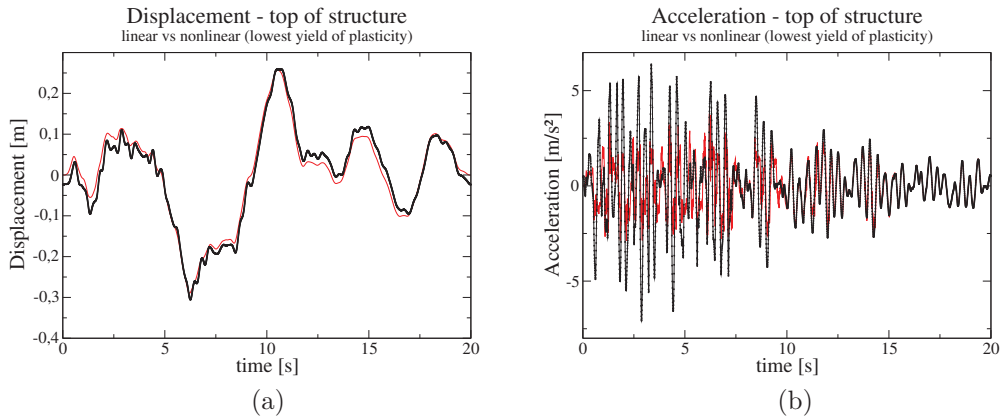


Figure 3.26: (a) Displacement and (b) acceleration at the top of the building for linear (black) and nonlinear (red) responses.

are obtained in respect to the reference solution but also no numerical damping is observed. In fact, the lower the yield load (that is a stronger nonlinear behaviour) the lower the relative error (see Tab. 3.3).

Table 3.3: Relative errors between acceleration response computed by the HLTA and the reference solution for different yield loads.

| F_y | $F_y/10$ | $F_y/20$ |
|-------|----------|----------|
| 5.40% | 4.45% | 4.06% |

Fig. 3.27 and 3.28 show the displacement and the acceleration in the x -direction at the top of the reactor building when the HLTA is used with MKC formulation.

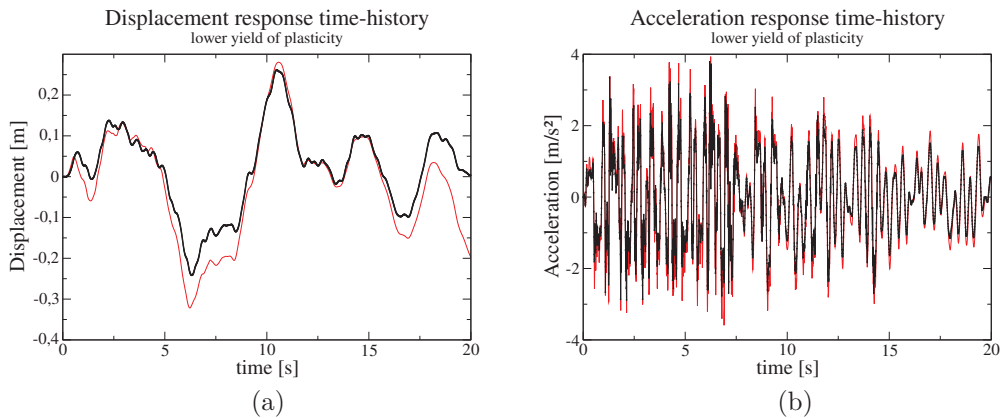


Figure 3.27: (a) Displacement and (b) acceleration in the x -direction using the HLTA with an MKC formulation.

If only inertial terms are used for the evaluation of SSI interaction forces, ie. a M decomposition is done as in previous section, the calculation yields to a wrong

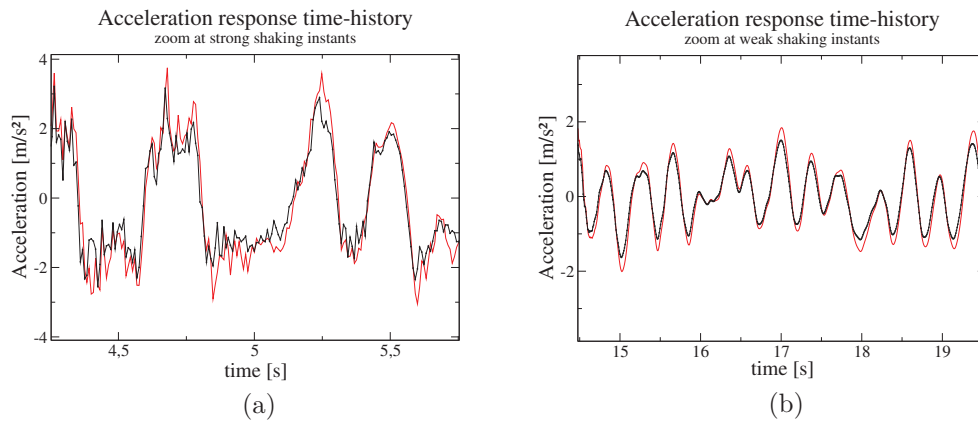


Figure 3.28: Zoom at the acceleration response obtained with an MKC formulation for (a) some strong shaking instants and (b) some weak shaking instants.

solution (see Fig. 3.29). In particular, whereas displacement response seems to be almost in phase with the reference solution –despite clear amplitude discrepancies–, acceleration response is completely dephased, probably due to an incorrect Newmark operator.

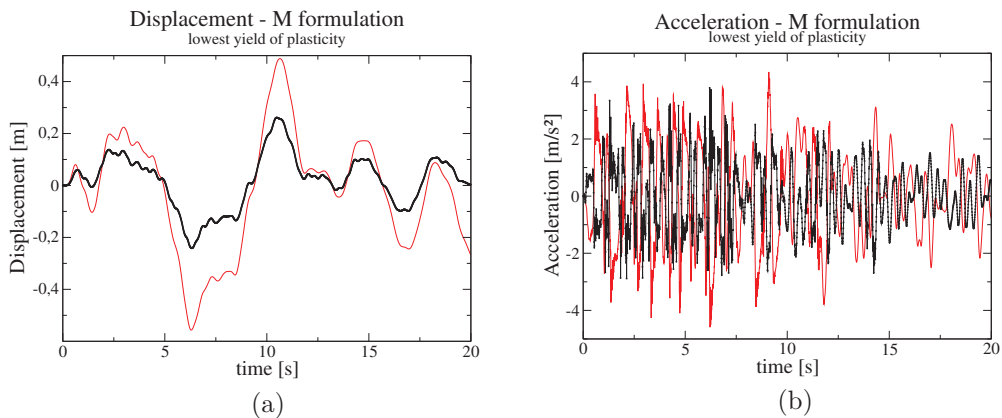


Figure 3.29: (a) Displacement and (b) acceleration at the top of the building (in the x -direction) for a HLTA applied with an M formulation.

3.4 Conclusions

Some considerations about HLTA numerical implementation have been listed. In particular, it should be recalled the fact that Convolution Quadrature Method can be straightforward implemented by using FFT algorithms. Moreover, it has been highlighted that SSI interaction forces are written in the form of a convolution integral because they account for ground-borne propagation phenomena. And so do time impedance functions.

Regarding the MKC identification to approximate the soil impedance matrix, a polynomial expression in the frequency domain can generally be used to identify its MKC matrices. This polynomial assumption is almost fully verified for homogeneous soils or regular layered soils. Nevertheless, in the case of embedded foundations or complex soil profiles, the identification of MKC matrices becomes more complex and the use of advanced algorithms, such as least squares, might be required. Whether or not such algorithms give better results remains unknown and future research works should be carried out.

Within a linear framework, HLTA has been tested on a lumped-parameter model, on a large scale FE model and on a 3SI application. Therefore, the computation of soil impedances in the Laplace domain has been validated in the case of different types of soils and foundations. Moreover, it has been concluded that the use of an MKC formulation gives better results, for both linear and nonlinear analyses, when MKC matrices can be determined. However, it is important to note that in the case of rigid surface foundations or embedded ones, conservative solutions have been obtained. Finally, it has been observed that accounting for nonlinear behaviour tends to reduce differences respect to the reference solution.

Chapter 4

Industrial numerical application

“We hope that, since the endless complexity and variety of natural phenomenon are caused by few basic elements and laws, their visual simulation can be achieved using few basic primitives and algorithms. We are still far from that goal, but then again we do not have as many processors or as much time as nature does.”

A. FOURNIER and W. T. REEVES, 1987

In this chapter, the HLTA is applied on a modified version of the numerical model used for the SMART project in 2008. Within linear and nonlinear analysis the HLTA is compared to a full FEM approach, assumed as the reference solution.

4.1 Introduction and methodology

The assessment of civil engineering structures under seismic loading is still a complex subject that remains a relevant research topic among the engineering community. In this framework, Électricité de France (EDF) and the Commissariat à l'Énergie Atomique et aux énergies alternatives (CEA) launched in 2007 an international benchmark under the name of SMART-2008 [77]. Seismic design and best-estimate Methods Assessment for Reinforced concrete buildings subjected to Torsion and non-linear effects (SMART) were thus tested on the prediction of the seismic response of the SMART specimen on the CEA Azalée shaking table (see Fig. 4.1). The correspondent numerical model, well-known by the scientific community, has been modified in order to construct a SSI system that could be used in the present study.



Figure 4.1: Experimental set-up.

Indeed, the already available SMART building has been first completed with a concrete slab (see Fig. 4.2). In order to build up the SSI system, a soil domain has been secondly added at the base of the foundations. Whereas the resulting superstructure is modelled using FE in *Code_Aster*, three different strategies have been considered for modelling the soil domain. The first one deals only with the FEM, ie. a large block of soil is discretized in FE till the bedrock. This technique is maybe the most versatile one since it is compatible with both frequency and time domain resolutions and it also allows for nonlinear soils. The second one, which is restricted to the frequency or Laplace domain, accounts for the (linear elastic) unbounded soil by means of an impedance function computed with a BEM and defined all over the base-slab of the structure. And the last one is a mixture of the other two approaches. It combines a bounded region of soil modelled with a FEM with the rest of the unbounded domain, also modelled by BE impedance function. Of course, in this case, the FE region of soil can exhibit nonlinear (in the time domain). Recall that code MISS3D is used for all BE calculations and thus, for the computation of the impedance function. In order to compare all these approaches within the present SSI analysis, the solution provided by the full FE approach will be considered as our *reference solution*.

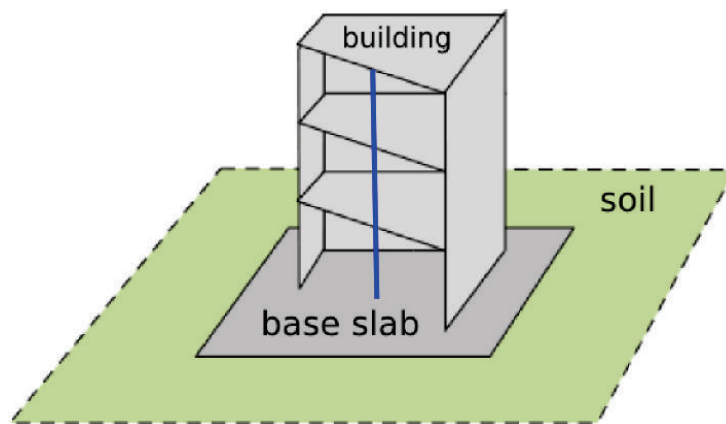


Figure 4.2: Schematic view of the soil-structure system to be modelled.

More details on the FE modelling of the SMART building and the soil properties are given in the following sections.

4.1.1 The structural FE model

The building, modelled in *Code_Aster* with 2D shell elements (floors and walls) except for a multi-fiber beam going from the bottom to the top the structure (blue line in Fig. 4.2), constitutes the only domain exhibiting a nonlinear behaviour. The FE model consists of 1 500 nodes and thus 9 000 degrees-of-freedom. Depending on the type of FE, different material laws are considered:

- For shell elements, reinforced concrete showing a global damage law known as GLRC_DM [51, 92] is used. The GLRC_DM law was originally developed for seismic calculations because of its global character which results in better performance results. However, it exhibits low dissipation rates and some current research looks for improvements on this way.

- For multi-fibers beams, the 1D-La Borderie constitutive law [19, 105] is adopted for concrete and a linear kinematic hardening law, for steels. The 1D-La Borderie law is well-adapted to the modelling of localized stiffness drops. It is thus particularly interesting for seismic analyses since it becomes an additional source of dissipation during loading cycles.

According to recommendations of reinforced concrete models and also of GLRC material law, the size of lateral element should be between 30 and 50 cm and, for the present study, the lower bound of 30 cm has been used for the building mesh.

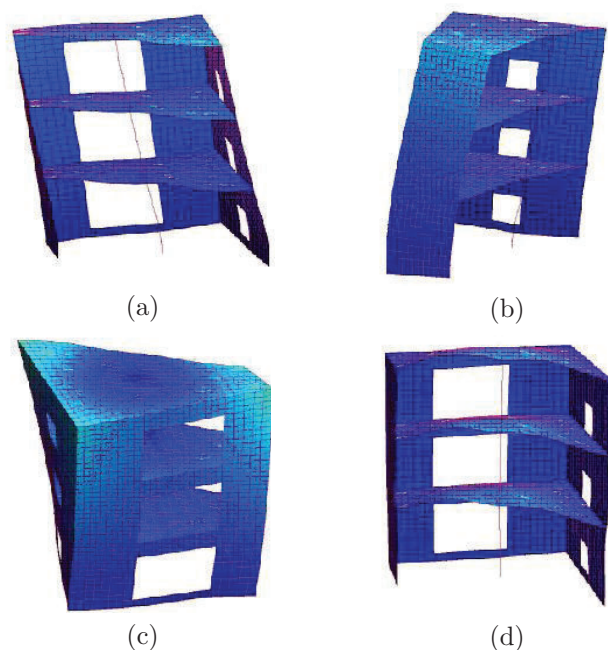


Figure 4.3: (a) and (b) Bending modes shape around x and y axis, (c) Torsional mode shape and (d) Pumping mode shape.

Table 4.1: First eigenfrequencies of the base-clamped SMART structure.

| | Bending 1 | Bending 2 | Torsional | Pumping |
|-----------------------|-----------|-----------|-----------|---------|
| Eigenfrequencies [Hz] | 9.0 | 15.9 | 31.6 | 32.3 |

In order to characterize the dynamic properties of the SMART building, the modal shapes of the first eigenmodes of the structure satisfying zero displacement at the base, as well as the value of the corresponding eigenfrequencies are given in Fig. 4.3 and Tab. 4.1 respectively. A Rayleigh damping model is used by considering a modal damping of 2% at the frequencies of 5 Hz and 15 Hz.

In the framework of this SSI analysis, the shaking table of the experimental set-up must be replaced by an unbounded domain of soil. Different choices could thus be selected in order to build the foundations of the structure but, for simplicity of modelling, a rigid and massive slab is added at the base of the building (see Fig. 4.4).

This squared base-slab with a side length of 4m is modelled with 2D shell elements and introduces 332 nodes. In addition, the foundations are assumed to lay on the soil and thus, a surface foundation is considered for the entire study. It is important to notice that the foundation and the SSI-interface does not always refer to the same part of the mesh. They usually coincide but, if the surrounding soil is also modelled, the SSI-interface would become embedded into the soil whereas the foundation (the base slab) would remain on the free-surface of the soil.

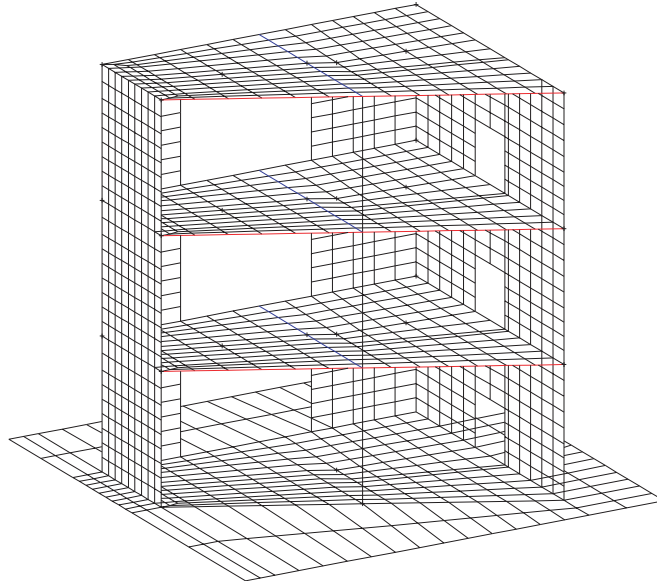


Figure 4.4: Numerical FE model of the SMART building and its foundations.

4.1.2 The viscoelastic soil domain

The soil is assumed to behave linearly in the whole domain. It consists of seven horizontal layers of different properties and thickness lying on a solid bedrock. In particular, the velocity-depth trend is presented in Fig. 4.5, where the z -coordinate denotes the downwards direction, ie. from the free-surface to the bedrock. As seen in previous chapter 3, soils showing a shear velocity pattern that increases with depth give time impedance waveforms that drop rapidly back to zero. In these cases, the mass, damping and stiffness matrices associated to the soil can easily be estimated by the approach proposed in Sec. 3.1.4. Therefore, the same technique is used in this chapter for the case of surface foundations.

Regarding the soil damping model, two different models are considered depending on the resolution domain. When a frequency domain calculation is carried out, a hysteretic soil damping model of coefficient β_s is used. On the contrary, when the problem is solved in the time domain, a Rayleigh damping model [129] is assumed for the soil, that is a damping matrix written as a linear combination of FE stiffness and mass matrices:

$$\mathbf{C} = \alpha_1 \mathbf{K} + \alpha_2 \mathbf{M} \quad (4.1)$$

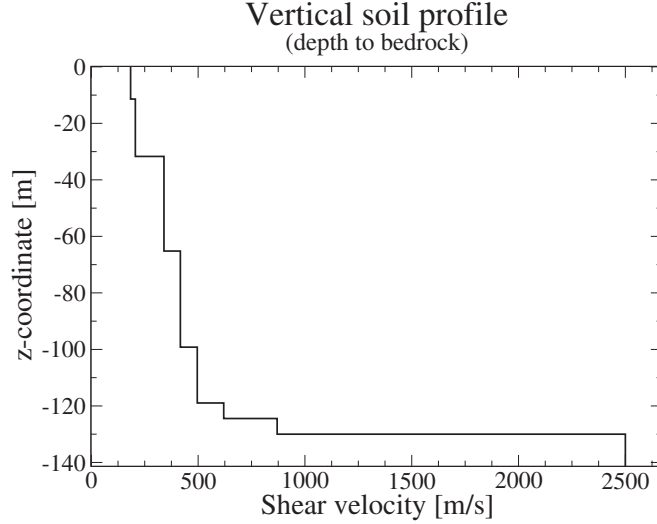


Figure 4.5: Vertical soil profile as a function of the shear velocity.

where α_1 and α_2 are some parameters arbitrarily tuned. Provided that vibration mode shapes are used to uncouple equations of motion, Eq. (4.1) can be rewritten in terms of the modal damping ratio ξ associated to the circular eigenfrequency ω as follows:

$$\xi = \frac{\alpha_1}{2}\omega + \frac{\alpha_2}{2}\frac{1}{\omega} \quad (4.2)$$

Factors α_1 and α_2 are determined so that the modal damping ratio is equal to a known value at the endpoints of an interval $[\omega_1, \omega_2]$. The frequency range of interest in this application is from 3 Hz to 30 Hz, which gives directly our $\omega_1 = 6\pi$ and $\omega_2 = 60\pi$. The choice of the modal damping values is discussed in the following. Remark that the expressions *eigenfrequency* and *modal damping ratio* are suitable only for bounded domains. As the present text concerns an unbounded domain, these expressions must be understood as the eigenvalues and eigenvectors of the FE matrices of the discretized soil domain and their associated damping ratio. However, they are indeed a good estimation of the resonance frequencies of the whole SSI system.

As mentioned before, one of the limitations encountered deals with the fact that frequency calculations, carried out with MISS3D, use a hysteretic damping model for the soil domain. In our case, the hysteretic parameter corresponding to our soil profile is $\beta_s = 0.05$ for all soil layers. To find the value of the modal damping ratio, the following well-known relation is used:

$$\beta_s = 2\xi = \alpha_1\omega + \alpha_2\frac{1}{\omega} \quad (4.3)$$

If the same hysteretic damping $\beta_s = 0.05$ applies for ω_1 and ω_2 , the following parameters are obtained: $\alpha_1 = 2.41 \cdot 10^{-4} \text{ s}$ and $\alpha_2 = 0.855 \text{ s}^{-1}$. Using this parameters in Eq. (4.2) results, as Fig. 4.6 can show, in a modal damping ratio below 2.5% over the frequency range of 3 Hz–30 Hz. In order to avoid this too low dissipation

level, an average modal damping ratio of 2.5% within the whole frequency interval is considered:

$$\beta_s = 2\xi = \frac{1}{\omega_2 - \omega_1} \int_{\omega_1}^{\omega_2} \left(\alpha_1 \omega + \alpha_2 \frac{1}{\omega} \right) d\omega \quad (4.4)$$

The latter gives values $\alpha_1 = 3.29 \cdot 10^{-4} \text{ s}$ and $\alpha_2 = 1.171 \text{ s}^{-1}$ when the same modal damping ratio is imposed at both ω_1 and ω_2 . The corresponding Eq. (4.2) is also presented in Fig. 4.6.

Further data on the soil properties, such as C_P or ρ_s , is not provided because of confidentiality clauses.

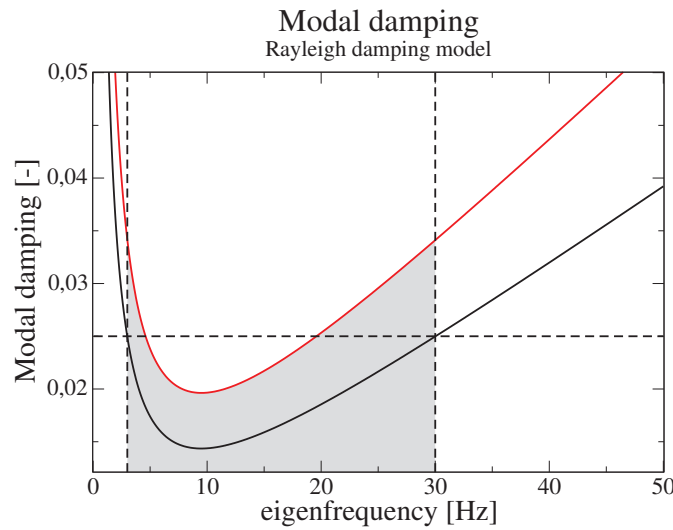


Figure 4.6: Modal damping ratio for an average value of 2.5% (red) between 3 Hz and 30 Hz and the original formula (black) enforcing 2.5% only at endpoints of the same frequency range.

4.2 Soil-structure interaction modelling

In this section three different types of modelling for the SSI system are detailed. The first one, which assumed as the reference solution, corresponds to a full FE modelling of the soil domain. The second one, which is limited to linear problems, is based on a frequency domain BE-FE coupling. And the last one, which uses the HLTA, is reserved to nonlinear analysis. For the last two approaches, a smaller block of soil modelled in FE is considered.

It is interesting to notice that, when the soil is taken into account, the eigenfrequencies of the system switch to lower frequencies. Tab. 4.2 show these results for the case of a full FEM modelling but no significant differences are observed for the two other approaches. Eigenfrequencies reduce approximately between 30% and 50%, standing out the importance of accounting for SSI in similar structures.

Table 4.2: First eigenfrequencies of the entire FE soil-structure system.

| | Bending 1 | Bending 2 | Torsional | Pumping |
|-----------------------|-----------|-----------|-----------|---------|
| Eigenfrequencies [Hz] | 5.9 | 8.7 | 15.3 | 20.1 |

4.2.1 Full FEM resolution

The more classical approach involves the FE discretization of the whole SSI system, that is the unbounded soil and the building. Thus, in order to correctly represent the semi-infinite character of the soil domain, a sufficiently large block of soil has to be considered. Besides, a structured FE mesh needs to be used, in order to avoid frequency filterings during waves propagation. Therefore, unless an efficient adapted parallel computing is available, this kind of full FEM approach usually results in very costly calculations, in both CPU time and memory.

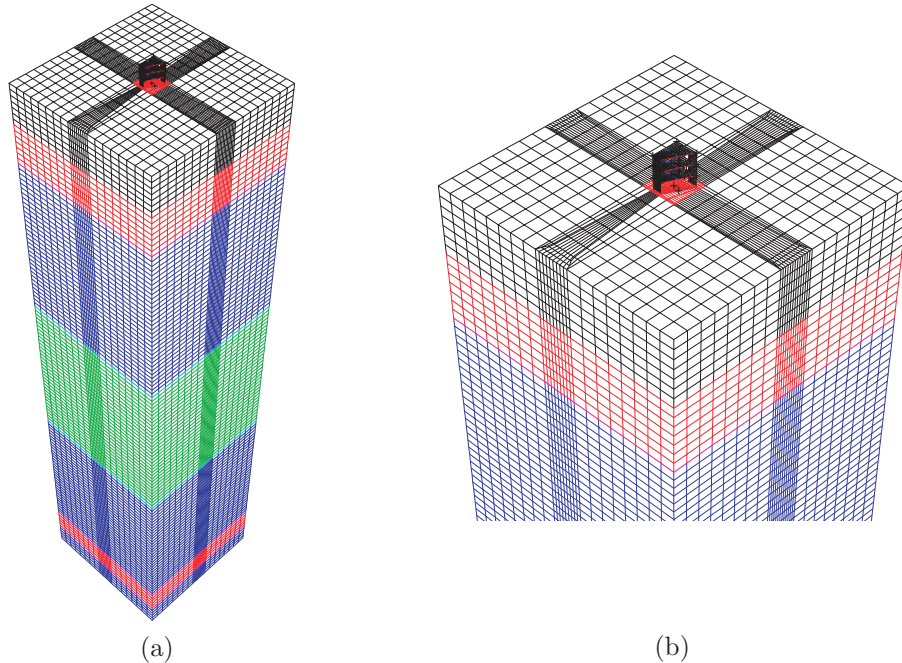


Figure 4.7: (a) FE model of the SSI system using a rectangular meshing. (b) Zoom of the same FE model near the structure.

The meshed soil block is 30 m of side length and 127 m of depth (until bedrock). A conforming meshing between the structural base-slab and the soil is considered, and also between two different layers. Two different meshing strategies have been used. The first one, which uses rectangular elements, resulted in 150 000 FE nodes and a non-regular mesh showing different element sizes, which is not recommended for seismic problems (see Fig. 4.7). The second one, the one that has been used, is based on radial meshing which results in 100 000 FE nodes (about 300 000 degrees-of-freedom) and a more regular mesh (see Fig. 4.8). Since for the latter approach the soil block is obtained by extruding a radially meshed surface, the number of elements

depends on the surface geometry and thus, it increases the total number of degrees-of-freedom. This limitation could have been avoided by meshing the volume of soil automatically but, in this case, an element size should have been imposed. Indeed, for a frequency domain formulation, it is recommended to use 8 nodes per S-wavelength [42]:

$$l_{EF} = \frac{\lambda_S}{8} = \frac{C_S}{8 f_{max}} \quad (4.5)$$

where $C_S = \sqrt{\frac{E_s}{2\rho_s(1+\nu_s)}}$ denotes the shear velocity of the soil and f_{max} the cut-off frequency of the nature of the problem, which is for seismic applications between 20 Hz and 50 Hz. Nevertheless, this criterion may be too severe for a full FEM modelling yielding to excessive computational costs. Therefore, engineers tend to relax it by considering 4 to 6 nodes per S-wavelength.

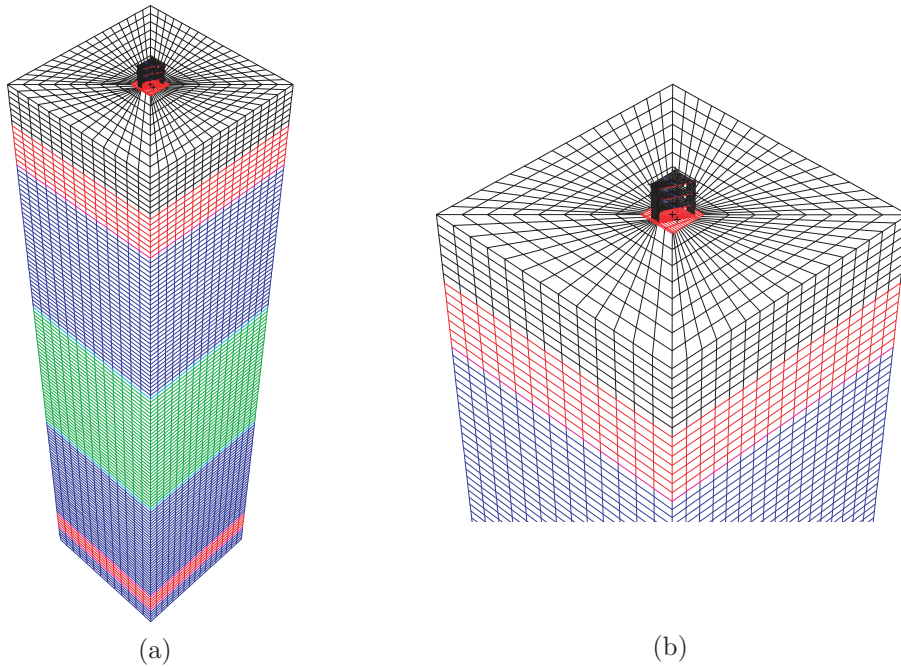


Figure 4.8: (a) FE model of the SSI system using a radial meshing. (b) Zoom of the same FE model near the structure.

In addition, when dealing with unbounded domains, Sommerfeld's radiation conditions have to be satisfied. Indeed, a FE modelling introduces spurious wave reflections because of the artificial boundaries delimiting the soil domain. In these cases, some kind of absorbing elements have to be used in order to get rid of this unwanted reflected waves. Different strategies can then be adopted, such as the use of PML or paraxial elements. It is interesting to notice that the paraxial approximation involves the total absorption of only normal incident waves on the boundaries. They are thus less efficient than PML-based approaches. Nevertheless, paraxial elements, which are available in *Code_Aster*, are used in this analysis to model radiating conditions at the base of the FE soil column. In particular, the zero-order paraxial approximation has been considered [93]. It is indeed equivalent to a set of dashpots of constant $\rho_s C_P$

and ρC_S respectively for P-waves and S-waves. As explained in the next paragraph, lateral sides of the soil domain do not contain absorbing elements.

The loading usually corresponds to a prescribed acceleration on the SSI-interface, however, when the soil domain is modelled with FE the equivalent acceleration at the bedrock has to be obtained. To do that, a one-dimension FE model of a soil column showing the same soil profile as the three-dimensional model is used. By knowing its transfer function, the equivalent acceleration at the bedrock is obtained using a deconvolution technique on the free-field accelerogram. Finally, this acceleration is applied on the whole FE model as a global body motion. In order to reproduce the 1D soil column model in the 3D problem, periodic boundary conditions are imposed on the lateral sides of the soil domain. The three-dimensional solution is not perturbed by these boundary conditions because lateral limits are far enough from the structure.

A full FE modelling of the whole SSI problem allows to account for nonlinear behaviour in a straightforward way. If nonlinear, a transient calculation has to be done, however, if the problem is entirely linear, i.e. a visco-elastic constitutive law is considered for both the soil and the building, the problem can be solved in the frequency domain. Therefore, FE allows for calculations in both frequency and time domains. Unfortunately, not all damping models used in the frequency domain can be used in the time domain. In fact, this is a real limitation when a nonlinear full FEM solution –in the time domain– is compared with solutions obtained using frequency-time hybrid approaches. Whereas in a frequency calculation, either a hysteretic damping or a Rayleigh damping can be used, a transient solution only applies for the latter model. Therefore, in the present analysis, an equivalent Rayleigh damping has been calculated (see Sec. 4.1.2) and used not only in transient calculations but, for simplicity, also in frequency ones. The equivalence between both Rayleigh and hysteretic damping models has been first validated with a harmonic calculation.

4.2.2 Frequency domain BE-FE coupling

When the problem is entirely linear, the more effective approach is based on the coupling of *Code_Aster* to MISS3D [42]. This technique, which underlies a BE-FE coupling, has been used in Sec. 3.2.1 to compute the linear reference solution. As mentioned there, the problem is projected on a Ritz basis and it is solved in the frequency domain. This method applies for rigid and flexible SSI-interfaces lying on the free-surface or being embedded into the soil but it is limited to elastic homogeneous soils and horizontally layered (local homogeneous) media.

In the present study, this approach is used for the case of a building lying on a bounded region of soil modelled in FE (see Fig. 4.9). The unbounded part of the soil is accounted by MISS3D using a frequency domain BE method. This FE part of soil measures 10 m of side length and 6 m of depth, within the first layer of soil. In order to avoid rocking modes by action of the building weight, this soil model, as well as the one for the full FEM solution, is centered horizontally according to the gravity center of the building. Because of the important number of degrees-of-freedom (3 500), the modal reduction technique described in Sec. 3.2.1 is used on the SSI-interface and its kinematics is thus represented by means of 240 interface eigenmodes, a sufficient number of modes to ensure the convergence of the solution [4]. For the building, the number of modes collected corresponds to the number of modal masses whose addition exceeds the 90% of the total mass of the structure. In order to reduce the

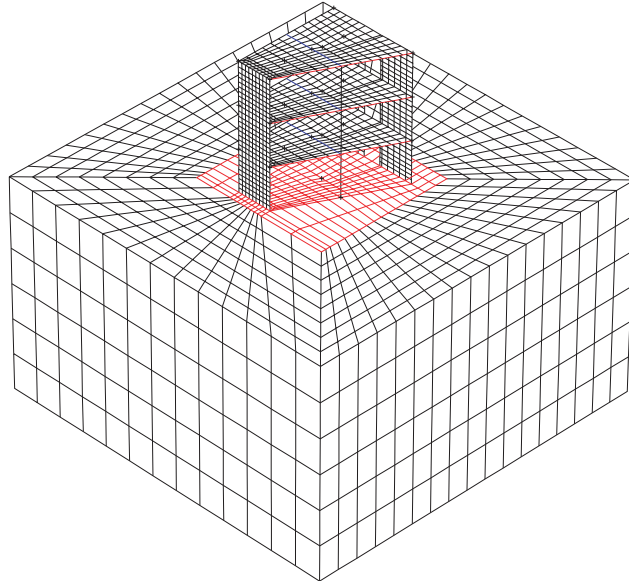


Figure 4.9: FE model used for the BE-FE coupling approach.

number of modes, not all the modal masses but only those which represent at least 0.1% of the total structural mass are retained.

The damping model considered in the FE region of soil corresponds to a Rayleigh model. It is calculated using the procedure described in Sec. 4.1.2 in order to get equivalent results to those that would be obtained with a hysteretic damping model (see Fig. 4.12). The rest of the unbounded soil, since it is accounted by a BE method in the frequency domain, is assumed to be modelled with hysteretic damping.

4.2.3 Hybrid Laplace-Time Domain Approach

In opposition to the previous section, the present approach, which is also applied on the model of Fig. 4.9, is reserved for nonlinear analysis and thus for transient calculations. Hence a Rayleigh damping model is used for the bounded soil region. As for the frequency domain BE-FE technique, the unbounded part of soil uses a hysteretic damping model. As well as for the frequency domain BE-FE coupling, the HLTA relies on a modal reduction technique of 240 eigenmodes for the representation of the interface dynamics, which results in an acceptable computational cost.

Chap. 3 concluded that an MKC decomposition is recommended when the SSI-interface is defined on the free-surface. Therefore, in order to test this approach with an MKC decomposition the model defined in Fig. 4.4, i.e. without a FE domain of soil, is also considered in this analysis. Indeed, in such a case, the whole domain of soil is assumed to behave with a hysteretic damping model.

When dealing with an embedded SSI-interface the base-slab is assumed to be flexible and its kinematics are accounted by the FE method. On the other hand, if the SSI-interface is on the free-surface the assumption of rigid foundation is adopted because is sufficiently stiff compared to the rest of the building.

4.3 Comparative study

In this section, a comparison of the three different modelling approaches of the same SSI problem presented in the previous section is addressed. First of all, the SSI system is analyzed in a linear framework and afterwards, nonlinear constitutive laws are introduced in the building. Nonlinearities within the soil domain are not considered in the present study.

In seismic analysis, comparisons in the time domain are sometimes not clear. A frequency analysis by using Fourier Transforms is therefore more useful to state conclusions. However, Response Spectra (RS), detailed in Appx. A, gives a good approximation that gets round some intrinsic problems [33]. For instance, if the Fourier Transform of the velocity field has values close to zero, higher values could be obtained for the displacements, yielding thus to unrealistic results. RS give in general more realistic values and this approach is the one used in the present study for post-processing responses.

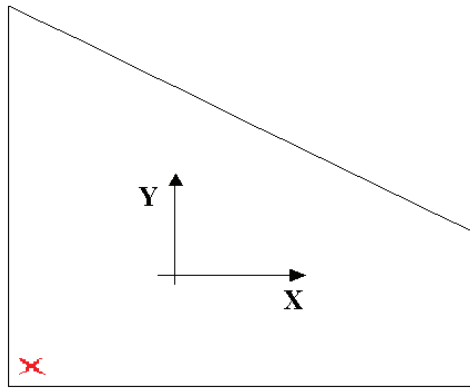


Figure 4.10: View from the top of the building. Red points indicate where acceleration responses have been measured.

In order to get rid of baseline problems, only acceleration results are analyzed. They are normalized with respect to gravity g and measured at one corner of the top of the building (see Fig. 4.10). The third floor has been chosen because more amplification effects are expected to be observed.

4.3.1 Loads

The dynamic response of the structure is the result of the superposition of static and dynamic loads. The first one is a static load corresponding to the weight of the structure. The weight of the soil is not taken into account because it remains linear during the whole calculation and thus, its possibly initial stress state would only translate the resulting structural response.

The second one corresponds to the dynamic loading of the earthquake, which is modelled by the free-field accelerograms used in the experimental tests of the shaking table. Particularly, in the present study, the measured accelerograms during the

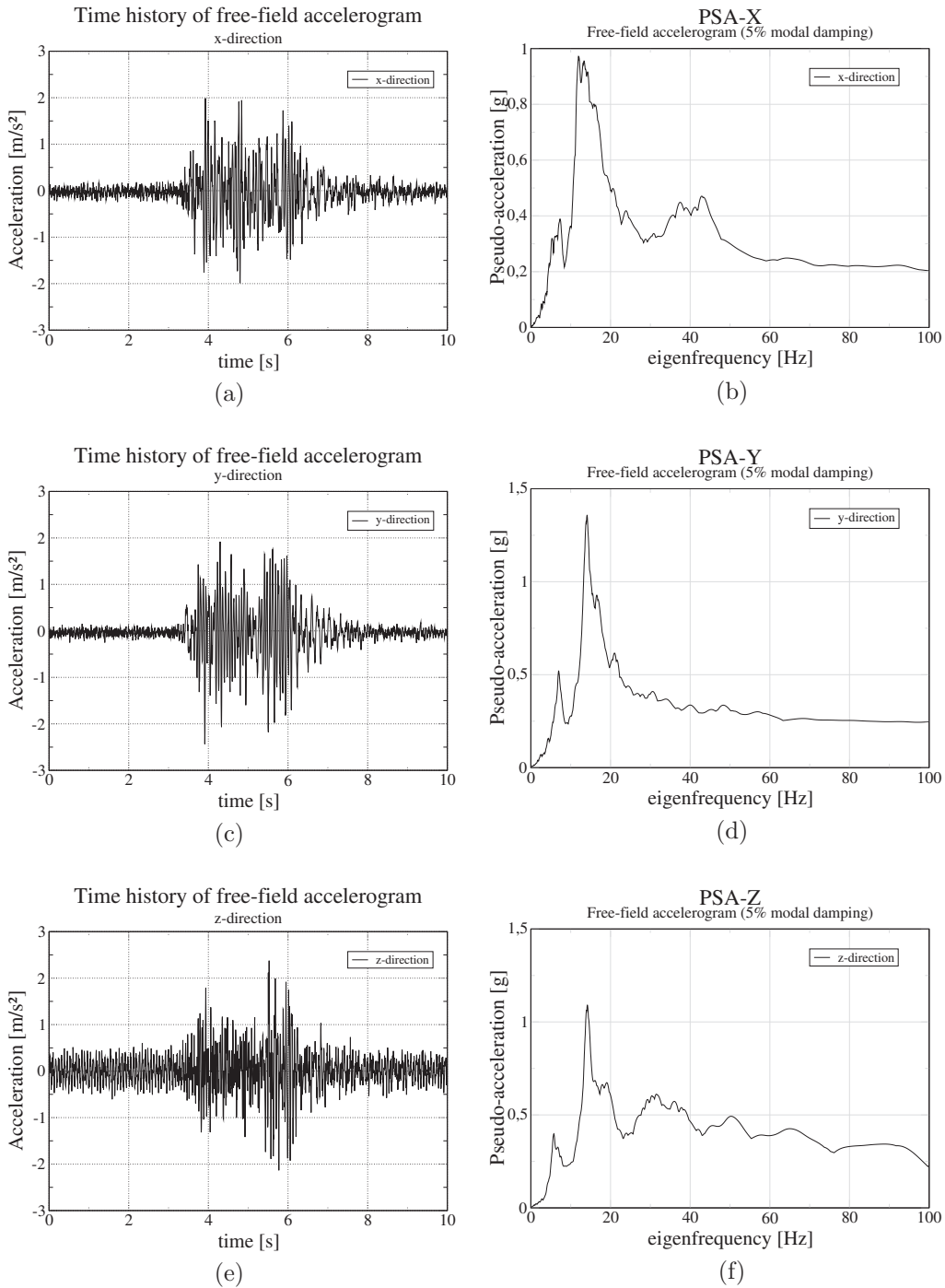


Figure 4.11: Time history and the corresponding Pseudo Spectral Acceleration (PSA) of the free-field accelerogram for (a) and (b) x -direction, (c) and (d) y -direction and, (e) and (f) z -direction.

experimental tests over the shaking table are used. Hence, instrumental noise can be observed in the time history of the accelerations. They are applied on x , y and z -directions in the present analysis. Their time and frequency characteristics can be observed in Fig. 4.11. A time step of $5 \cdot 10^{-3}$ s has been used for the time sampling of the accelerograms. They show a strong phase between $t = 3$ s and $t = 7$ s but during the other time instants the level of acceleration is quite important. Indeed, it remains around 0.5 m.s^{-2} for the vertical direction and lower than 0.2 m.s^{-2} for the other two directions. In addition, the three accelerograms concentrates the most of their energy on the frequency range of 10 to 20 Hz. A cut-off frequency of 50 Hz seems thus acceptable.

Enforcing vanishing conditions at both beginning and end of the three accelerograms allows to satisfy causality conditions and to avoid unwanted oscillations during the first time steps of the calculation. The latter could indeed yield to non realistic damaged parts of the building in a nonlinear analysis.

4.3.2 Linear analysis

First of all, the proper use of the Rayleigh damping model is verified by using the frequency domain BE-FE approach (hereafter FreqBFA). To do that, the model with a bounded FE region of soil is considered. As mentioned before, Fig. 4.12 shows satisfactory results when the frequency response obtained with a hysteretic FE soil are compared with that of viscous FE soil.

Indeed the discrepancies between damping models in each direction are not significant, maybe because the region of soil subjected to damping variations is small with respect to the unbounded domain of soil. Thus, the Rayleigh damping model considered in that region is validated for the following assessments.

To this validation, it follows a comparison between a harmonic full FEM solution and the one obtained with the FreqBFA. Since the comparison is done in terms of PSA (see Fig. 4.13), corresponding transient responses are obtained by means of FFT algorithms. Let the frequency range of interest be only discussed: although responses coincide quite well for the first peak around $f = 7.8$ Hz for y and z -directions, an error of 10.7% is produced for the same peak in the x -direction. If one focuses on the maximum peak around $f = 14.28$ Hz, differences of 14.8% can be observed in all directions. Regarding the rest of the spectrum, one realizes that the full-FEM solution is in general higher than the FreqBFA response. The latter may be explained in terms of the amount of energy dissipated within the soil domain: the use of paraxial elements at the boundaries of the FE domain of soil are not perfectly matching or consistent and hence, levels of acceleration are expected to be higher in the full FEM case. However, the difference between x and y directions is more difficult to explain and may be related to the asymmetric behaviour of the building.

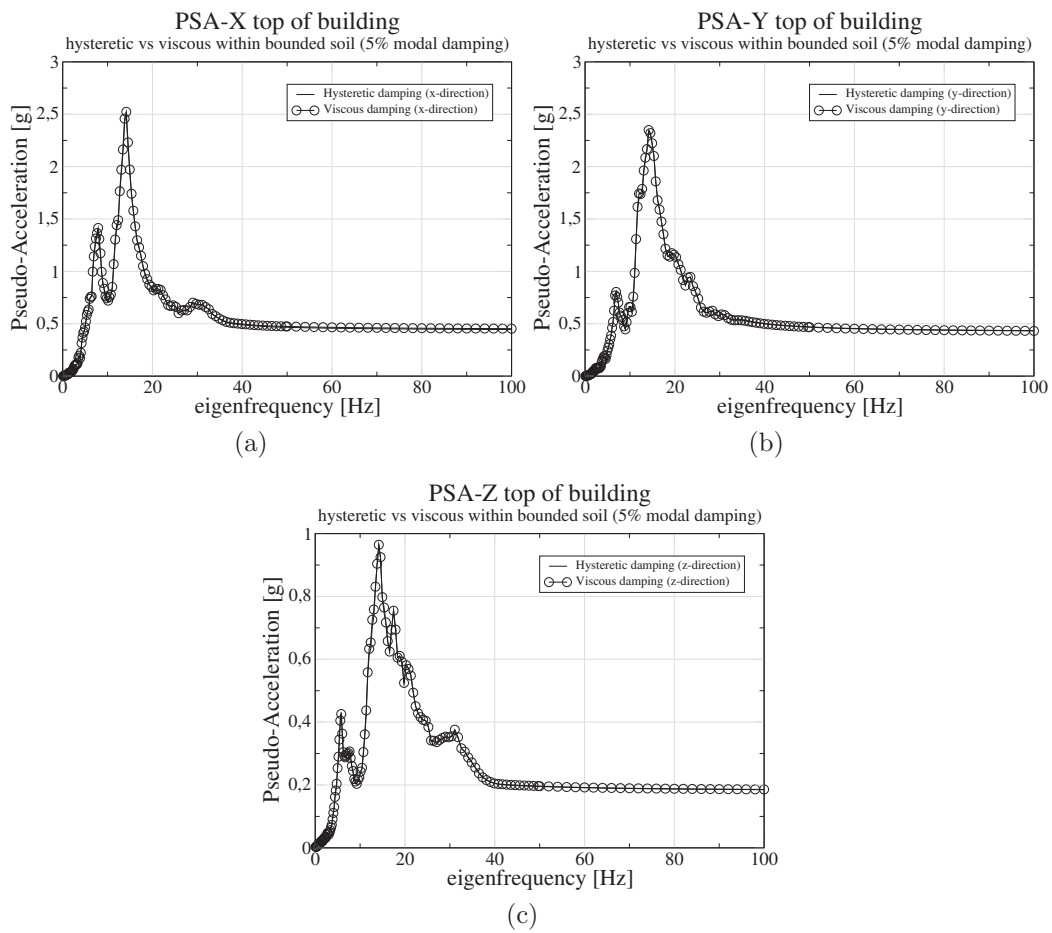


Figure 4.12: Comparison between PSA's: one with a hysteric damping model within the the bounded FE soil and the other, with a viscous damping for (a) x -direction, (b) y -direction and (c) z -direction.

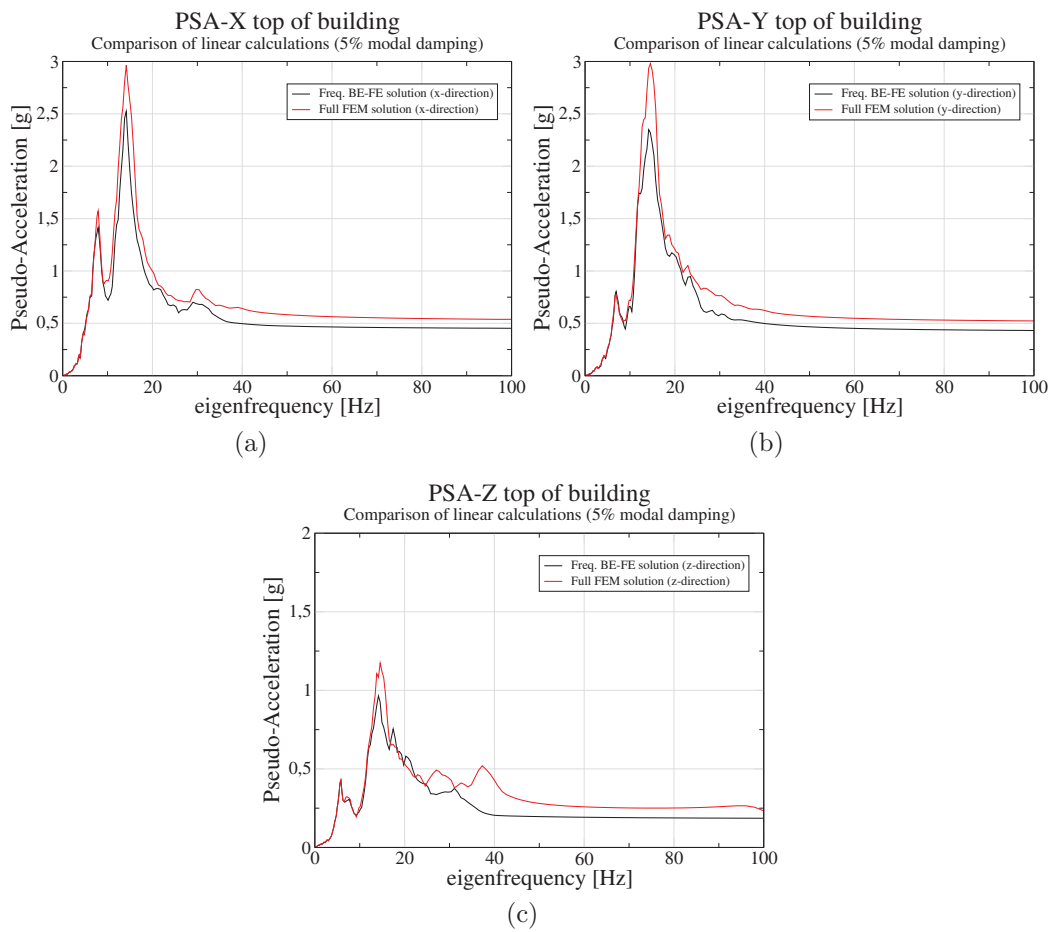


Figure 4.13: Linear calculation comparing FreqBFA and full FE solutions in (a) *x*-direction, (b) *y*-direction and (c) *z*-direction.

4.3.3 Nonlinear analysis

In this section nonlinear phenomena is accounted for and therefore, the FreqBFA cannot be used. The comparison is thus between a transient full FEM solution and the one provided by using the HLTA. As nonlinearities are concentrated in the structural domain, the solution with a surface SSI-interface is also considered. But first of all, the influence of damaging nonlinearities is highlighted. Hence Fig. 4.14 shows the superposition of the PSA's that correspond to linear and nonlinear full FEM responses in each spatial direction. Regardless the spatial coordinate-direction, the

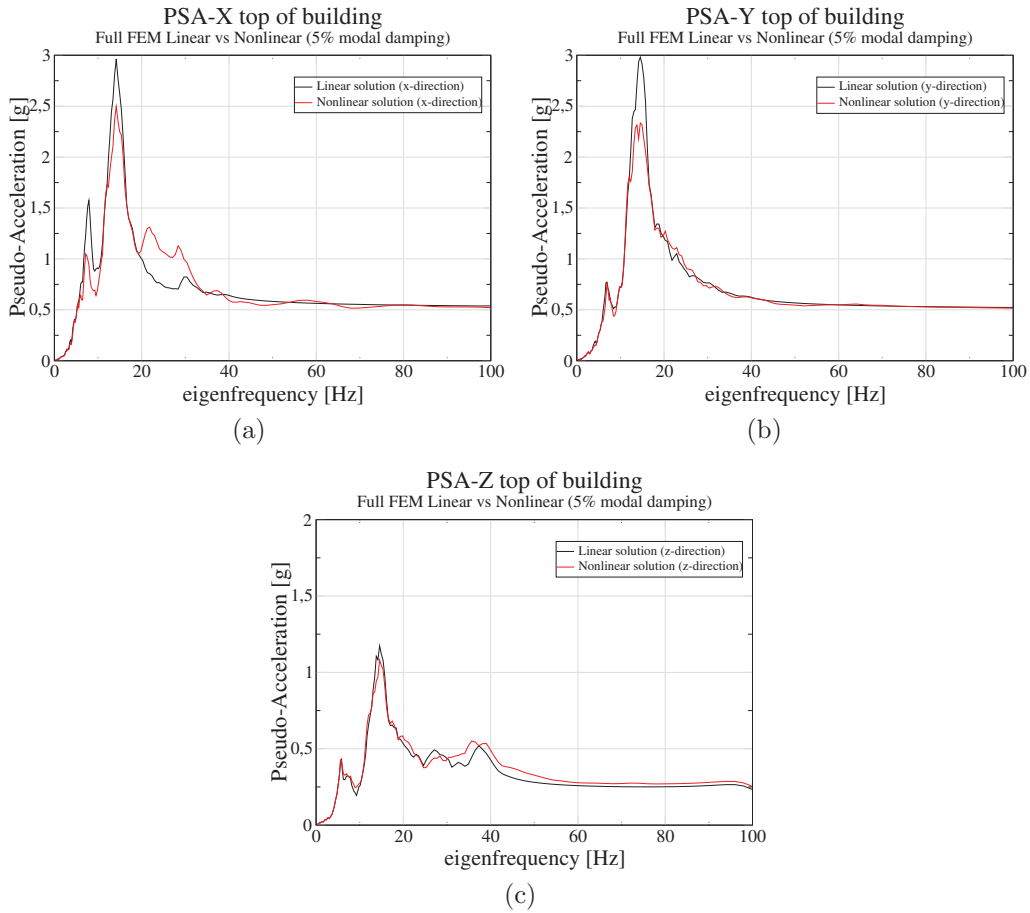


Figure 4.14: PSA of linear and nonlinear transient full FEM solution in (a) x -direction, (b) y -direction and (c) z -direction.

nonlinear responses are globally lower than the linear ones. This is mainly due to the dissipative character of the damaging constitutive law of reinforced concrete. However, and probably because of the asymmetry of the building, differences are observed depending on the direction. Then, no significant difference stand out for z -direction and y -direction except for the most important peak around $f = 14.28$ Hz. In particular, for y -direction the maximum of acceleration is reduced of 22.4%. On the contrary, in the x -direction, peak at $f = 14.28$ Hz is lowered of 15.9% but peak at $f = 7.8$ Hz descends from 1.54 m.s^{-2} to 1.04 m.s^{-2} , this is a reduction of 32.4%. Moreover, a sig-

nificant amplification between 20 Hz and 30 Hz suddenly appears. This phenomenon of amplification has also been observed in the work of Sewell *et al.* [131].

It is interesting to notice that, even though the free-field acceleration considered in the x -direction shows the lower amplitudes, it seems to correspond to the most damaged direction. Recall that the building was designed for torsion analysis so coupling terms certainly exist in the model. Anyway, the effect of nonlinear phenomena globally change the structural response and therefore, within a *best-estimate strategy*, it is important to be accounted for.

In the following, the full FEM solution is compared with the HLTA approach, with and without MKC formulation. As recommended in previous chapter, the MKC formulation is only used for a SSI-interface lying on the free-surface. However, in this case, the base-slab is assumed to be rigid. Recall that the use of rigid foundations yields to higher amplitudes in the final response (see Sec. 3.2.3). Obtained results are plotted in Fig. 4.15.

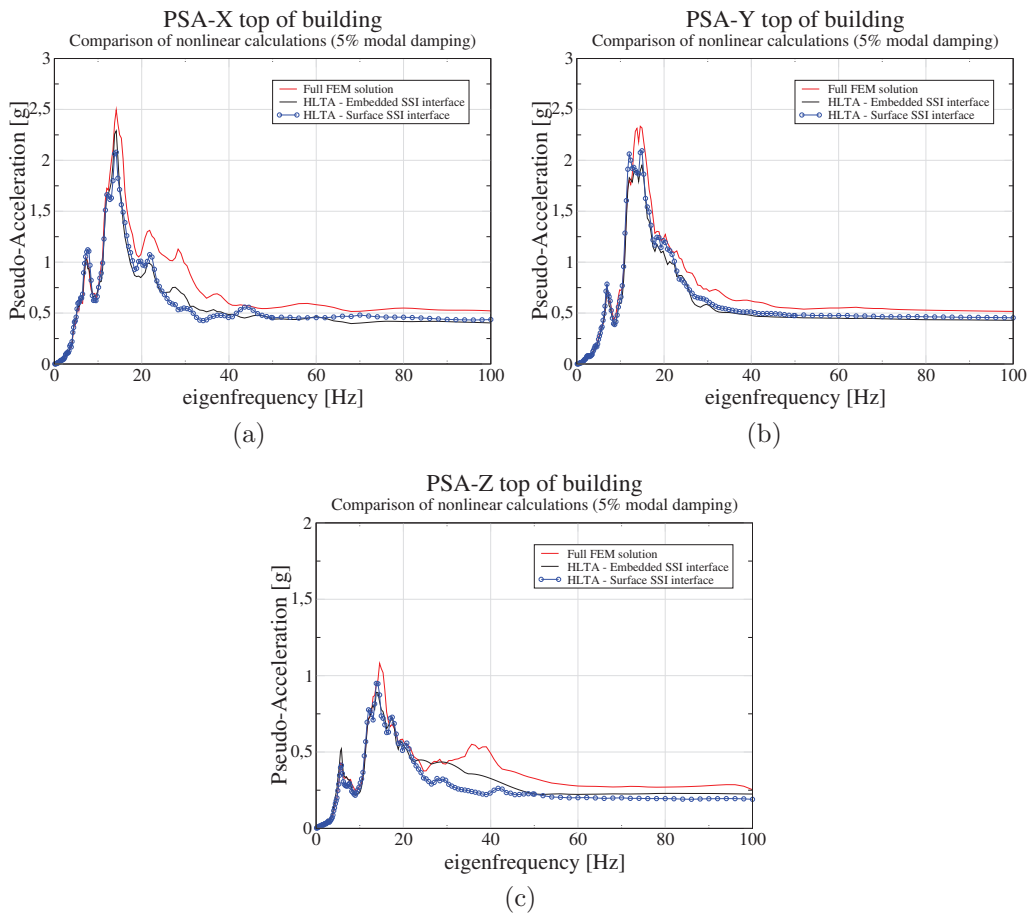


Figure 4.15: PSA of the nonlinear transient full FEM solution compared with the HLTA based on both surface and embedded SSI-interface, for (a) x -direction, (b) y -direction and (c) z -direction.

The analysis of these results must be addressed separately for each direction. In the x -direction, approaches based on the HLTA give lower levels than the one based on the FE method. In fact, very close results are obtained for low frequencies (0 – 20 Hz). In the y -direction, even if the main peak at $f = 14.28$ Hz is not very well approximated, HLTA with surface SSI-interface gives satisfactory results compared with the full FEM solution until $f = 20$ Hz. For higher frequencies, amplitudes are reduced resulting in fact in the lowest PGA among the three approaches. However, the HLTA with embedded SSI-interface behaves in opposition, giving lower levels before the main peak and higher (but not as for a full FE modelling) afterwards. In the z -direction, the HLTA with surface SSI-interface gives similar results as in y -direction. In contrast, the HLTA with embedded SSI-interface gives levels even higher than the full FEM ones for almost all the frequency range.

These differences are not easy to justify and complementary analyses should be done to clarify some points, also for the full FE modelling. However, a phenomenon observed in Chap. 3 seems to repeat again: the nonlinear behaviour tends to reduce the discrepancies with respect to a reference solution. Indeed, as mentioned before, the main damaging state takes place in the x -direction and it is in this direction where HLTA results match the better the reference solution.

Damage assessment

In order to assess building damage, the iso-values of damage of only floors and walls, that is those corresponding to the GLRC.DM law, are plotted. Two variables of damage are analyzed: the one corresponding to traction and the one corresponding to bending forces. All results are normalized by the maximum value.

First, the damage of the building is studied under the action of its own weight. Two different views of the building show that, in traction, the building is already damaged by its body load, in particular, values of 0.20 are reached in the junctions between walls and floors, and floors and multi-fiber beams. As no bending forces are present, no damaging is observed for this reason. Fig. 4.16 the results of the full FEM solution.

After accounting for the weight, seismic loading is considered. At the end of the earthquake, the building is subjected to high levels of damage. It reaches maximum values of 0.95 for traction and 0.87 for bending in a full FE modelling (see Fig. 4.17). The damage is mainly concentrated on the walls, near the ground. When HLTA is used, the levels of damage decrease, being the case of surface SSI-interface the one giving better results. It gives 0.93 for tensile damage and 0.84 for bending, yielding to errors of 2.1% and 3.1% respectively. If the SSI-interface is embedded into the soil, a damage of 0.92 for tensile damage and 0.83 for bending is obtained. The corresponding damage iso-values are shown in Fig. 4.18.

4.3.4 Efficiency of the considered approaches

In this section some remarks regarding the CPU time and memory requirements are addressed.

For linear calculations, the use of the FreqBFA is more efficient than to model the whole SSI system with FE. Indeed, with full FEM approach the calculation takes

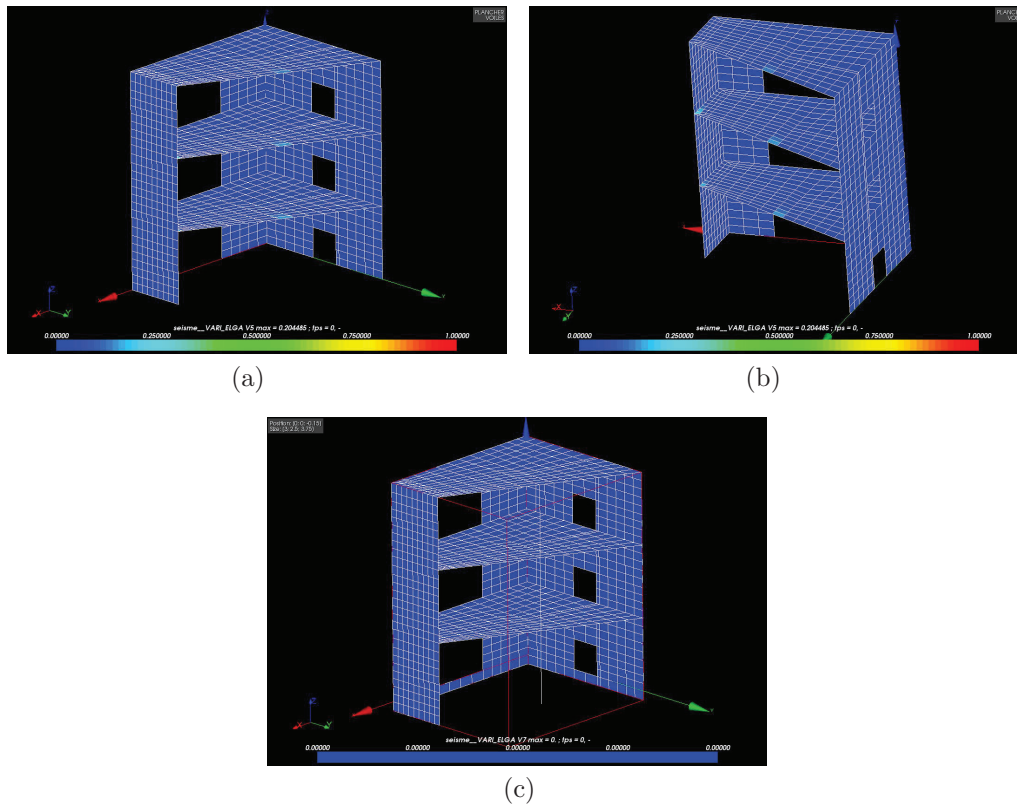


Figure 4.16: For a full FEM modelling under the action of the weight: damage iso-values to traction, (a) front view and (b) side view. (c) Damage iso-values to bending, front view.

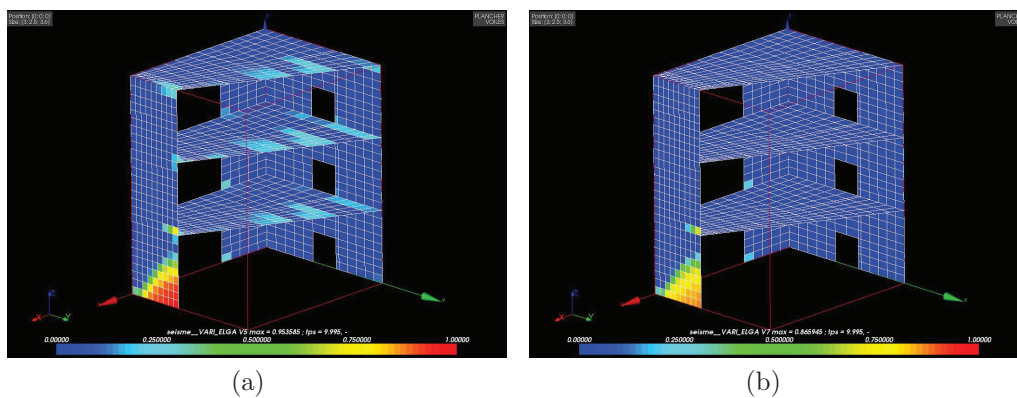


Figure 4.17: For a full FEM modelling under the action of the earthquake: ultimate damage iso-values on traction, (a) front view and (b) side view. (c) Ultimate damage iso-values on bending, front view.

about 200 000 s of elapsed CPU time (no parallelisation is done), whereas the other approach takes only 29 000 s, from which 23 000 s are for the computation of the soil impedance and the equivalent seismic force.

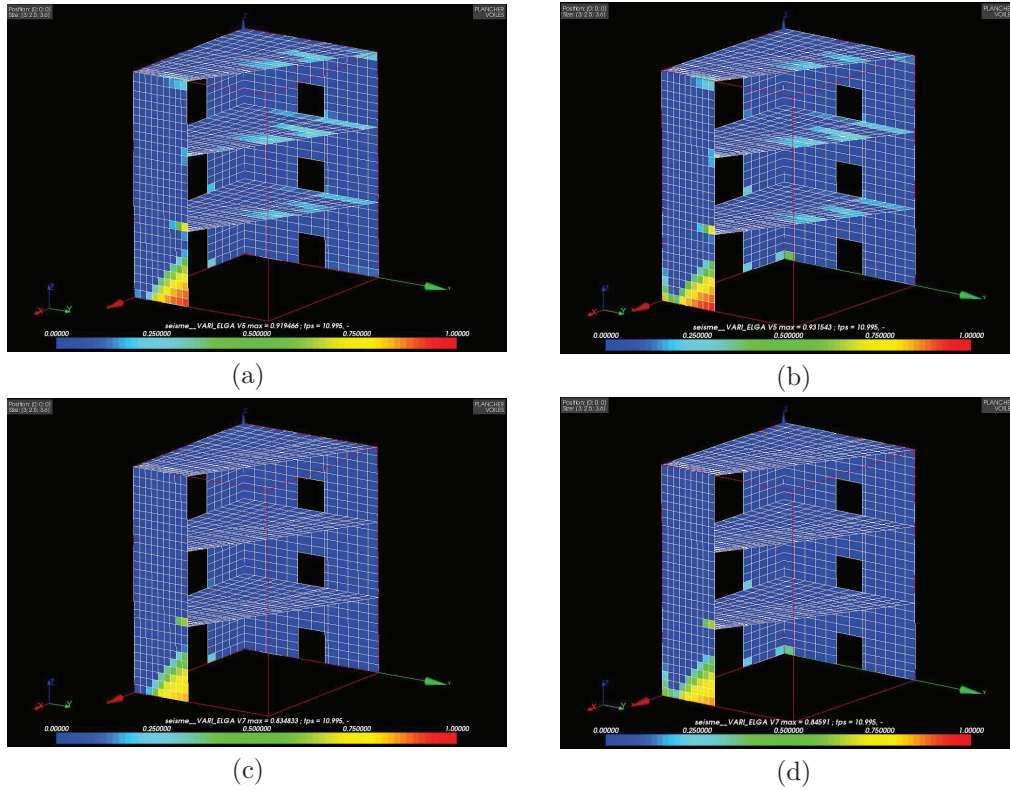


Figure 4.18: For the HLTA solution: damage iso-values on traction when (a) an embedded SSI-interface and (b) a surface SSI-interface are considered. The same for the case of damage on bending: (c) embedded SSI-interface and (d) surface SSI-interface.

For nonlinear calculations and a full FEM modelling, the GMRES algorithm (PETSC package¹) combined to an LDLT preconditionner gives an speed-up of 3.05 since the CPU time is almost reduced by four in four different processors (from 223 000 s to 73 000 s). In the same situation, the CPU time elapsed with a HLTA and embedded SSI-interface is about 129 000 s from which 105 000 s is for the computation of the time impedance function and 3 100 s for the real resolution. For a surface SSI-interface the CPU time elapsed is about 4 900 s without parallelisation, from which 1 500 s comes from the time impedance evaluation and 2 800 s for the nonlinear solver.

It has to be highlighted that even if it seems that the HLTA (for an embedded SSI-interface) needs a more computational effort than a full FEM modelling, the advantage of the former is that the time impedance matrices are computed once for all. This is a very interesting point for parametric industrial studies or even for probabilistic assessments. Moreover, the way in which the BE-FE coupling has been implemented allows the parallelisation of the impedance computation. Indeed, the impedance can be computed at each complex frequency at the same time, since each calculation is independent to each other. In that way, important gains of CPU time can be achieved. Nevertheless, the memory requirements to stock all the time history of the impedance remain the same.

¹<http://www.mcs.anl.gov/petsc/>

4.4 Conclusions

This chapter details the validation of the Hybrid Laplace-Time domain Approach (HLTA) on an industrial structure, the SMART building. In order to validate this technique, a comparison to a full FEM solution (assumed as the reference) is done in linear and nonlinear regime. Nonlinearities come essentially from the damage constitutive law of the reinforced concrete of the building but steel plasticity has also been accounted for. The GLRC_DM and the 1D-La Borderie law are used for the damaging material behaviour. The soil is assumed linear within the entire domain. Recall that the HLTA is based on Laplace BE method which uses a hysteretic damping model for the soil.

Different limitations arise at modelling the SSI system, in particular, during the construction of the reference solution. In fact, no hysteretic damping model can be used in a transient resolution and thus, the nonlinear reference solution obtained by a full FEM modelling involves a Rayleigh damping model. An equivalent damping model is calculated. It is also important to remark that paraxial elements on the boundaries are used. Therefore, spurious reflections might be created inside the soil domain.

In linear framework, the full FEM solution is first compared to a frequency domain BE-FE coupling procedure. Satisfactory results are obtained in terms of response spectra. In nonlinear analysis, the reference solution has been compared to the HLTA with an SSI-interface lying on the free-surface and embedded into the soil. For the latter, a bounded domain of soil has been modelled using the FE method. In this analysis, maximum errors of less than 15% are obtained for acceleration response spectra and 4% for the structural damage assessment at the end of the loading. Better results are obtained with a surface SSI-interface than with an embedded one, but using an MKC formulation as recommended in Chapter 3. Different conclusions can be stated depending on loading direction but globally, one can affirm that the direction involving more damage is the one that shows more concordance between the reference solution and the HLTA.

Regarding time performance, the FreqBFA is the best choice for a linear calculation. For nonlinear analysis, both HLTA (with embedded SSI-interface) and the full FEM solution gives similar computational elapsed times (about 200 000 s). However, for the HLTA, more than a half of the time is due to the computation of time impedance matrices. Therefore, for parametric or probabilistic studies, the latter approach seems to be more performant. Still, CPU time can be reduced in a near future by processor parallelisation. For a surface SSI-interface, computational effort is much more acceptable (< 5 000 s).

Conclusions and perspectives

“The world is round and the place which may seem like the end may also be only the beginning.” IVY BAKER PRIEST, 1958

DYNAMIC soil-structure interaction (SSI) problems mainly focus, in most of the engineering analysis, on computing the response of the building, while the response in the soil is usually the subject of less attention. The global problem is therefore solved directly in the building and the impedance operator, defined on the boundary, is used as a particular type of boundary conditions that accounts for the effects of the unbounded soil. This impedance operator is assumed to be known either in the frequency or Laplace domain. However, if nonlinearities are taken into account, the problem formulated within the superstructure has to be solved in the time domain. In such a case, this particular type of boundary conditions, that depends on a frequency (or Laplace) domain impedance operator, corresponds to a convolution integral in the time domain. As this convolution is homogeneous to a force, it is usually known under the name of SSI interaction forces.

In the first chapter, different approaches to deal with unbounded domains have been reviewed. Following a substructuring procedure, the SSI problem has been formulated and the impedance operator, introduced by means of boundary integral operators. In this framework, a FE method is used for the spatial discretization of the structural domain and the impedance operator is computed by means of a Laplace domain BE method. In particular, this BE-FE coupling approach relies on the chaining of MISS3D (which is a BE code) and Code_Aster (which is a FE code). The use of a BE-FE procedure makes possible to take profit of FE methods, which are well-adapted for complex geometries showing nonlinear material laws, and of BE methods, which implicitly accounts for radiation conditions when dealing with unbounded domains.

Regarding time domain discretization –compulsory for nonlinear applications– the Convolution Quadrature Method (CQM) has been used for the approximation of convolution integrals. Litterature proposes several techniques for the evaluation of these SSI interaction forces and so does the approach presented in second chapter, called Hybrid Laplace-Time domain Approach (HLTA). This approach, which is based on the CQM and on a MKC formulation, consists in the factorization of the polynomial part of the impedance operator. This allows the introduction of acceleration, velocity and displacement quantities coming from the soil domain in the time integration scheme. When MKC matrices are correctly chosen according to the soil domain, the convergence of the calculation is improved. The coupling of the HLTA using a

MKC formulation to a Newmark's time integration scheme is also addressed, mainly because this is the time integration procedure used in the majority of FE analysis. Nevertheless, the HLTA is not limited to the use of Newmark integrators and, *a priori*, it should also work with other time integration schemes such as the HHT method.

Chapter three tries to experiment with the HLTA in different applications. After clarifying some points related to the implementation (the CQM can be combined to IFFT algorithms to improve performance), the notion of time impedance function has been addressed. Within these preliminaries, an interpolation technique for the interaction forces in the time domain has also been proposed. Finally, different numerical applications have been studied in both linear and nonlinear conditions. Different positions of the SSI interface have also been considered as well as the possibly modal formulation of the problem in terms of the HLTA. Chapter essentially concludes that an MKC formulation gives better results if inertial, damping and stiffness soil matrices can be identified. And this can be done when the soil profile is regular with depth or the SSI-interface coincides with the free-surface.

Chapter four is focused on the SSI analysis of an industrial application, the SMART building. Damaging nonlinear behaviour is considered within the reinforced concrete of the building. Linear elastic soil is assumed. The recommendations stated in previous chapter are used for that assessment and results are validated by comparison with a full FE solution. Satisfactory results are observed in a linear framework. However, further research has to be done in order to understand other numerical aspects of the HLTA when adopted in a nonlinear frame.

Perspectives

Some future work is detailed in the following. The main works turn around the HLTA and its numerical improvements. However, rendering the approach user-friendly and ergonomic within the framework of *Code_Aster* is also of great importance for its future capitalisation.

Improving accuracy and performance of HLTA

Regarding accuracy, just recall that quadrature weights (this is time impedance coefficients) can be related to the p -th order approximation of the inverse Laplace transform $Z(t)$ for $t = n\Delta t$ bounded away from zero as follows:

$$Z_n = \frac{\Phi_n}{\Delta t}$$

with Δt being the time step. The quality of this approximation can be improved by adding a few correction terms [84].

Accuracy seems that would be also improved if the CQM is combined to Runge-Kutta schemes instead of multistep methods [6, 7, 88].

Regarding performance, the parallelisation of the evaluation of complex frequencies for the computation of the soil impedance matrix can significantly improve the computational cost. Still, performance can be augmented by introducing an interpolation scheme in the Laplace domain allowing less samples to be collected for the evaluation of SSI interaction forces.

Validation of the HLTA with a nonlinear soil application

Next step to chapter four is to introduce nonlinearities in the bounded region of soil. However, further research has to be done to a better understanding of the model. Particularly, improvements in the FE modelling, such as adding PML's instead of paraxial elements, should be considered to be done in a near future.

***MKC* identification for soils with embedded foundations**

Further research has to be pursued in order to optimize the identification of the inertial, damping and stiffness soil matrices [35]. This research work would aim at allowing an MKC formulation, within the HLTA, not only for surface SSI-interfaces but also for embedded foundations or nonlinear soils.

Time integration scheme coupling

Theoretical developments in numerical analysis can be elaborated. Particularly interesting is the stability analysis of the coupled Newmark time integration scheme and the CQM. Since analysis based on the growing matrix has not yielded to satisfactory results, energy-based methodologies are encouraged to be explored for the same purpose [87].

Probabilistic analysis

The present dissertation is written in a deterministic framework. The extension to a probabilistic analysis can be done as a perspective. In particular, it may be interesting to use the SMART model in order to study the effect of the nonlinear SSI on fragility curves [120]. Besides, also spatial variability effects can also be taken into account.

Bibliography

- [1] E.L. Albuquerque, P. Sollero, and P. Fedelinski. Dual reciprocity boundary element method in Laplace domain applied to anisotropic dynamic crack problems. *Computers and Structures*, 81:1703–1713, 2003.
- [2] R.J. Astley. Wave envelope and infinite elements for acoustic radiation. *International Journal for Numerical Methods in Fluids*, 3:507–526, 1983.
- [3] R.J. Astley and J.A. Hamilton. The stability of infinite element schemes for transient wave problems. *Computer Methods in Applied Mechanics and Engineering*, 195(29 - 32):3553–3571, 2006.
- [4] E. Balmes. Use of generalized interface degrees of freedom in component mode synthesis. In *International Modal Analysis Conference*, pages 204–210, 1996.
- [5] A. Bamberger and T.H. Duong. Formulation variationnelle espace-temps pour le calcul par potentiel retardé de la diffraction d’une onde acoustique. i. *Mathematical Methods in the Applied Sciences*, 8(3):405–435, 1986.
- [6] L. Banjai and C. Lubich. An error analysis of runge-kutta convolution quadrature. *Preprint 27/2010*, 2010.
- [7] L. Banjai, C. Lubich, and J.M. Melenk. Runge-kutta convolution quadrature for operators arising in wave propagation. *Numerische Mathematik*, 119(1):1–20, 2011.
- [8] J.M.O. Barbosa, J. Park, and E. Kausel. Perfectly matched layers in the thin layer method. *Comp. Methods in Applied Mech. Engineering*, 217-220:262–274, 2012.
- [9] F.C.P. De Barros and J.E. Luco. Discrete models for vertical vibrations of surface and embedded foundations. *Earthquake Engineering and Structural Dynamics*, 19(2):289–303, 1990.
- [10] U. Basu and A.K. Chopra. Perfectly matched layers for transient elastodynamics of unbounded domains. *International Journal for Numerical Methods in Engineering*, 59:1039–1074, 2004.
- [11] K.J. Bathe and M.M.I. Baig. On a composite implicit time integration procedure for nonlinear dynamics. *Computers and Structures*, 83:2513–2524, 2005.
- [12] T. Belytschko and Y.Y. Lu. A variationally coupled FE-BE method for transient problems. *International Journal for Numerical Methods in Engineering*, 37:91–105, 1994.

- [13] J.P. Berenger. A perfectly matched layer for the absorption of electromagnetic waves. *Journal of Computational Physics*, 114:185–200, 1994.
- [14] D. Bernal and A. Youssef. A hybrid time frequency domain formulation for non-linear soil-structure interaction. *Earthquake Engineering and Structural Dynamics*, 27(7):673–685, 1998.
- [15] P. Bettess. Infinite elements. *International Journal for Numerical Methods in Engineering*, 13:53–64, 1977.
- [16] P. Bettess. *Infinite Elements*. Penshaw press edition, 1992.
- [17] C. Birk and R. Behnke. A modified scaled boundary finite element method for three-dimensional dynamic soil-structure interaction in layered soil. *International Journal for Numerical Methods in Engineering*, 89(3):371–402, 2012.
- [18] M. Bonnet. *Boundary Integral Equation Methods for Solids and Fluids*. John Wiley & Sons, 1995.
- [19] C.L. La Borderie. *Phénomènes unilatéraux dans un matériaux endommageable: modélisation et application à l'analyse des structures en béton*. PhD thesis, Université Paris VI, 1991.
- [20] S. Bougacha and J.L. Tassoulas. Seismic analysis of gravity dams i: modeling of the sediments. *Journal of Engineering Mechanics (ASCE)*, 117(8):1826–1837, 1991.
- [21] M. Bransch and L. Lehmann. A nonlinear HHT-alpha method with elastic-plastic soil-structure interaction in a coupled SBFEM/FEM approach. *Computers and Geotechnics*, 38(1):80–87, 2011.
- [22] D.S. Burnett. A three-dimensional acoustic infinite element based on a prolate spheroidal multipole expansion. *Journal of Acoustic Society of America*, 96: 2798–2816, 1994.
- [23] S. Chaillat, M. Bonnet, and J.F. Semblat. A multi-level fast multipole BEM for 3-D elastodynamics in the frequency domain. *Comp. Methods in Applied Mech. Engineering*, 197:4233–4249, 2009.
- [24] C.T. Chatzigogos, A. Pecker, and J. Salencon. Macroelement modeling of shallow foundations. *Soil Dynamics and Earthquake Engineering*, 29(5):765–781, 2009.
- [25] W.C. Chew and Q.H. Liu. Perfectly matched layers for elastodynamics: a new absorbing boundary condition. *Journal of Computational Acoustics*, 4(4):341–359, 1996.
- [26] J.S. Choi, C.B. Yun, and J.M. Kim. Earthquake response analysis of the hualien soil-structure interaction system on based updated soil properties using forced vibration test data. *Earthquake Engineering and Structural Dynamics*, 30:1–26, 2001.
- [27] J.S. Choi, J.S. Lee, and J.M. Kim. Nonlinear earthquake response analysis of 2-d underground structures with soil-structure interaction including separation and sliding at interface. In *15th ASCE Engineering Mechanics Conference*, New York (USA), June 2002.

- [28] Z. Chuhan and Z. Chongbin. Coupling method of finite and infinite elements for strip foundation wave problems. *Earthquake Engineering and Structural Dynamics*, 15:839–851, 1987.
- [29] R. Clayton and B. Engquist. Absorbing boundary conditions for acoustic and elastic wave equations. *Bulletin of the Seismological Society of America*, 67(6):1529–1540, 1977.
- [30] D. Clouteau and D. Aubry. MISS 6.4: Manuel scientifique. Version 1.2. Technical report, École Centrale Paris, 2005.
- [31] D. Clouteau and G. Devésá. Décollement des fondations sous chargement sismique méthodes temporelle et temps/fréquence. In *Actes du cinquième colloque national en Calcul des structures*, volume II, pages 1065–1072, Giens, 2001.
- [32] D. Clouteau, A. Baroni, and D. Aubry. Boundary integrals and ray method coupling for seismic borehole modeling. In J. A. DeSanto editors, *Fourth international conference on Mathematical and Numerical Aspects of Wave Propagation: SIAM*, page 768, 1998.
- [33] D. Clouteau, D. Broc, G. Devésá, V. Guyonvarh, and P. Massin. Calculation methods of Structure-Soil-Structure Interaction (3si) for embedded buildings. application to NUPEC tests. *Soil Dynamics and Earthquake Engineering*, 32(1):129–142, 2012.
- [34] F. Collino and C. Tsogka. Application of the perfectly matched absorbing layer model to the linear elastodynamic problem in anisotropic heterogeneous media. *Geophysics*, 66(1):294–307, 2001.
- [35] R. Cottureau. *Probabilistic models of impedance matrices. Application to dynamic soil-structure interaction*. PhD thesis, Ecole Centrale Paris, 2006.
- [36] R. Courant, K. Friedrichs, and H. Lewy. On the partial difference equations of mathematical physics. *IBM Journal of Research and Development*, 11(2):215–234, 1967.
- [37] E. Şafak. Time-domain representation of frequency-dependent foundation impedance functions. *Soil Dynamics and Earthquake Engineering*, 26:65–70, 2005.
- [38] P.R. Cummins, N. Takeuchi, and R.J. Geller. Computation of complete synthetic seismograms for laterally heterogeneous models using the Direct Solution Method. *Geophysical Journal International*, 130(1):1–16, 1997.
- [39] G. Dahlquist. A special stability problem for linear multistep methods. *BIT Numerical Mathematics*, 3:27–43, 1963.
- [40] G.R. Darbre and J.P. Wolf. Criterion of stability and implementation issues of hybrid frequency time domain procedure for non-linear dynamic analysis. *Earthquake Engineering and Structural Dynamics*, 16(4):569–581, 1988.
- [41] G. Dasgupta. A finite element formulation for unbounded homogeneous continua. *Journal of Applied Mechanics (ASME)*, 49:136–140, 1982.

- [42] G. Devésá. Interaction sol-structure (ISS) en analyse sismique. Technical report, EDF R&D/AMA, 2009.
- [43] G. Devésá and V. Guyonvarh. Décollement dynamique de fondation en interaction sol-structure (ISS) par méthode de ressorts de sol. Technical Report U2.06.08, EDF R&D/AMA.
- [44] J. Domínguez. *Boundary elements in dynamics*. Computational Mechanics Publications and Elsevier Applied Science, 1993.
- [45] X. Du and M. Zhao. Stability and identification for rational approximation of frequency response function of unbounded soil. *Earthquake Engineering and Structural Dynamics*, 39:165–186, 2010.
- [46] W.M. Elleithy and M. Tanaka. Interface relaxation algorithms for BEM-BEM coupling and FEM-BEM coupling. *Computational Methods Applied to Mechanical Engineering*, 192:2977–2992, 2003.
- [47] F. Elsabee. *Static Stiffness Coefficients for Circular Foundations Embedded in an Elastic Medium*. PhD thesis, Massachusetts Institute of Technology, 1975.
- [48] O.von Estorff and H. Antes. On FEM-BEM coupling for fluid-structure interaction analyses in the time domain. *IJNME*, 31:1151–1168, 1991.
- [49] O.von Estorff and M. Firuziaan. Coupled BEM/FEM approach for nonlinear soil/structure interaction. *Engineering Analysis with Boundary Elements*, 24: 715–725, 2000.
- [50] O.von Estorff and M.J. Prabucki. Dynamic response in the time domain by coupled boundary and finite elements. *Computational Mechanics*, 6:35–46, 1990.
- [51] S. Fayolle. Loi de comportement GLRC-DM. Technical Report R7.01.32, EDF R&D/AMA, 2009.
- [52] M.L. Fernández, C. Lubich, and A. Schädle. Fast and oblivious convolution in evolution equations with memory. *SIAM Journal on Scientific Computing*, 28 (2):421–431, 2006.
- [53] S. François. *Nonlinear modelling of the response of structures due to ground vibrations*. PhD thesis, Katholieke Universiteit Leuven, 2008.
- [54] S. François and G. Degrande. Application of a time domain coupled finite element-boundary element method to traffic induced vibrations. In M. Papadrakis, E. Oñate and B. Schrefler editors, *Computational Methods for Coupled Problems in Science and Engineering*, Santorini, Greece, 2005. CD-ROM.
- [55] L. Gaul and M. Schanz. A comparative study of three boundary element approaches to calculate the transient response of viscoelastic solids with unbounded domains. *Computer methods in applied mechanics and engineering*, 179:111–123, 1999.
- [56] R.J. Geller and T. Hatori. DSM synthetic seismograms using analytic trial functions: plane layered, isotropic, case. *Geophysical Journal International*, 120:163–172.

- [57] R.J. Geller and T. Ohminato. Computation of synthetic seismograms and their partial derivatives for heterogeneous media with arbitrary natural boundary conditions using the Direct Solution Method. *Geophysical Journal International*, 116:421–446, 1994.
- [58] M. Cemal Genes. Dynamic analysis of large-scale ssi systems for layered unbounded media via a parallelized coupled finite-element/boundary-element/scaled boundary finite-element model. *Engineering Analysis with Boundary Elements*, 36:845–857, 2012.
- [59] S. Grange, P. Kotronis, and J. Mazars. A macro-element to simulate dynamic soil-structure interaction. *Engineering Structures*, 31(12):3034–3046, 2009.
- [60] A. Gravouil. *Méthode multi-échelles en temps et en espace avec décomposition de domaines pour la dynamique non-linéaire des structures*. PhD thesis, ENS Cachan, 2000.
- [61] N.A. Haskell. The Dispersion of Surface Waves on Multilayered Media. *Bulletin of the Seismological Society of America*, 13(1), 1953.
- [62] Y. Hayashi and H. Katukura. Effective time-domain soil-structure interaction analysis based on FFT algorithm with causality condition. *Earthquake Engineering and Structural Dynamics*, 19(5):693–708, 1990.
- [63] I. Herrera and J. Bielak. Soil-structure interaction as a diffraction problem. In *Proceedings of the 6th World Conference on Earthquake Engineering*, pages 19–24, New Delhi (India), 1977.
- [64] R.L. Higdon. Absorbing boundary conditions for elastic waves. *Geophysics*, 56(2):231–241, 1991.
- [65] H.M. Hilber, T.J.R. Hughes, and R.M. Taylor. Improved numerical dissipation for time integration algorithms in structural dynamics. *Earthquake Engineering and Structural Dynamics*, 5:283–292, 1977.
- [66] T.J.R. Hugues, K.S. Pister, and R.L. Taylor. Implicit-explicit finite elements in nonlinear transient analysis. *Computer Methods in Applied Mechanics and Engineering*, 17/18:159–182, 1979.
- [67] E.I. Jury. *Theory and application of the z transform method*. Wiley, 1964.
- [68] M. Karpel. Design for active flutter suppression and gust alleviating using state-space unsteady aeroelastic modelling. *Journal of Aircraft*, 19(3):221–227, 1982.
- [69] E. Kausel. Thin layer method: formulation in the time domain. *International Journal for Numerical Methods in Engineering*, 37:927–941, 1994.
- [70] E. Kausel and R. Peek. Dynamic loads in the interior of a layered stratum: an explicit solution. *Bulletin of the Seismological Society of America*, 72(5):1459–1481, 1982.
- [71] E. Kausel and J.M. Roesset. Stiffness matrices for layered soils. *Bulletin of the Seismological Society of America*, 71(6):1743–1761, 1981.

- [72] E. Kausel and S.H. Seale. Static loads in layered halfspaces. *Journal of Applied Mechanics (ASME)*, 54(2):403–408, 1987.
- [73] E. Kausel, R.V. Whitman, J.P. Morray, and F. Elsabee. The spring method for embedded foundations. *Nuclear Engineering and Design*, 48(2–3):1039–1074, 1978.
- [74] Y. Kitada, T. Hirotani, and M. Iguchi. Model Test on Dynamic Structure-Structure Interaction of Nuclear Power Plant Buildings. *Nuclear Engineering and Design*, 192:205–216, 1999.
- [75] A. Laliena and F.J. Sayas. Theoretical aspects of the application of convolution quadrature to scattering of acoustic waves. *Numerische Mathematik*, 112(4):637–678, 2009.
- [76] V.I. Lebedev and V.I. Agoshkov. *Poincaré-Steklov operators*. In *International Congress of Mathematicians*, Warsaw, 1982.
- [77] S. Lermite, T. Chaudat, T. Payen, D. Vandeputte, and E. Viallet. Smart 2008: Seismic design and best-estimate methods assessment for RC buildings subjected to torsion. In *The 14th World Conference on Earthquake Engineering*, Beijing, China, 2008.
- [78] A.R. Levander. Use of the telegraphy equation to improve absorbing boundary efficiency for fourth-order acoustic wave finite difference schemes. *Bulletin of the Seismological Society of America*, 75(6):1847–1852, 1985.
- [79] B. Li, L. Cheng, A.J. Deeks, and B. Teng. A modified scaled boundary finite-element method for problems with parallel side-faces. part I. theoretical developments. *Applied Ocean Research*, 27(4-5):216–223.
- [80] S.T. Lie and G.Y. Yu. Stability improvement to BEM/FEM coupling scheme for 2d scalar wave problems. *Advances in Engineering Software*, 33:17–26, 2002.
- [81] S.T. Lie, G. Yu, and C. Fan. Further improvement to the stability of the coupling BEM/FEM scheme for 2-d elastodynamic problems. *Computers and Structures*, 25:468–476, 2000.
- [82] G. Lin, J. Du, and Z. Hu. Dynamic dam-reservoir interaction analysis including effect of reservoir boundary absorption. *Science in China Series E: Technological Sciences*, 50(1):1–10, 2007.
- [83] F.S. Loureiro and W.J. Mansur. An efficient hybrid time-Laplace domain method for elastodynamic analysis based on the explicit Green’s approach. *International Journal of Solids and Structures*, 46:3093–3102, 2009.
- [84] C. Lubich. Convolution quadrature and discretized operational calculus i. *Numerische Mathematik*, 52:129–145, 1988.
- [85] C. Lubich. Convolution quadrature and discretized operational calculus ii. *Numerische Mathematik*, 52:413–425, 1988.
- [86] C. Lubich. On the multistep time discretization of linear initial-boundary value problems and their boundary integral equations. *Numerische Mathematik*, 67:365–389, 1994.

- [87] C. Lubich. Stable FEM & BEM & Leapfrog & Convolution Quadratures coupling for the wave equation. In *6th Workshop Numerical Methods for Evolution Problems*, Heraklion, Crete, 2012.
- [88] C. Lubich and A. Ostermann. Runge-kutta methods for parabolic equations and convolution quadrature. *Mathematics of Computation*, 60:105–131, 1993.
- [89] J. Lysmer. Lumped mass method for rayleigh waves. *Bulletin of the Seismological Society of America*, 60(1):89–104, 1970.
- [90] J. Lysmer and R.L. Kuhlemeyer. Finite dynamic model for infinite media. *Journal of Engineering Mechanics Division (ASCE)*, 95(EM4):859–877, 1969.
- [91] J. Lysmer and G. Waas. Shear waves in plane infinite structures. *Journal of Engineering Mechanics (ASCE)*, 18:85–105, 1972.
- [92] D. Markovic, P. Koechlin, and F. Voldoire. Reinforced concrete structures under extreme loading: Stress resultant Global Reinforced Concrete models (GLRC). In *Proceedings of Computational Methods in Structural Dynamics and Earthquake Engineering (COMPdyn)*, 2007.
- [93] F. De Martin, H. Modaressi, and H. Aochi. Coupling of FDM and FEM in seismic wave propagation. In *4th International Conference on Earthquake Geotechnical Engineering*, Greece, June 2007.
- [94] H.R. Masoumi. *Numerical modeling of free field vibrations due to pile driving*. PhD thesis, Katholieke Universiteit Leuven, 2008.
- [95] F. Medina and R.L. Taylor. Infinite elements for elastodynamics. *Earthquake Engineering and Structural Dynamics*, 10:699–709, 1982.
- [96] E. Mesquita and R. Pavanello. Numerical methods for the dynamics of unbounded domains. *Computational and Applied Mathematics*, 24(1):1–26, 2005.
- [97] W. Moser, H. Antes, and G. Beer. A Duhamel integral based approach to one-dimensional wave propagation analysis in layered media. *Computational Mechanics*, 35:115–126, 2005.
- [98] W. Moser, H. Antes, and G. Beer. Soil-structure interaction and wave propagation problems in 2D by a Duhamel integral based approach and the convolution quadrature method. *Computational Mechanics*, 36:431–443, 2005.
- [99] N. Nakamura. A practical method for estimating dynamic soil stiffness on surface of multi-layered soil. *Earthquake Engineering and Structural Dynamics*, 34(11):1391–1406, 2005.
- [100] N. Nakamura. A practical method to transform frequency dependent impedance to time domain. *Earthquake Engineering and Structural Dynamics*, 35(2):217–231, 2005.
- [101] N. Nakamura. Improved methods to transform frequency-dependent complex stiffness to time domain. *Earthquake Engineering and Structural Dynamics*, 35(8):1037–1050, 2006.

- [102] N. Nakamura. Transform methods for frequency-dependent complex stiffness to time domain using real or imaginary data only. *Earthquake Engineering and Structural Dynamics*, 37(4):495–515, 2007.
- [103] N. Nakamura. Seismic response analysis of deeply embedded nuclear reactor buildings considering frequency-dependent soil impedance in time domain. *Nuclear Engineering and Design*, 238:1845–1854, 2008.
- [104] N.M. Newmark. A method of computation for structural dynamics. *ASCE Journal of Engineering Mechanics Division*, 85:67–94, 1959.
- [105] X.H. Nguyen and N. Ile. Finite elements models for earthquake engineering: the case of reinforced concrete building. In *The 3rd ACF International Conference ACF/VCA*, 2008.
- [106] R. Nova and L. Montrasio. Settlements of shallow foundations on sand. *Géotechnique*, 41(2):243–256, 1991.
- [107] C. Obrembski, D. Clouteau, and N. Greffet. Algorithme temps-fréquence pour la dynamique non-linéaire en interaction sol-structure. In *Cinquième colloque national en Calcul des structures*, volume II, pages 615–620, Giens, 2005.
- [108] A.V. Oppenheim, A.S. Willsky, and S.H. Nawab. *Signals and Systems*. Prentice-Hall edition, 1997.
- [109] R.Y.S. Pak and B.B. Guzina. Seismic soil-structure interaction analysis by direct boundary element methods. *International Journal of Solids and Structures*, 36:4743–4766, 1999.
- [110] A. Paronesso and J.P. Wolf. Global lumped-parameter model with physical representation for unbounded medium. *Earthquake Engineering and Structural Dynamics*, 24(5):637–654, 1995.
- [111] A. Paronesso and J.P. Wolf. Recursive evaluation of interaction forces and property matrices from unit-impulse response functions of unbounded medium based on balancing approximation. *Earthquake Engineering and Structural Dynamics*, 27(6):609–618, 1998.
- [112] A. Peirce and E. Siebrits. Stability analysis and design of time-stepping schemes for general elastodynamic boundary element models. *International Journal for Numerical Methods in Engineering*, 40:319–342, 1997.
- [113] A. Pereira and G. Beer. Interface dynamic stiffness matrix approach for three-dimensional transient multi-region boundary element analysis. *International Journal for Numerical Methods in Engineering*, 80:1463–1495, 2009.
- [114] T. Von Petersdorff and R. Leis. Boundary integral equations for mixed Dirichlet, Neumann and transmission problems. *Mathematical Methods in the Applied Sciences*, 11(2):185–213, 1989.
- [115] L. Pyl, D. Clouteau, and G. Degrande. The soil impedance of embedded structures in the higher frequency range, computed with the Boundary Element Method. In *16th ASCE Engineering Mechanics Conference*, University of Washington, Seattle, 2003.

- [116] R.K.N.D. Rajapakse and P. Karasudhi. Efficient elastodynamic infinite element. *International Journal of Solids and Structures*, 22:643–657, 1986.
- [117] J.R. Retherford. *Hilbert space: Compact Operators and the Trace Theorem*. Cambridge University Press, 1993.
- [118] A.C. Reynolds. Boundary conditions for the numerical solution of wave propagation problems. *Geophysics*, 43(6):1099–1110, 1978.
- [119] F.J. Rizzo. An integral equation approach to boundary value problems of classical elastostatics. *Quarterly of Applied Mathematics*, 25:83–95, 1967.
- [120] E.P. Saez Robert. *Dynamic nonlinear soil-structure interaction*. PhD thesis, Ecole Centrale Paris, 2009.
- [121] I. Romero. Stability analysis of linear multistep methods for classical elastodynamics. *Comp. Methods in Applied Mech. Engineering*, 193:2169–2189, 2004.
- [122] J.S. Ryu, C.G. Seo, and C.B. Yun. Seismic response analysis of soil-structure interactive system using a coupled three-dimensional FE-IE method. *Nuclear Engineering and Design*, 240:1949–1966, 2010.
- [123] A. Schädle, M.L. Fernández, and C. Lubich. Fast and oblivious convolution quadrature. *SIAM Journal on Scientific Computing*, 28(2):403–420, 2006.
- [124] M. Schanz. *Wave propagation in Viscoelastic and Poroelastic Continua: A Boundary Element Approach*. Springer, 2001.
- [125] M. Schanz and H. Antes. A new visco- and elastodynamics time domain boundary element formulation. *Computational Mechanics*, 20(5):452–459, 1997.
- [126] M. Schanz and H. Antes. Application of 'Operational Quadrature Methods' in time domain boundary element methods. *Meccanica*, 32:179–186, 2006.
- [127] M. Schanz, H. Antes, and T. Rüberg. Convolution quadrature boundary element method for quasi-static visco- and poroelastic continua. *Computers and Structures*, 83:673–684, 2005.
- [128] S.H. Seale and E. Kausel. Dynamic and static impedances of cross-anisotropic halfspaces. *Journal of Engineering Mechanics (ASCE)*, 115(3):509–524, 1989.
- [129] J.F. Semblat and A. Pecker. *Waves and Vibrations in Soils: Earthquakes, Traffic, Shocks, Construction works*. IUSS Press, 2009.
- [130] C.G. Seo, C.B. Yun, and J.M. Kim. Three-dimensional frequency dependent infinite elements for soil-structure interaction. *Engineering Structures*, 29:3106–3120, 2007.
- [131] R.T. Sewell, C.A. Cornell, G.R. Toro, and R.K. McGuire. A study of factors influencing floor response spectra in nonlinear multi-degree-of-freedom structures. Technical Report Report No.86, The John A. Blume Earthquake Engineering Center, 1986.
- [132] S.G. Shah, C.H. Solanki, and J.A. Desai. Soil structure interaction analysis methods - state of art - review. *International Journal of Civil and Structural Engineering*, 2(1):176–204, 2011.

- [133] A. Sommerfeld. *Partial differential equations*. Academic Press, New York (USA), 1949.
- [134] C. Song and J.P. Wolf. Consistent infinitesimal finite-element-cell method: out-of-plane motion. *Journal of Engineering Mechanics*, 121(5):613–619, 1995.
- [135] C. Song and J.P. Wolf. Consistent infinitesimal finite-element cell method: three-dimensional vector wave equation. *International Journal for Numerical Methods in Engineering*, 39(13):2189–2208, 1996.
- [136] C. Song and J.P. Wolf. The scaled boundary finite-element method –alias consistent infinitesimal finite-element cell method– for elastodynamics. *Computer Methods in Applied Mechanics and Engineering*, 147:329–355, 1997.
- [137] C.C. Spyrakos and C. Xu. Dynamic analysis of flexible massive strip-foundations embedded in layered soils by hybrid BEM-FEM. *Computers and Structures*, 82: 2541–2550, 2004.
- [138] A. Talbot. The accurate numerical inversion of Laplace transforms. *Journal of the Institute of Mathematics and its Applications*, 23:97–120, 1979.
- [139] J.L. Tassoulas and E. Kausel. On the dynamic stiffness of circular ring footings on an elastic stratum. *International Journal for Numerical and Analytical Methods in Geomechanics*, 8:411–426, 1983.
- [140] W.T. Thomson. Transmission of Elastic Waves through a Stratified soil Medium. *Journal of Applied Physics*, 21, 1950.
- [141] T. Triantafyllidis. 3-D time domain BEM using half-space green’s functions. *Engineering Analysis with Boundary Elements*, 8(3):115–124, 1991.
- [142] R.F. Ungless. *An infinite finite element*. PhD thesis, *M.A.Sc. Thesis*, University of British Columbia, 1973.
- [143] O. von Estorff and E. Kausel. Coupling of boundary and finite elements for soil-structure interaction problems. *Earthquake Engineering and Structural Dynamics*, 18:1065–1075, 1989.
- [144] J.P. Wolf. *Dynamic soil-structure interaction*. Prentice-Hall, 1985.
- [145] J.P. Wolf. *Soil-structure interaction analysis in the time domain*. Prentice-Hall, 1988.
- [146] J.P. Wolf and M. Motosaka. Recursive evaluation of interaction forces of unbounded soil in the time domain. *Earthquake Engineering and Structural Dynamics*, 18(3):345–363, 1989.
- [147] J.P. Wolf and M. Motosaka. Recursive evaluation of interaction forces of unbounded soil in the time domain from dynamic-stiffness coefficients in the frequency-domain. *Earthquake Engineering and Structural Dynamics*, 18(3): 365–376, 1989.
- [148] J.P. Wolf and P. Oberhuber. Non-linear soil structure-interaction analysis using dynamic stiffness or flexibility of soil in the time domain. *Earthquake Engineering and Structural Dynamics*, 13(2):195–212, 1985.

- [149] J.P. Wolf and D.R. Somaini. Approximate dynamic model of embedded foundation in time domain. *Earthquake Engineering and Structural Dynamics*, 14(5):683–703, 1986.
- [150] J.P. Wolf and C. Song. Consistent infinitesimal finite-element cell method: in-plane motion. *Computer Methods in Applied Mechanics and Engineering*, 123:355–370, 1995.
- [151] J.P. Wolf and C. Song. *Finite-element Modelling of Unbounded Media*. John Wiley & Sons, 1996.
- [152] J.Y. Yan, C.H. Zhang, and F. Jin. A coupling procedure of FE and SBFEM for soil-structure interaction in the time domain. *International Journal for Numerical Methods in Engineering*, 59(11):1453–1471, 2004.
- [153] S.C. Yang and C.B. Yun. Axisymmetric infinite elements for soil-structure interaction analysis. *Engineering Structures*, 14:361–370, 1992.
- [154] G.Y. Yu, W.J. Mansur, J.A.M. Carrer, and S.T. Lie. A more stable scheme for BEM/FEM coupling applied to two-dimensional elastodynamics. *Computers and Structures*, 79:811–823, 2001.
- [155] W.J. Mansur J.A.M. Carrer G.Y. Yu and S.T. Lie. A more stable scheme for BEM/FEM coupling applied to two-dimensional elastodynamics. *Computers and Structures*, 79:811–823, 2001.
- [156] I. Zentner. *Étude de la stabilité de systèmes aéroélastiques en présence d'excitations aléatoires multiplicatives*. PhD thesis, Ecole Nationale des Ponts et Chaussées, 2005.
- [157] L. Zhenpeng. Dynamic Interaction of Natural and Man-Made Structures with Earth Medium. *Earthquake Research in China*, 13(3), 1999.
- [158] O.C. Zienkiewicz and P. Bettess. A novel boundary infinite element. *International Journal for Numerical Methods in Engineering*, 19:393–404, 1983.
- [159] O.C. Zienkiewicz, R.L. Taylor, and J.Z. Zhu. *The Finite Element Method: Its Basis and Fundamentals*. Elsevier, 1988.

Appendix A

Functional spaces

Let $L^p(\Omega)$ be the Banach space of p th-power integrable real-valued functions defined on an open set $\Omega \in \mathbb{R}^n$ for a Lebesgue measure. This space is equipped with the norm $\|u\|_{0,p} = (\int_{\Omega} |u(x)|^p d\Omega)^{\frac{1}{p}}$ and, for the particular case of $p = 2$, $L^2(\Omega)$ is a Hilbert space with inner product:

$$(u, v) = \int_{\Omega} u(x)v(x) d\Omega \quad (\text{A.1})$$

and whose norm is denoted by $\|\cdot\|$. For non-negative integer m and $p \geq 1$, the classical Sobolev spaces can be defined:

$$W^{m,p}(\Omega) = \{u \in L^p(\Omega) \mid \partial^k u \in L^p(\Omega) \forall |k| \leq m\} \quad (\text{A.2})$$

whose associated norm is defined as:

$$\|u\|_{m,p} := \|u\|_{W^{m,p}(\Omega)} = \left(\sum_{0 \leq |k| \leq m} \|\partial^k u\|_{L^p(\Omega)}^p \right)^{\frac{1}{p}} \quad (\text{A.3})$$

where k denotes a multi-index. Because of its Hilbert space structure, the case of $W^{m,2}(\Omega)$ is commonly denoted by $H^m(\Omega)$ (remark that $H^0(\Omega) = L^2(\Omega)$) and its associated norm by $\|\cdot\|_{m,\Omega}$ or simply by $\|\cdot\|_m$. Moreover, for the case of $m = 1$, the following norm can also be defined:

$$\|u\|_{a,\Omega} := \left(\int_{\Omega} |\nabla u|^2 + a^2 \int_{\Omega} |u|^2 \right)^{\frac{1}{2}} \quad (\text{A.4})$$

where $a > 0$. In particular, for $s \in \mathbb{C}$ and $\sigma = \Re e(s) > 0$, the previous norm is equivalent to the one usually used in $H^1(\Omega)$:

$$\underline{\sigma} \|u\|_{1,\Omega} \leq \|u\|_{|s|,\Omega} \leq \frac{|s|}{\underline{\sigma}} \|u\|_{1,\Omega} \quad (\text{A.5})$$

where $\underline{\sigma} := \min(1, \sigma)$. For the last inequality, identity $\underline{\sigma} \max(1, |s|) \leq |s|$ has been used.

For the case of Ω having Lipschitz boundary, which is denoted Γ , similar Sobolev spaces $H^r(\Gamma)$ endowed with norm $\|\cdot\|_{r,\Gamma}$ (or $\|\cdot\|_r$) can be defined for $r \in \mathbb{R}^+$. Particularly interesting are $H^{\frac{1}{2}}(\Gamma) \subset L^2(\Gamma)$ and its dual $H^{-\frac{1}{2}}(\Gamma) \supset L^2(\Gamma)$. If duality pairings are denoted by $\langle \cdot, \cdot \rangle$, the duality is written as:

$$\langle \lambda, \psi \rangle = \int_{\Gamma} \lambda(x)\psi(x) d\Gamma. \quad (\text{A.6})$$

Appendix B

Earthquake Response Spectra

Response Spectra are very employed in earthquake engineering. In particular, they are used to predict how equipments would respond under a seismic loading by considering their individual mass m and stiffness k .

In this framework, consider N SDOF systems with different fundamental periods $T_i, i = 1..N$ –but the same modal damping ξ – subjected to a ground excitation $\ddot{u}_g(t)$. Then, the Spectral Displacement (SD) S_d is defined as the maximum of the displacement response $u_i(t)$ of each SDOF system as a function of the corresponding fundamental period:

$$S_d(T) = \max|u_i(t)|, \quad i = 1..N \quad (\text{B.1})$$

Analogously, the Spectral Acceleration (SA) reads:

$$S_a(T) = \max|\ddot{u}_i(t) + \ddot{u}_g(t)|, \quad i = 1..N \quad (\text{B.2})$$

where the absolute acceleration has been considered.

In fact, both SD and SA are, not only a function of the fundamental period but also a function of the modal damping, $S_d(T) = S_d(T, \xi)$ and $S_a(T) = S_a(T, \xi)$. The family of all these curves is called Displacement Response Spectra or Acceleration Response Spectra of an earthquake, respectively.

When $T_i = 0$ (i.e. the system is infinitely stiff), the SA equals the Peak Ground Acceleration (PGA) $S_a = \ddot{u}_{g,max}(t)$ while $S_d = 0$. On the other hand, when T_i approaches infinity (i.e. the system is infinitely flexible), S_a tends to zero and S_d to the Peak Ground Displacement (PGD).

In order to estimate the maximum base shear force $F_{sh,max}$ at the base of a SDOF, the Pseudo Spectral Acceleration (PSA) has to be defined:

$$PSA(T, \xi) = \left(\frac{2\pi}{T_i}\right)^2 S_d(T, \xi) \quad (\text{B.3})$$

It coincides to S_a for $\xi < 20\%$ and it allows to evaluate:

$$F_{sh,max} = mPSA. \quad (\text{B.4})$$

